STELLINGEN

behorende bij het proefschrift:

"Simulation of volume changes
in hardening cement-based materials"

van

Eddie Koenders

Delft, 23 september 1997

1

Thermodynamisch evenwicht in het poriesysteem van cementgebonden materialen bepaalt de grootte van de interne krachten die aangrijpen op de microstructuur tijdens het verhardingsproces.

2

De grootte van de autogene krimp (krimp door zelfuitdroging) van cementgebonden materialen wordt bepaald door de spanning die optreedt in de geadsorbeerde laag tegen de poriewand.

3

Door zogenaamde 'interne nabehandeling' blijft de relatieve-vochtigheid in cementgebonden materialen op een hoger niveau, waardoor de spanning in de geadsorbeerde laag tegen de poriewand lager blijft.

4

De constitutieve relatie betreffende het verband tussen oppervlaktespanning in de geadsorbeerde laag en vervorming, zoals oorspronkelijk voorgesteld door Bangham (1931), is ook toepasbaar voor verhardende cementpasta mits het effect van de veranderingen in de microstructuur op de waarde van de grootheden in de Bangham-vergelijking wordt verdisconteerd.

Bangham, D. H. and Fakhoury, N. (1931), The Swelling of Charcoal, Royal Society of London ,CXXX,(Series A),81-89.

5

Vervormingen, die verklaard kunnen worden uit veranderingen van de relatieve-vochtigheid in een cementpasta, kunnen slechts voor een deel de vervormingen verklaren die optreden tijdens de vroege fase van het verhardingsproces. Een ander deel wordt bepaald door het type cement.

6

Dat, overeenkomstig de literatuur, de hydratatiegraad van beton hoger is dan de hydratatiegraad van zuivere cementpasta, kan deels worden verklaard op grond van de resultaten van numerieke-simulaties van het verhardingsproces. De invloed van zowel de ruimtelijke verdeling van de cementkorrels alswel het effect van vloeistofstroming door de matrix als gevolg van drukgradienten, hebben hierop grote invloed.

7

De ontwikkeling van numerieke-simulatiemodellen ten behoeve van wetenschappelijk onderzoek biedt mogelijkheden voor het inzichtelijk maken van zeer complexe problemen. Het algoritmiseren van mechanismen en/of physische processen draagt daarom zowel bij aan de voortgang van fundamenteel onderzoek als aan het inititëren van nieuwe onderzoeksvragen.

8

Naarmate een onderzoeksprobleem verder wordt uitgediept ontstaat er meer behoefte aan interdisciplinair overleg.

9

Op het gebied van het besteden van onderzoeksgelden is het ozongat een gat in de markt.

10

Laboratoriumexperimenten worden pas overbodig indien computers "materiaaleigenschappen" bezitten.

11

Beton is niet hard maar wordt hard.

12

De NS doet er goed aan de dienstregeling enkele minuten te verschuiven. Op deze manier zal een groot deel van de treinvertragingen verdwijnen.

13

Het fietsverkeer zou er zeer bij gebaat zijn indien regen wordt betrokken in het voorrangverleen-algoritme van verkeersregelinstallaties.

Simulation of Volume Changes in Hardening Cement-Based Materials

Simulation of Volume Changes in Hardening Cement-Based Materials

PROEFSCHRIFT
ter verkrijging van de graad van doctor
aan de Technische Universiteit Delft,
op gezag van de Rector Magnificus Prof. dr. ir. J. Blaauwendraad
in het openbaar te verdedigen ten overstaan van een commissie,
door het College van Dekanen aangewezen,
op dinsdag 23 september 1997 te 13.30 uur

door

Eduardus Aloysius Bernardus KOENDERS

civiel ingenieur

geboren te Groenlo

Dit proefschrift is goedgekeurd door de promotor:
Prof. dr. ir. J.C. Walraven

Toegevoegd promotor:
Dr. ir. K. van Breugel

Samenstelling promotiecommissie:

Rector Magnificus, Voorzitter	Technische Universiteit Delft
Prof. dr. ir. J.C. Walraven, promotor	Technische Universiteit Delft
Dr. ir. K. van Breugel, toegevoegd promotor	Technische Universiteit Delft
Prof. ir H.W. Bennenk	Technische Universiteit Eindhoven
Prof. dr. ir. J.M.J.M. Bijen	Technische Universiteit Delft
Prof. Dr. -Ing. F.S. Rostásy	Technische Universiteit Braunschweig, Duitsland
Prof. dr. ir. L.Taerwe	Universiteit Gent, België
Prof. dr. ir. A. Verruijt	Technische Universiteit Delft

Published and distributed by:
Delft University Press
Mekelweg 4
2628 CD DELFT
The Netherlands
Telephone: +31 15 2783254
Fax: +31 15 2781661
E-mail: DUP@DUP.TUDelft.NL

CIP-GEGEVENS KONINKLIJKE BIBLIOTHEEK, DEN HAAG
Koenders, Eduardus A.B.
Simulation of Volume Changes in Hardening Cement-Based Materials / E.A.B. Koenders. - Delft : Delft University Press. - Illustrations.
Thesis Delft University of Technology. - With ref. - With summary in Dutch.
ISBN 90-407-1499-1
NUGI 841
Subject headings: cement hydration / modelling / volume changes / pore structure

It's just a temporary thing
(Lou Reed, 1978)

Acknowledgements

The research work that is described in this thesis was carried out at the Stevin Laboratory of the Civil Engineering Department of Delft University of Technology in the Netherlands.

I would like to express my gratitude to my supervisor dr K. van Breugel for his guidance and fruitful discussions during the period of this research.

I also like to thank prof. J.C. Walraven for his valuable comments and his supporting and stimulating words that I needed, especially at the start of this research.

The help and support of all colleagues of the Concrete Structures Group has contributed to the final result of this work. I am particular indebted to Fred Schilperoort for his assistance and expertise in performing the experiments and his helpful comments on the computer programming language C.

I am also grateful to prof. A. Verruijt for his patience and help with the derivation of the differential equation for the description of the moisture transport mechanism.

The permission of the Dutch Ministry of Transport, Public works and Water Management in Tilburg in The Netherlands, to allow for the use of the experimental data of the TSTM set-up is gratefully mentioned.

The full scale structure in chapter 7 of this thesis is part of a research project *"First office building in high strength concrete"*. This project was managed by NBM-Amstelland building contractors.

Most of the figures are prepared by Henk Spiewakowski and Theo Steijn. Their work is gratefully acknowledged.

I like to express my deepest gratitude to my roommate Sander Lokhorst with which I shared room 1.06 for almost four years. I will miss the synergy in not only the technical but also in the social part of the PhD study. In addition, I also like to thank him and dr Cor van der Veen for carefully reading the preliminary version of this thesis and their critical remarks.

I like to thank my friends Roeland Ris and Arjen Kort for the turbulent time we had during this PhD study. I also like to mention my friends Edwin Dado, Rob Damink and Erwin Lammertink with whom I spent many pleasurable hours after working time.

Finally, I like to thank Susan Lensink for her support and interest during the writing of this thesis.

TABLE OF CONTENTS

Acknowledgements
Table of contents

1. INTRODUCTION **1**
1.1 General scope of the project 1
1.2 Practical relevance 3
1.3 Aim of the project 4
1.4 Research strategy and set-up of the thesis 4

2. FEATURES OF LOW WATER/CEMENT RATIO CONCRETES **7**
2.1 General 7
2.2 Mix composition 8
2.2.1 Water/binder ratio 8
2.2.2 Cement fineness 8
2.2.3 Cement content and type of cement 8
2.2.4 Aggregates 9
2.2.5 Microfillers 9
2.2.6 Admixtures 10
2.3 Degree of hydration 10
2.3.1 General 10
2.3.2 Definition 11
2.3.3 Degree of hydration measurements on HSC 11
2.4 Rate of hydration 12
2.5 Volume changes during hardening 13
2.5.1 General 13
2.5.2 Definitions 13
2.6 Special locations in concrete 15
2.6.1 Interfacial transition zone and bulk paste 15
2.6.2 Plain paste 16
2.7 Moisture transport during hardening 17
2.7.1 Microstructural phase changes 17
2.7.2 Transport of capillary water 18
2.8 Discussion 19

3. MODELLING HYDRATION AND MICROSTRUCTURE **21**
3.1 General 21

3.2 Existing numerical models 22
3.2.1 NIST-model 22
3.2.2 Jennings and Johnson model 23
3.2.3 Basic HYMOSTRUC model 24
3.2.3.1 Basic features of the simulation model 24
3.2.3.2 Stereological aspects 24
3.2.3.3 Particle expansion and particle interaction mechanism 24
3.2.3.4 Classification of pores 25
3.2.3.5 Modelling the pore size distribution 26
3.2.3.6 Pore structure constant "a" determined from experiments 29
3.3 Extension of the basic HYMOSTRUC model 30
3.3.1 General 30
3.3.2 Random particle structure 30
3.3.3 Theoretical background 31
3.3.4 Mean particle spacing 34
3.3.5 Formation of microstructure 36
3.3.6 Pore structure constant "a" determined from random particle structure 37
3.4 Discussion 41

4. MODELLING OF AUTOGENOUS SHRINKAGE 43
4.1 General 43
4.2 Thermodynamic analysis of the moisture state in a changing pore system 44
4.2.1 Literature survey 44
4.2.2 Basic mechanism of thermodynamic analysis 45
4.2.3 Existing models based on a thermodynamic approach 45
4.2.4 Description of a thermodynamic analysis of a pore system 47
4.2.5 Adsorption layer at the pore wall area 50
4.2.6 Relative humidity in empty pore space 51
4.2.7 Gas pressure in empty pore space 52
4.2.8 Surface tension in the adsorption layer 52
4.3 Deformation of the cement paste 53
4.3.1 General 53
4.3.2 Deformation mechanism 54
4.3.3 Pore wall area of the empty pores 55
4.3.4 Specific mass of plain cement paste 56
4.3.5 Modulus of elasticity of hardening cement paste 56
4.3.6 Validity range of the thermodynamic approach 58
4.3.7 Discussion 61
4.4 Flow chart of the iteration procedure 62
4.4.1 General 62

4.4.2 Description of the flow chart 62
4.5 Parameter study and model features 65
4.5.1 General 65
4.5.2 Evolution of the degree of hydration 65
4.5.3 Relative humidity in the empty pore space 67
4.5.4 Thickness of the adsorption layer in the pore space 69
4.5.5 Gas pressure in the empty pore space 70
4.5.6 Surface tension in the adsorption layer 72
4.6 Discussion 73

5. AUTOGENOUS SHRINKAGE: EXPERIMENTS VS SIMULATIONS 75
5.1 Introduction 75
5.2 Experimental program on autogenous shrinkage of cement paste 76
5.3 Description of the experimental set-up 77
5.4 Experiments on neat Portland cement pastes 78
5.4.1 Cement of high fineness (Blaine 550 m²/kg) 78
5.4.2 Cement of medium fineness (Blaine 420 m²/kg) 79
5.4.3 Cement of low fineness (Blaine 300 m²/kg) 80
5.5 Experiment on cement paste with silica fume 81
5.6 Numerical simulations versus literature data 84
5.7 Autogenous shrinkage of concrete 84
5.7.1 Internal restraint by aggregates 84
5.7.2 Parallel-series model 85
5.7.3 Lattice model approach 88
5.8 Discussion 91

6. RIBBON PASTE HYDRATION 93
6.1 General 93
6.2 Interfacial transition zone 94
6.3 Concrete RIBBON model 95
6.3.1 General 95
6.3.2 Ribbon thickness 97
6.4 Pore system properties 99
6.5 Current HYMOSTRUC potential on ribbon hydration 103
6.5.1 Paste density and water/cement ratio 103
6.5.2 Degree of hydration 104
6.5.3 Porosity 104
6.5.4 Degree of saturation 106
6.6 Ribbon hydration of random particle structures 107
6.6.1 General 107

6.6.2 Random particle size distribution in sphere 107
6.6.2.1 Paste density and water/cement ratio 107
6.6.3 Random particle size distribution in tube 109
6.6.3.1 Evolution of the degree of hydration over the ribbon thickness 109
6.6.3.2 Porosity 111
6.6.3.3 Degree of saturation 111
6.7 Towards the effect of modelling of moisture transport on ribbon paste hydration .. 112
6.7.1 General 112
6.7.2 Derivation of a differential equation for moisture transport 114
6.7.3 Permeability of hardening cement paste for water and gas 116
6.7.4 Permeability of ribbon paste 119
6.8 Ribbon hydration with transport of water and gas 120
6.8.1 General 120
6.8.2 Pressure in capillary water 121
6.8.3 Evolution of the degree of hydration in the ribbon paste 122
6.8.4 Degree of saturation in ribbon paste 122
6.8.5 Relative humidity in the empty pore space 124
6.8.6 Gas pressure in the empty pore space 124
6.8.7 Thickness of the adsorption layer in the pore space 125
6.8.8 Surface tension in the adsorption layer 126
6.8.9 Elastic modulus over the ribbon thickness 127
6.8.10 Autogenous shrinkage over the ribbon thickness 128
6.8.11 Autogenous shrinkage of paste in concrete 129
6.9 Discussion 130

7. APPLICATIONS: AUTOGENOUS SHRINKAGE INDUCED CRACKING .. 131
7.1 General 131
7.2 Case study I: lab-scale structure 132
7.2.1 Temperature-Stress Testing Machine (TSTM) 132
7.2.2 Outline of the experimental set-up 133
7.2.3 Description of experimental results 133
7.2.4 Prediction of autogenous shrinkage of blended cement concrete 135
7.2.5 Discussion 136
7.3 Case study II: full-scale structure 136
7.3.1 Description of the structure 137
7.3.2 Temperature development in the wall 139
7.3.3 Stress development in the wall 139
7.3.4 Probability of cracking 140
7.3.5 Safety against cracking 141
7.3.6 Discussion 141

8. DISCUSSION OF RESULTS AND CONCLUSIONS 143
8.1 Discussion of results.....143
8.2 Conclusions.....145
8.3 Recommendations and outlook.....146

References 149
Appendices
A: Cement characteristics 155
B: Numerical solution of differential equation for moisture transport 157
C: The program TEMPSPAN 159
D: Description of the drying-wetting model 161
Notations and symbols 165
Summary 167
Samenvatting 169
Curriculum vitae 171

1.

Introduction

1.1 General scope of the project

In the design of civil structures, durability is gaining more and more the interest of the construction principals. The way how to realise a durable structure can be categorised roughly into two main disciplines. At first, designers and engineers have to design a building project in such a way, that the desired lifetime of this project is guaranteed. This can be considered as the designers approach. At a conference in Brisbane in Australia [84] , Somerville called this: *Durability by design.*
Secondly, the quality of the building material plays an important role. In order to come to a durable structure with low and maintenance costs, the material of which the structure is made must satisfy certain quality requirements. If the building material is concrete, the demands on quality of the concrete microstructure becomes increasingly important.

In order to be able to meet the increasing higher demands on the material level, new types of concrete were designed. This led to the introduction of special types of concrete that were more durable and also had improved material properties. Generally, these types of concrete are called: high performance concrete's (HPC) or high strength concrete's (HSC). Although the material properties of these types of concrete, generally, show a substantial improvement in comparison with conventional concretes, these types of concrete also have some properties that require due attention. The development of high quality concretes has introduced the substantial volume changes which occur during hardening of the material. Generally, this type of volume change is called: *autogenous shrinkage*. A reduction of the pressure in the emptied pore space (see Fig. 1.1) may cause an external volume reduction. For low water/cement ratio mixes, the volume reduction may exceed the (Fig. 1.2) maximum tensile strain capacity of the concrete (0.1 á 0.2‰). Any restraint of the deformation strain will induce tensile stresses in the hardening concrete. This may cause cracking of the concrete and an associated

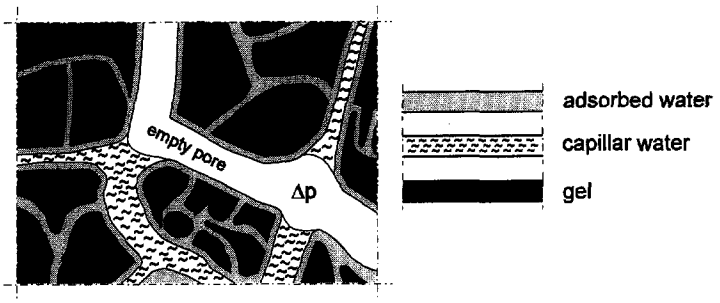

Fig. 1.1. Schematical presentation of the relationship between the volumetric chance of the microstructure and the pressure reduction Δp in the emptied pore space.

reduction of the durability. Therefore, although the structure is designed correctly, a substantial reduction of durability may be introduced by the deformations and stresses that develop during hardening of the concrete. Large macro or micro-cracks may serve as "canals" for e.g. chlorides, to be carried from the concrete's surface via the damaged microstructure to the reinforcement. The quality of the concrete structure may be reduced dramatically by this particular phenomenon. Generally, this reduction of quality of a concrete structure can be considered as self-destruction of the hardening microstructure that is caused by a mechanism that acts from the "inside". Most annoying in this respect is the fact that these volumetric changes, as they develop during the hardening process, can not be influenced from the exterior. The existence of this type of volume change is directly related to the mix-design and the hydration process. The contributions of the individual mix-components determine this mechanism. A change of the contributions of the different mix-ingredients or a variation of the properties of the ingredients will directly affect the volume changes of the hardening material. To which extent the contributions of the individual mix-components influence

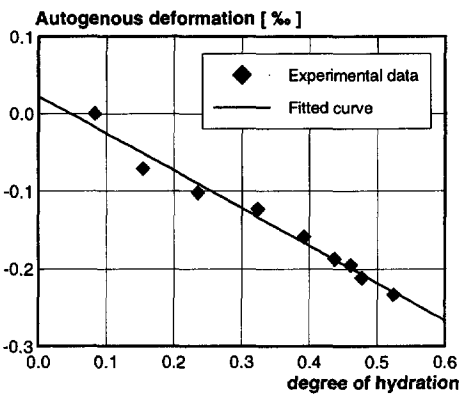

Fig. 1.2. Autogenous shrinkage of an ordinary HSC [47, 48, 49]

this volumetric change of the hardening microstructure is still very unclear. As yet, there is no clear description of the mechanism behind this type of volumetric contraction. i.e. autogenous shrinkage, of the hardening microstructure.

1.2 Practical relevance

The hydration process of an ordinary concrete goes along with an increase of the temperature and also with the development of autogenous shrinkage. Autogenous shrinkage of a concrete may introduce additional stresses in a hardening structure. Together, the stresses induced by temperature and by autogenous shrinkage may exceed the actual tensile strength of an arbitrary concrete during hardening. This may cause cracking and associating damage of the concrete structure.
In order to gain more insight in the order of magnitude of the additional stresses which are introduced by autogenous shrinkage, an example will be given of an ordinary wall which is cast on a rigid slab [50].
A wall with a thickness of 0.16 m and a height of 3.5 m is cast on a rigid slab. A HSC mixture is used with a mix temperature of 20°C. The adopted autogenous shrinkage is shown in Fig. 1.2. The ambient temperature is 18 ± 1°C. On the left hand side of Fig. 1.3, the temperature development is shown for a location which is situated 0.5 m above the slab. A maximum temperature of 33°C is reached after 16 hours of hardening. At that particular time, stripping of the formwork takes place.
The stress development in the hardening wall is calculated with TEMPSPAN [57]. The stresses are calculated with and without the effect of autogenous shrinkage. The wall is considered to be fully restrained by the slab. From the results presented on the right

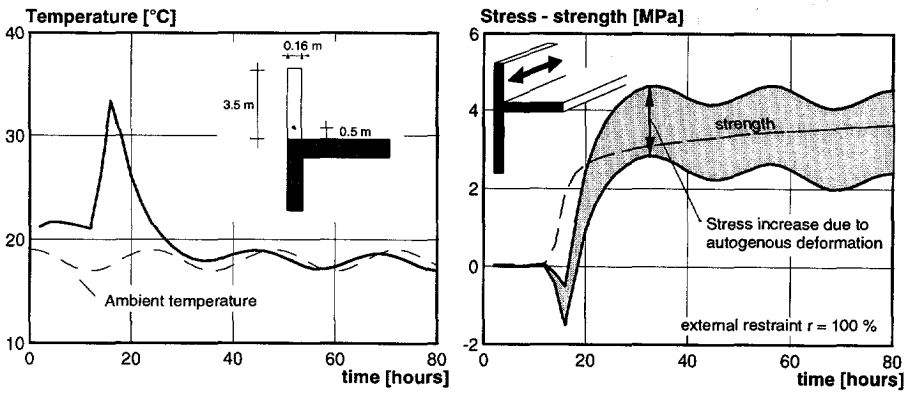

Fig. 1.3. Concrete wall cast on a rigid sub-base. Left: Temperature development versus time. Right: Calculated stress and strength development in the wall with and without autogenous shrinkage.

hand side of Fig. 1.3, it can be seen that the additional stress which is induced by autogenous shrinkage is about 2 MPa. Neglecting the effect of autogenous shrinkage in the stress calculations would give the impression that the stresses will not exceed the actual tensile strength. However, autogenous shrinkage will substantially enhance the stresses. For an accurate prediction of the probability of cracking of a hardening concrete structure the influence of autogenous shrinkage may therefore not be neglected.

1.3 Aim of the project

The main goal of this research project is to describe the main mechanism behind the process that causes the non-thermal hydration induced volume changes of hardening cement-based materials and to develop a numerical model for simulation of these volume changes.

A description of the main mechanism that causes volume changes during the hardening process may certainly contribute to realise durable concrete structures. A clear understanding of the magnitude of the "internal" strains that will develop is of paramount importance. It may decide whether a concrete mixture is suitable to perform satisfactory for a predetermined lifetime.

Together, the thermal strains that may develop during hydration and the micro-structural volume changes determine the quality of a concrete structure if hardened. The restraint of the "internal" strains by either external factors, e.g. stiff construction parts, or by internal influences, e.g. addition of stiff aggregates, may introduce macro- or microcracks, respectively.

The development of numerical tools for the evaluation of the hardening behaviour of concrete structures will contribute to the assessment of the quality of concrete structures. In order to develop a model that is consistent and reliable, it is encouraged to descend from the macro-scale to the micro-scale level. Modelling physical and chemical processes at this particular level may contribute to a clear understanding of the material behaviour that is generally observed at the macro-scale level. The micro-scale level is, therefore, also the level at which the mechanism is modelled to predict the volume changes during hardening.

1.4 Research strategy and set-up of the thesis

In order to reach the aims as outlined in the previous sections, this thesis has been outlined according to the following research strategy. In chapter 2 the research starts with a detailed discussion on the mix proportions of an arbitrary high strength concrete.

The main material properties and the most striking differences with ordinary concrete will be discussed. Other aspects like the definition of the degree of hydration and also a definition for chemical and autogenous shrinkage will also be discussed. The chapter ends with a discussion on the special locations in concrete and on the moisture transport through the hardening microstructure.

In chapter 3, an overview will be presented of the numerical modelling of the microstructure of hardening cement-based materials. The single particle model of Jander and Pommersheim [41, 66] is considered as the starting point of the numerical modelling of cement hydration. Three different numerical models, among which the HYMOSTRUC[1)] model, will be discussed and outlined. This overview forms the basis and the motivation for an extension of the current HYMOSTRUC model to a model where the description of the microstructure is based on a random distribution of cement grains in water. The formation of structure as well as the development of the pore structure will be discussed in detail.

Knowledge on the development of the pore structure is of paramount importance for an accurate prediction of the volumetric changes which develop during hardening. In chapter 4, a model is presented with which thermodynamic equilibrium in the continuously changing pore structure can be established. The model is based on the balance between the pressure in the empty pore volume and the surface tension in the adsorbed layer at the pore wall area of the microstructure. From the surface tension, the microstructural deformation of the hardening cement-based material can be determined using the constitutive equation as originally proposed by Bangham [7]. A parameter study is performed to show the sensitivity of the model results and to verify the results obtained.

In chapter 5, the experimental program is discussed that has been used to validate the predictive potential of a model regarding the simulation of microstructural deformations of plain cement paste during hardening. The experimental program concerns cement pastes with different water/cement ratios and application of three different finenesses of cement. The influence of the addition of a microfiller, such as silica fume, is also dealt with. Emphasis is on the increase of the volumetric contraction due to the addition of silica fume.
The volumetric deformation of concrete is considered to be driven by the volumetric deformation of the hardening paste. The stiff aggregate particles prevent the hardening cement paste to deform. Two different approaches will be discussed to model this

---

[1)] HYMOSTRUC: A numerical simulation program with the potential to simulate and predict, among other things, adiabatic hydration curves as a function of the particle size distribution and chemical composition of the cement, the water/cement ratio and the temperature [17].

effect. Firstly, a parallel-series model will be proposed with which the effect of the stiff aggregate particles on the volumetric changes of the hardening cement paste can be simulated. Secondly, a more advanced approach will be discussed. A lattice model will be used to simulated volumetric changes of a concrete sample. The model turned out to be able to predict the deformational behaviour of a concrete sample and to identify the areas which are prone to microcracking. With this model, the relationship between processes that act on a micro-scale level and the response of the material on a macro-scale level was simulated.

To look more closely at the hydration process between two aggregate particles a ribbon paste[2)] model is proposed in chapter 6. The matrix ribbon is considered to be a representative part of the cement paste. This part of the matrix comprises the interfacial transition zone and the bulk paste region. These regions have different material properties due to the different packing of the cement particles. With the proposed ribbon model, the development of the material properties can be determined as a function of the hydration process. The autogenous shrinkage, the gas pressure in the empty pore space and the hydration process are considered to drive the transport of capillary water and gas through the hardening ribbon paste. The influence of the "water-rich" interfacial zone on the hydration of the bulk paste is also considered.

The importance of the microstructural volume changes, e.g. autogenous shrinkage, on the stress development of micro and macro level structures will be discussed in detail in chapter 7. Two different test cases are discussed with the aim to give a clear overview of the effect of the hydration induced volume change on the stress development of a hardening structure. The influence of the degree of external restraint on the stress development is also taken into account.
The thesis ends with a discussion on the results obtained, conclusions and recommendations on the further development of numerical modelling of microstructural volume changes in hardening cement-based materials.

[2)] Ribbon paste: cement paste that is bordered by two aggregate particles.

2.

Features of low water/cement ratio concretes

2.1 General

In this chapter, the most characteristic properties of low water/cement ratio concretes, like High Strength Concrete (HSC), will be outlined and discussed. HSC is considered to be a concrete with addition of a microfiller, e.g. silica fume, and having a mean compressive strength above 60 MPa after 28 days of hardening. In comparison with ordinary concrete, HSC has a different mix composition. As a result of this, the development of the microstructure of HSC will be different from an ordinary concrete. This means that also the development of the material properties differ. Another important aspect in this respect is also the rate at which the hydration process proceeds. The rate of hydration of HSC mixtures is generally much higher than for ordinary concrete mixtures. During hydration, HSC mixtures also show a very pronounced volume change.

Due to these characteristic properties, the material behaviour of hardening HSC will be discussed, seen from the microstructural point of view. Therefore, this chapter is outlined as follows: to become familiar with the different ingredients of an HSC mixture, an extended discussion will be held on the individual constituents and their purpose in the mix. Next, the hardening process is discussed in terms of the degree of hydration. This discussion is followed by an outline on the rate at which the hardening process of HSC mixtures proceeds. The volumetric changes which develop during the hardening process are considered next. In this section, the emphasis is on the definition of the chemical shrinkage and the autogenous shrinkage. After this, a discussion will be held on the moisture transport in the hardening microstructure. The transport of capillary water as well as the main driving forces behind the moisture flow will be discussed. The final topic in this chapter is on the different regions inside a concrete. The differences between the interfacial transition zone, the bulk paste and plain paste are discussed in detail. The chapter ends with a brief discussion on the most important features of low water/cement ratio concretes. This, in view of numerical modelling of the microstructure.

2.2 Mix composition

2.2.1 Water/binder ratio

Generally, HSC mixtures have a relatively low water/binder ratio. Indicative values taken form the literature show a range between 0.25 and 0.35 [1]. Most often, a value of about 0.3 is adopted. Application of such a low water/binder ratio requires additional care regarding the workability of the concrete mix. The use of a plasticizer is inevitable in order to obtain a stable and homogenous mix.

In low water/cement ratio cement pastes, cement particles are situated very close to each other. Only little hydration is necessary to bridge the distance between the hydrating cement particles. After a certain period of hardening, the hydrating cement particles start to form a load bearing structure. The strength of this structure increases when the hydration process proceeds. Due to the low water/cement ratio, there will not be enough water for the hydration of all cement particles. A certain volume of anhydrous cement will remain in the paste after the hydration process has ceased. This volume of anhydrous cement will also contribute to the strength and stiffness of the developing microstructre.

2.2.2 Cement fineness

Cement particles exhibit a certain distribution. The number of particles per fraction depends on the fineness of the cement and on its distribution. A rough way to quantify the fineness of a certain cement can be obtained by application of the specific surface (m^2/kg). This has been proposed by Blaine (see [16]). It is also possible to relate the particle size distribution of a cement to its fineness [16]. Cement of high fineness contains a large number of fine particles. This goes along with a large specific surface and also with a highly reactive potentiality of the cement. A way to describe the particle size distribution of cement mathematically is proposed by Rosin-Rammler. This description can be formulated as follows:

$$G(x) = 1 - e^{-b_{RR} x^{n_{RR}}} \qquad (2.1)$$

in which the G(x) is the cumulative weight of the cement particles of diameter x. With the constants n_{RR} and b_{RR}, the distribution of the particles can be defined (see Fig. 2.1).

2.2.3 Cement content and type of cement

In comparison with conventional concrete, high strength concrete contains a relatively large amount of cement. For conventional concrete, the amount of cement ranges roughly between 300 and 400 kg/m^3, whereas the cement content for high strength concrete ranges between 400 and 500 kg/m^3 [19]. The most common used type of cement for HSC is Portland cement with a high specific surface (Blaine≈550m^2/kg). However, in The Netherlands, a blended cement mix is frequently used. Mostly, this type of cement consists of a combination of Portland cement and Blast furnace slag cement [48]. The application of a blended cement in a concrete mixture has a favourable

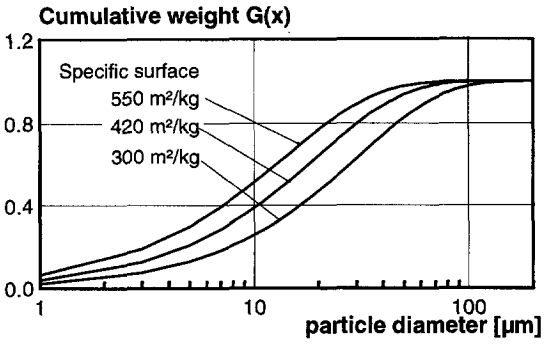

Cement fineness

Fine:	n_{RR}=1.030,
550 m^2/kg,	b_{RR}=0.067
Medium:	
420 m^2/kg,	n_{RR}=1.076,
	b_{RR}=0.041
Coarse:	
300 m^2/kg,	n_{RR}=1.107,
	b_{RR}=0.023

Fig. 2.1. Particle size distribution for cements with different fineness.

effect on some material properties. The addition of the low reactive Blast furnace slag cement may for instance contribute to a more moderate liberation of the heat of hydration. This may reduce the temperature rise of the mix [56].
To compensate for the volumetric contraction of the concrete during hardening [87], it is also possible to use some type of cement which exhibit some swelling.

2.2.4 Aggregates

Another characteristic feature of high strength concrete is the maximum aggregate size, the shape and the distribution of the aggregate particles. A maximum aggregate diameter of 16 mm is most commonly used for HSC mixtures. In the Netherlands, these aggregates are generally manufactured by crushing river stones.
Aggregates are generally subdivided into two ranges with respect to their diameter. Aggregate particles that have a diameter in a range between 4 and 16 mm and particles that have a diameter between 0 and 4 mm. This is generally adopted as the border between coarse and fine aggregates. The finer part of the aggregates is considered to be the sand.
The addition of relatively fine aggregate particles to a HSC mixture has the purpose of controlling the packing continuity of the aggregate structure. It will also have a positive influence on the stability of the concrete mix. A better distribution of the stresses through the aggregate structure is also an additional advantage.

2.2.5 Microfillers

The most characteristic feature of high strength concrete is the addition of a latent reactive material. This can be: *-Silica fume*
-Fly ash
-Trass

The most commonly used latent reactive material is silica fume. It consists of almost pure silicon dioxide. Silica fume can be used as a dry powder material or as a slurry (water + silica powder). Silica particles are very fine. The average particle diameter is

approximately 0.1 μm and the specific area is generally 100 times larger in comparison with cement [63, 86]. This relatively high specific area (ultra fine particle diameters) gives the silica fume a high reactive potentiality. Experiments have shown partly reacted particles at one day and coagulation and gel formation after seven days of hydration [74]. This implies that silica fume must be considered as an highly pozzolanic active material. Silica fume will therefore consume a substantial amount of water. A secondary reaction will appear, in combination with the calcium hydroxide, resulting in stable Calcium Silicate Hydrates [10, 63]. This may lead to a very dense and strong microstructure and a very strong matrix-aggregate interface. It may also contribute to a reduction of the actual pore volume.
The addition of fly-ash or trass will result in lower performance. This is mainly caused by the relatively lower amount of silicon dioxide (SiO_2) and the relatively larger particle size. Due to these properties, these latent reactive materials will result in lower strength development caused by a more moderate rate of reaction (1/7 of Portland cement).

2.2.6 Admixtures

Additives are indispensable for the homogeneity of high strength concrete mixture. The mix-stability and slump will be controlled and the material properties may be improved. In general these admixtures can be divided in three categories. These are the plasticizers, superplasticizers and the retarders. The first two admixtures control the workability of the mix, while the latter admixture controls the length of the dormant period. If no retarder would be added to the mixture, the hydration process would start very soon after the addition of the mixing water.

2.3 Degree of hydration

2.3.1 General

For ordinary Portland cement-based mixtures, the determination of the degree of hydration is generally described in terms of the amount of liberated heat or the amount of non-evaporable water (chemically bound water). It must be born in mind that even for a plain Portland cement this is an approximation. The fact that the individual clinker compounds hydrate at different rates while liberating different amounts of heat and binding different amounts of water makes that the degree of hydration of a poly-mineral system should in fact be considered as a "weighted" value. In case non-Portland cements are used the approximative character of these parameters must be emphasised even more strongly [3, 29]. The same holds for high strength concrete mixes which contain a certain amount of latent reactive silica fume. The rate of reaction of the silica fume differs from that of the individual clinker components and of the cement as a whole [34, 63, 74].

2.3.2 Definition

Based on the motivation as outlined in the previous section, we are nevertheless inclined to define the degree of hydration $\alpha(t)$ as the ratio between the amount of cement that has reacted, i.e. that has been dissolved, at time t, relative to the original amount of cement [16]. Or formulated:

$$\alpha(t) = \frac{\text{amount of cement that has reacted at time t}}{\text{total amount of cement at time t = 0}} \qquad (2.2)$$

2.3.3 Degree of hydration measurements on HSC

Being aware of the approximative character of the heat of hydration and the non-evaporable water as indicators of the actual state of the hydration process of a mix containing silica fume, these parameters have nevertheless been applied here in an attempt to characterise the actual state of the hydration process. In Fig. 2.2 the degree of hydration based on non-evaporable water measurements [95] is compared with the degree of hydration based on heat of hydration measurements. It appears that, although some deviations between the results obtained according to the two methods are obvious, the correlation between the two quantities is fairly good. It should also be born in mind that in the case of a plain Portland cement, some deviation between the two methods have to be considered. The data-points of the non-evaporable water measurements (Fig. 2.2) are average values of three specimens which were also used for compressive strength tests at the indicated curing temperatures (20, 40 and 60 °C). The maximum degree of hydration for this high strength concrete mixture appeared to be approximately 0.6. The water- cement ratio for this mixture is 0.3. Theoretically, this degree of hydration could reach a

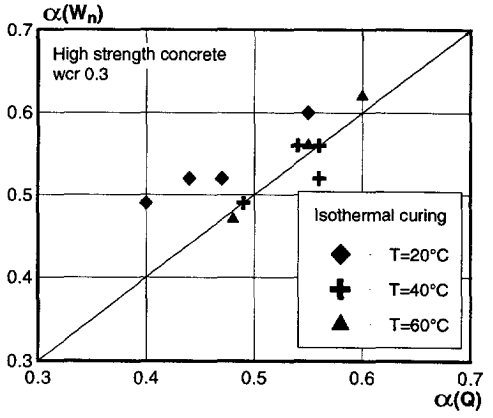

Fig. 2.2. Degree of hydration based on non-evaporable water measurements (W_n) versus the degree of hydration based on heat of hydration measurement (Q). Tests carried out at isothermal curing temperatures (T=20, 40 and 60 °C).

maximum value of 0.75. However, there will be a certain amount of water in the pore system which is not available for cement hydration. Depending on the ultra fine pore structure of high strength concrete, this amount may be quite substantial [10]. The data-points shown in Fig. 2.2 are determined at 1,2,3,7 and 28 days. The degree of hydration appeared to range only from approximately 0.4 to 0.6. This is a result of the fact that the major part of the cement hydration of high strength concrete takes place in the early phase of the hardening process. The agreement between both methods is quite satisfactory and justify the determination of the degree of hydration on the basis of heat of hydration measurements. This method is very suitable for computer modelling purposes.

2.4 Rate of hydration

In comparison with ordinary concrete, the hydration process of a HSC proceeds very fast. This is mainly the result of the relatively larger specific surface of the cement which is commonly used in HSC mixtures, viz. Blaine 550m^2/kg. A coarser type of cement has a lower reactive potential and hydration will proceed slower. From Fig. 2.3, it can be seen that this influence can be quite substantial. The finest cement with a specific surface of 550m^2/kg reaches a degree of hydration of ca. 0.5 after about 50 hours of hardening while the coarser cement with a specific surface of 300 m^2/kg needs about 1000 hours of hydration to reach this value. It is noticed that the rate of the hydration process depends also on the water/cement ratio. For low water/cement ratio concretes like HSC, the rate of the hydration process may cease due to a lack of water.
The differences in the rate of hydration will strongly influence the rate at which the material properties develop.

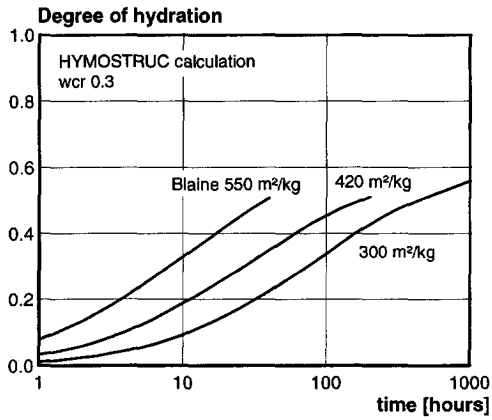

Fig. 2.3. Degree of hydration versus time for three different finenesses of cement.

2.5 Volume changes during hardening

2.5.1 General

The hardening process of concrete goes along with a reduction of the original mix volume. The development of a microstructure introduces internal forces that deform the hardening material. Under sealed conditions, these "hardening deformations" can be attributed to three main factors. Firstly, the *chemical shrinkage*, secondly the *autogenous swelling* and thirdly the *autogenous shrinkage*. Different mechanisms conceal these three volume changes. In the next section, definitions will be given on the chemical shrinkage and the autogenous shrinkage. In these definitions, the volumetric changes due to chemical shrinkage is the result of the chemical reaction between the water and the cement. The autogenous shrinkage is the volume reduction due to the self-desiccation of the microstructure during hardening. The effect of autogenous swelling is disregarded in these definitions.

2.5.2 Definitions

In [78], Sellevold shows a relationship between the external and total chemical shrinkage for a cement paste with a water/cement ratio of 0.4 (see Fig. 2.4). Two hardening conditions were considered. Firstly, the total chemical shrinkage was measured of a continuously rotating specimen were no load bearing microstructure could be formed. Secondly, the external chemical shrinkage was measured for a specimen which was not rotated during hardening. The difference between these two types of shrinkage can be attributed to the formation of a load bearing microstructure. At a certain stage of the hardening process, this microstructure will resist the cement paste to shrink further than it would like to in case of free chemical shrinkage. Evidently, the shrinkage volume which is resisted will manifest itself into empty pore space. This additional pore volume will also contribute to the total pore volume that develops during hardening of a cement paste microstructure.

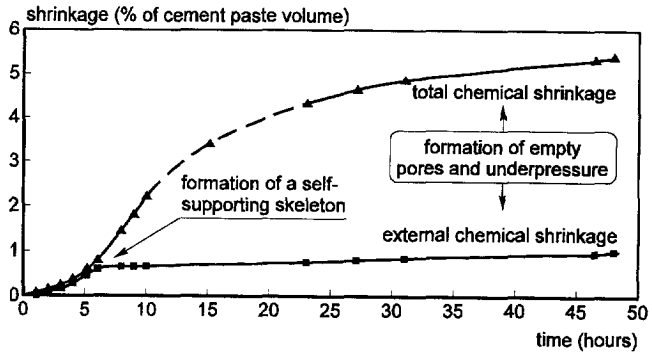

Fig. 2.4. Total and external chemical shrinkage for cement paste with a water/cement ratio of 0.4 (Definitions according to Sellevold [78]).

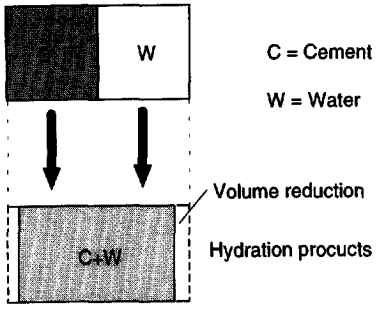

Fig. 2.5. Schematic representation of chemical shrinkage mechanism

Chemical shrinkage:
is a volume reduction that finds its origin in the fact that the resulting volume of the reaction product that is formed by the water/cement reaction is smaller than the volume of the original constituents (see Fig. 2.5). The net result is an increase of the pore volume in the hardening paste with hardly any external volume change.

The pore volume which is generated by the development of chemical shrinkage will be filled with gas (air). The chemical shrinkage induced pore volume will increase with progress of the hydration process. According to Boyle's law, an increase of the pore volume associates with a decrease of the gas pressure. The gas pressure in the pore volume equilibrates with the surface tension in the adsorption layer. This surface tension will act on the hardening cement paste from the interior, and may associate with the development of additional external deformations. In this thesis, this mechanism is called autogenous shrinkage (self-desiccation) .

Autogenous shrinkage (in this thesis):
is a volume reduction of a hardening element that finds its origin in the fact that the self-desiccation of hardening cement-based material is accompanied by an increase of the surface tension in the adsorption layer (see Fig. 2.6).

From the definitions, it becomes clear that the volume reduction induced by chemical shrinkage interfere with the volume reduction that is defined as autogenous shrinkage. In fact, the additional pore volume caused by chemical shrinkage is plays a role in the calculation of the autogenous shrinkage during hardening. The calculation of the autogenous shrinkage of a hardening cementitious material is, therefore, also affected by the chemical shrinkage.

The definitions on chemical shrinkage and autogenous shrinkage are indispensable in view of modelling the volumetric changes in hardening cement-based materials. Therefore, the given definitions are adopted throughout this thesis.

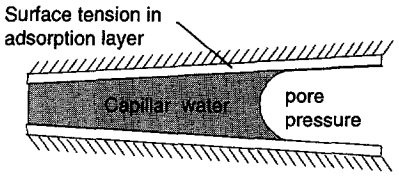

Fig. 2.6. Schematic representation of the mechanism behind autogenous shrinkage.

2.6 Special locations in concrete

Concrete can be subdivided into zones which have different properties. In order to get a clear understanding of these zones and to become familiar with their particular properties, an overview will be given in this section. Therefore, emphasis will be on the differences between the interfacial transition zone, the bulk paste. The difference with plain paste will also be discussed.

2.6.1 Interfacial transition zone and bulk paste

Generally, concrete can be subdivided into three main parts that contain different (characteristic) material properties. These are: the Aggregate, the Interfacial transition zone (ITZ) and the Bulk paste. Although there exists no clear border between the ITZ and the bulk paste, this distinction makes it possible to define concrete as a three phase system. The interfacial transition zone (ITZ) is defined as the region between the aggregate surface and the bulk paste (see Fig. 2.7). Some authors have proposed a more detailed distinction of the regions within the ITZ. For instance in [55], the interfacial zone is subdivided in:

a. *Contact layer*, a dense layer of 2-3 μm thickness , located directly at the aggregate surface and composed essentially of $Ca(OH)_2$ crystals.
b. *Intermediate layer*, located adjacent to the contact layer with a thickness of about 5-10 μm. This layer consists for the most part of needle shaped ettringite crystals.
c. *Transition zone*, located adjacent to he intermediate layer with a thickness of about 10 μm. This layer is characterised by a dense paste merged into the bulk paste

From this detailed distinction, it can be derived that the average thickness of the ITZ ranges between the 15 and 25 μm. The exact thickness depends on the water/cement ratio and the fineness of the cement. The thickness of the ITZ is expected to be larger for a coarse type of cement and will decrease if the cement becomes finer. This is not very

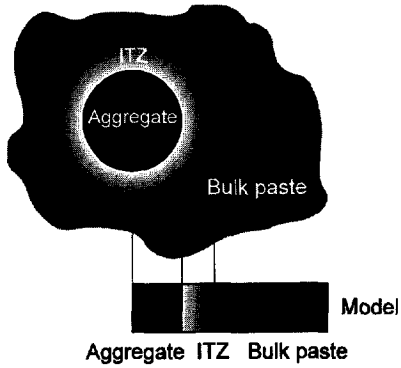

Fig. 2.7. Schematic representation of three different parts distinguished in concrete.

remarkable since the finer cement grains are able to form a closer packing close to the aggregate surface. Variations of the particle to particle distance close to the aggregate surface also has its impact on the paste density and porosity in that particular area. From Fig. 2.8 it can be seen that the paste density reduces almost to zero when approaching the aggregate surface. In the bulk paste, the paste density remains almost constant. The water/cement ratio shows a similar tendency. Since the development of the material properties depends strongly on the water/cement ratio, a change of the water/cement ratio close to the aggregate surface will result in a region where the material properties are different from the material properties in the bulk paste. It is generally accepted that the ITZ is very important in view of the ultimate strength of a concrete mixture.

2.6.2 Plain paste

Plain paste is cement paste which is not affected by moisture transport due to pressure differences in the capillary water (see 2.7.2). The capillary water is considered to be

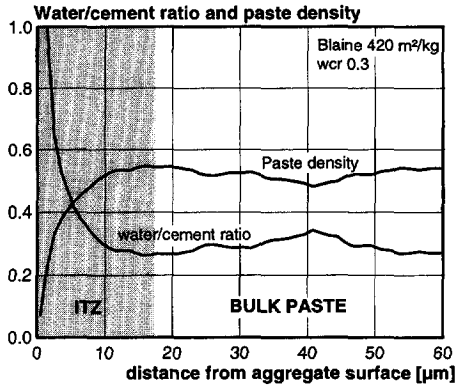

Fig. 2.8. Representation of the development of the water/cement ratio and the paste density as a function of the distance from the aggregate surface (see chapter 6).

homogeneously distributed throughout the paste and can only be consumed by cement hydration. Plain paste can be considered as a reference paste. Hardening proceeds under ideal conditions and stereological packing discontinuities that exist in concrete (ITZ) will not effect the hydration process. Generally, these ideal conditions do not occur in an arbitrary concrete mixture.

The discontinuity in the packing of the cement particles in the close vicinity of the aggregate surface is accompanied by differences in the water/cement ratio and also in the rate of the hydration process. This will, on its turn, introduce pressure differences in the capillary water and cause moisture flow. This means that plain paste is different from bulk paste

2.7 Moisture transport during hardening

2.7.1 Microstructural phase changes

The formation of the microstructure of a cement-based material is a process of continuously changing phases. For a plain cement paste, the continuously changing phases are the anhydrous cement, hydration products (gel), capillary water and gas (air voids and pore gas). The rate of this process is driven by the degree of hydration. Generally, a phase change is associated with a decrease of the volume of unhydrated cement, an increase of the volume of hydration products, a reduction of the capillary water volume and an increase of the gas volume. The volume of the newly formed hydration products is larger than the volume of the unhydrated cement. On the other hand, the volume of the original phases, water and unhydrated cement, is larger than the volume of the newly formed hydration products. This leads to an increase of the pore volume.

An increase of the pore volume accompanies with a decrease of the gas pressure in that particular volume. Additional gas may become dissolved from the capillary water. Parallel with this process, capillary pore water is consumed by the chemical water/cement reaction and is, therefore, taken out of the system. The volume which was originally occupied by this water will now be filled with gas. Since it concerns a closed system, the pressure in this newly formed space will decrease. This complex system of consumption of capillary water and formation of pore space can be subdivided into two parts. These are the chemical shrinkage and the volume originally occupied by the capillary water. Together, this can be formulated as:

Gas volume = Chemical shrinkage volume + Consumption of volume capillary water

Emphasis must be on the fact that initially the (cement-based) system consists of a volume of cement and a volume of water (that includes dissolved gas). The emptied pore

space becomes filled with gas due to the phase changes as described before. The volume of water in the pore space can be defined by the degree of saturation. This degree of saturation is defined as the ratio between the total volume of capillary water in the cement-based system and the total pore volume (both empty and filled pore space) [93]. The degree of saturation can never be equal to 100%[1)]. There is always a certain volume of gas dissolved in the capillary pore water, depending on the pressure. In Dorcey (1940), [25] values are given for the dissolubility of gas in water for different isothermal temperatures. At 20 °C, a value of 1.87% is given. Therefore, before the hydration process has started, the degree of saturation will be equal to about 98%. This value may be affected by the transport of capillary water through the microstructure.

2.7.2 Transport of capillary water

As hydration proceeds, the volume of capillary water, e.g. the degree of saturation, may become affected by three different factors. Firstly, capillary water will be consumed by the chemical reaction process between water and cement. Secondly, capillary water may also be transported through the pore system due to pressure differences within the paste. Finally, the volume of capillary water may also become effected by different microstructural volume changes.

Pressure differences in the capillary water occur due to a statistical variation of the development of the material property in a hardening microstructure. For instance, the microstructure in the ITZ develops differently from the microstructure in the bulk paste. Differences in the local water/cement ratio and in the packing of the cement particles cause a different rate of hydration. Depending on the local permeability of the microstructure, quite substantial pressure differences can develop. These processes take place on a micro-scale level. This means that there exists a mechanism that drives capillary water through the paste. Capillary water may become discharged from the "water-rich" interfacial zone into the bulk paste or the other way around. This process will have an effect on the rate of hydration and also on the volumetric changes of the hardening microstructure.

A transport of capillary water may intensify the self-desiccation effect in the hardening microstructure. Due to the discharge of capillary water, additional deformations are introduced at certain locations in the concrete. It may cause microcracking in the interfacial region, in the close vicinity of the aggregate surface. The contraction of the hardening cement paste close to the aggregate surface will experience a substantial restraint by the much stiffer aggregate particles. On the one hand, this may lead to micro-cracks, but, on the other, it will also influence the volume changes of the hardening concrete.

[1)] This effect is disregarded in the model as proposed in this thesis.

2.8 Discussion

Low water/cement ratio concretes behave differently from ordinary concretes. These differences are mainly the result of different mix proportions which are used in HSC. Of special interest is the very high fineness of the cement (Blaine 550m^2/kg) and the relatively low water/cement ratio. Due to high specific surface of the cement, hydration proceeds very fast. The low water/cement ratio is mainly responsible for a very dense microstructure. Generally, the microstructure of low water/cement ratio concretes (HSC) develops relatively fast.

Due to the addition of a microfiller in HSC mixtures, like silica fume, a very fine pore system will develop. This may intensify the self-desiccation of the hardening microstructure and may cause a very pronounced volume reduction.
A purpose of aggregates in a concrete is to get a stiffer and stronger material. Due to the aggregate addition, the stereological packing of the cement particles change. Close to the aggregate surface (ITZ), the packing differs from the packing in the bulk paste. A highly porous material will be formed at the ITZ, while in the bulk paste a dense material will develop. The water/cement ratio at the ITZ will be substantially higher than in the bulk paste.

Both the microstructure that is formed at the ITZ and the microstructure that is formed in the bulk paste differ from the microstructure of a plain paste. This means that the microstructure of concrete is different from the microstructure of plain cement paste. Two different materials must be considered. Therefore, in the following chapters, an outline will be given on what these differences are and how they can be quantified by using numerical models. It will be investigated how the microstructure can be modelled numerically, and how the model can be used for the analysis of the pore structure.
In order to get more insight in the mechanisms which play a role in the hardening process of concrete and plain paste, a thermodynamic analysis of the moisture evaluation of the pore structure will be proposed and discussed. Based on this thermodynamic analysis and with help of the hydration model HYMOSTRUC, the differences in the hydration of a concrete ribbon and a plain paste are quantified and the results will be compared. To reach this goal, the topics as outlined in this chapter must be considered as information which is necessary for a better understanding of the processes which play an important role at the hardening process of low water/cement ratio concretes.

Note: In this thesis, for all calculations which are carried out with the HYMOSTRUC model, isothermal boundary conditions are considered at 20°C.

3.

Modelling hydration and microstructure

3.1 General

The introduction of the 'single particle' models by, among others, Jander [66] and Pommersheim et. al. [41] can be considered as a "take-off" for the development of several types of numerical models to simulate hardening process of cement-based materials. The 'single particle' model as proposed by Jander describes the hydration of one single cement particle. Hydration products will be formed at the surface of the hydrating cement particle.

In the category of 'single particle' models, the model as proposed by Pommersheim appears to be most advanced (Fig. 3.1). The model is derived for the hydration of the tri-calcium silicate (C_3S) clinker. In this model, distinction is made between the different types of hydration products. The so called 'outer product' is assumed to grow from the original cement surface of the cement grain in outward direction. The 'inner product' is considered to grow from the original cement grain surface towards the centre of the particle. The layer that separates the inner and outer product layer is called the middle layer. The middle layer is assumed to dissolve gradually during hydration. The inner and outer product have different densities and, from this, also different diffusion properties. With numerical techniques, the rate of the hydration process can be determined. This also includes the effect of the particle size distribution. However, the main disadvantage of the 'single particle' model was the absence of a formulation which accounts for the contacts between hydrating cement grains explicitly. Without this, the formation of structure can not be modelled. Therefore, the development of strength and stiffness and material properties can not be predicted in a reliable way. From this point on, it was Jennings [43] who proposed a model to quantify the interparticle contacts between hydrating cement grains. Later on, more models have been developed that include the formation of a microstructure.

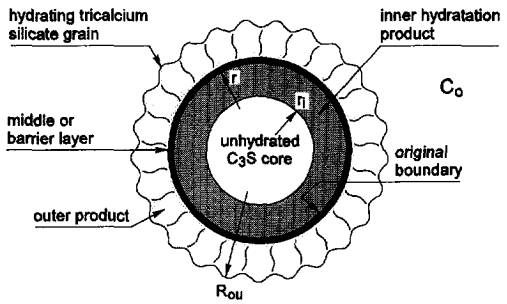

Fig. 3.1. Model for hydration of tri-calcium silicate according to Pommersheim [66].

At this stage of the research, several numerical models have been developed which can be categorised, roughly, into two different numerical simulation techniques. These are the *digital image approach* and the *particle approach*. In order to become more familiar with these different approaches on cement hydration, some of these types of numerical models will be discussed briefly in the next sections. After this, an overview will be given of the extension of the HYMOSTRUC model. Hereby, emphasis is on the formation of the microstructure and on the pore size distribution.

3.2 Existing numerical models

3.2.1 NIST-model

At the National Institute of Standardisation (NIST) in Washington USA, a digital image model has been developed that is currently assumed to be the most advanced model on the hydration of cement-based materials. The model is developed by Bentz and Garboczi [11, 12]. A digital image of a cement paste sample is subdivided into elements which are represented by pixels (see Fig. 3.2). Each pixel stores information on the current position in the system and on the current chemical composition. A pixel has a volume of 1 μm^3. Pixels that are situated at the border of a cement grain are considered to come into solution and are able to react chemically with other hydration products in the aqueous system. The reaction products that are formed will precipitate on a cement grain surface. This process is driven randomly. With this model, the relevance of parameters involved in the cement hydration process can be investigated very accurately. It gives also a good impression on the development of the pore structure of the developing microstructure. A disadvantage of the model is the enormous consumption of CPU-time that is required for a single calculation. Due to the large number of pixels that are imposed by the required fineness of the grid, a lot of memory storage capacity is necessary. However, the model turned out be an advanced tool for fundamental research on hydration processes of cement-based materials.

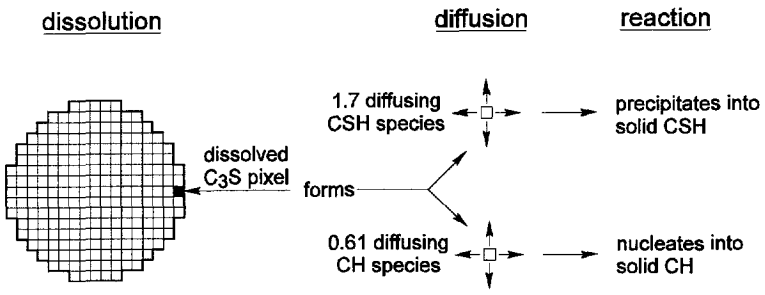

Fig. 3.2. Schematical representation of the Pixel-model of NIST

3.2.2 Jennings and Johnson model

A model that is based on the particle approach was developed by Jennings and Johnson [43] in 1986. The model simulates the development of the microstructure during the hydration of tri-calcium silicate (C3S). A random distribution of the cement particles forms the initial state of the model. The hydrating cement particles are represented as expanding spheres. At the contact zone where two hydrating cement grains meet, the overlapping volume of hydration products is smeared out around the outer shells of the two touching cement particles. The formation of these types of interparticle contacts represent the development of the microstructure.

The model has the potential to predict the development of the microstructure and the bulk properties for a wide range of hardening conditions.

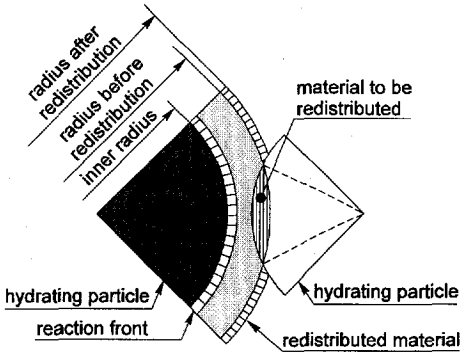

Fig. 3.3. Schematical representation of the formation of contacts between hydrating cement grains according to Jennings and Johnson [43].

3.2.3 Basic HYMOSTRUC model

3.2.3.1 Basic features of the simulation model

In the computer-based simulation model HYMOSTRUC hydration curves are calculated as a function of the particle size distribution and the chemical composition of the cement, the water/cement ratio and the reaction temperature. Unlike most previously proposed models the effect of physical interactions between hydrating cement particles on the rate of hydration of individual cement particles is modelled explicitly.

3.2.3.2 Stereological aspects

In HYMOSTRUC [16], cement particles are considered to be distributed in the paste. An arbitrary particle is considered to be located in the centre of a so called "cell" (Fig. 3.4). A cell is defined as a cubic space with a rib size S_x in which the central particle has a diameter of x μm. The rib size S_x further depends on the water/cement ratio of the paste and the particle size distribution of the cement. The amount of cement found in a fictitious cell with a certain thickness, surrounding a central particle x, will also depend on the water/cement ratio and the particle size distribution of the cement. This amount of cement plays an important role in the formation of interparticle contacts during hydration.

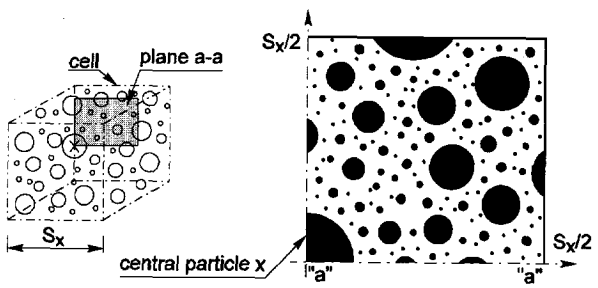

Fig. 3.4. Cell concept - schematic [17].

3.2.3.3 Particle expansion and particle interaction mechanism

The volume of the reaction products is about twice the volume of the reacting cement. When the larger portion of the reaction products are formed in the close vicinity of the anhydrous cement grains, the latter can be considered as gradually 'expanding' particles. Because of this 'expansion', interparticle contacts are made and a microstructure is formed. In order to obtain a workable algorithm for the determination of the interaction between hydrating cement particles the following assumptions were made:

- Particles of the same size hydrate at the same rate.
- The ratio between the volumes of the reaction products and the reactant decreases with increasing temperatures, i.e. $v = v(T)$ (see later eq. 6.22)
- Reaction products precipitate in the close vicinity of hydrating cement particles.

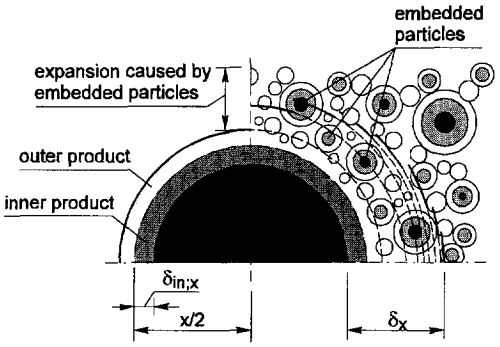

Fig. 3.5. Interaction mechanism for expanding particles. Left part: free expansion, formation of inner and outer product. Right part: embedding of particles, several iteration steps (Modified, after [16]).

The expansion and interaction mechanisms are schematically shown in Fig. 3.5. On contact with water an arbitrary cement particle x starts to dissolve under formation of reaction products. These product are formed partly inside and partly outside the original surface of the particle. In this way cement particles exhibit an outward expansion, thereby making contact with neighbouring particles. At a certain time, the degree of hydration of this central particle x is α_x and the depth of penetration of the reaction front is δ_{in}. Further hydration of this particle goes along with further expansion and embedding of neighbouring particles. The embedding of other particles causes an extra expansion and, as a consequence of this, the embedding of even more particles. An algorithm has been developed for this expansion mechanism of continuous expansion and embedding of particles, with which the stereological aspect of microstructural development can be simulated.

3.2.3.4 Classification of pores

The pore volume of cement paste is generally defined as the initial paste volume minus the volume of the solid material. The ratio between the pore volume and the initial paste volume is defined as the porosity. For cement paste, it is generally assumed that these pores form a continuous pore size distribution [16]. For neat cement paste, the pore system consist of pores with diameters that range between 10 Å to 10^7 Å [104]. The pore diameters involved in the pore size distribution of a cement-based material can be subdivided into different categories that characterise a certain type of porosity. These are: the *gel pores*, *the capillary pores* and the *air voids*. Several authors have proposed upper and lower boundaries for these three types of pores. However, no general agreement exists on the border limits that should be applied. As an example, in Table 3.1, limits as proposed by Young [104] are given.

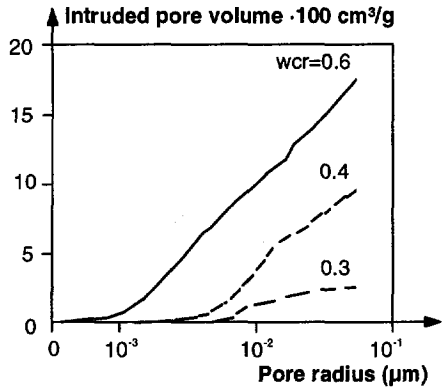

Fig. 3.6. Cumulative pore size distribution: Effect of water/cement ratio [71].

For the proposed classification of pores, only the pores within the range of the capillary pores are considered to be able to transport water or gas through the hardening microstructure. The diameter of the capillary pores range from 0.002 μm ≤ ϕ ≤ 10 μm, where ϕ is the pore diameter.

The porosity and the pore size distribution are effected by several factors. These are, the degree of hydration, the water/cement ratio, the temperature, the cement composition and the particle size distribution of the cement.

3.2.3.5 Modelling the pore size distribution

During the hydration process, the cement paste changes gradually from an aqueous liquid into a hardened porous material. During hardening, the pore size distribution changes as well. The pore size distribution of a cementitious material can either be measured by, for example, mercury intrusion, or can be obtained by numerical simulations. In Fig. 3.6, a typical pore size distribution is presented for three cement pastes with different water/cement ratios. It can be seen that the capillary pore volume is larger for a higher water/cement ratio.

Table 3.1. Classification of pores in cement paste (after [104]).

Classification of pores in cement paste			
Type	Diameter [μm]	Description	Role of water (adopted in model)
Air voids	>10	Entrained air	No transport of water or gas.
Capillary pores	10 - 0.002	Meso-macro pores	Able to transport water or gas.
Gel pores	< 0.002	Micro pores	No transport of water or gas.

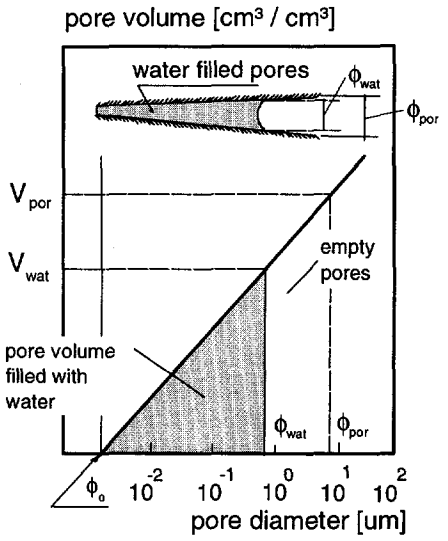

Fig. 3.7. Schematical representation of the pore size distribution with emphasis on the state of the pore water in the actual pore volume (Source after [16]).

The cumulative pore size distribution for the capillary pore water can be described mathematically with the expression (see Fig. 3.7) [16]:

$$V_{por} = a \ln\left(\frac{\phi}{\phi_0}\right) \tag{3.1}$$

where V_{por} is the pore volume, ϕ the diameter of the capillary pore, ϕ_0 the minimum capillary pore diameter and "a" a pore structure constant. The pore volume formed by pores smaller than ϕ_0=0.002 μm (see Table 3.1), i.e. gel porosity, is not included in this formulation. The total pore volume in a cement paste depends on the state of the hydration process, viz. the degree of hydration α. At the initial stage of the hardening process, the total pore volume is equal to the paste volume minus the volume of cement. This ratio is determined by the water/cement ratio. At that particular stage, the total pore volume is completely filled with water[1]. After some hydration has occurred (α>0), the capillary pore volume has decreased due to the formation of hydration products. The pores do not remain completely filled with water since some part of the water volume has been used up by the reaction process with cement. The pores with the largest diameter are emptied first. From this, a distinction can be made between pores that are still completely filled with water, i.e. with diameter $\leq\phi_{wat}$ and empty pores. The diameter of the pore that is still completely filled with water will be within the border limits of the capillary pores, e.g. $\phi_0 \leq \phi_{wat} \leq \phi_{por}$, where ϕ_{por} is the maximum

[1] The dissolved gas in the capillary pore water is disregarded.

pore diameter involved in the pore size distribution. This maximum pore diameter can be derived from equation (3.1). At a certain degree of hydration, the maximum pore diameter involved in the pore system can be determined with:

$$\phi_{por}(\alpha(t)) = \phi_0 \exp\left(\frac{V_{por}(\alpha(t))}{a}\right) \tag{3.2}$$

The actual total pore volume $V_{por}(\alpha(t))$ changes continuously throughout the hardening process. The pore space will reduce due to the formation of hydration products but, on the other hand, new pore space will be formed due to the volumetric reduction that is a result of the chemical reaction between the water and the cement (chemical or "Le Chatelier shrinkage). Therefore, in this equation, the total pore space $V_{por}(\alpha(t))$ is considered to be built up from two contributions. These are the actual pore volume that is occupied currently by capillary water and an additional volume that is the result of the chemical shrinkage. The relative contributions of both volumes change continuously during the hydration process. The changes of the total pore volume are accompanied by changes of the pore wall area.

The pore wall area of the hardening cement paste is considered to be covered by a thin adsorption layer of water molecules. The thickness of this layer depends mainly on the relative humidity in the pore system. Changes of the actual water volume in the system due to hydration, will change the relative humidity in the pore space and, therefore, also effect the thickness of this adsorption layer. It is assumed that the water volume that is occupied by the adsorption layer goes at the cost of the free capillary pore water volume that is available for further hydration. Therefore, the diameter of the pore that is still completely filled with water will become smaller due to adsorption of water at the pore wall area.

When adopting the modelling approach as it is proposed up till now, detailed information on the properties of pore structure of a hardening cement paste is available. The only parameter in the formulation (eq. (3.1)) that remains unknown, is the pore structure constant "a". The value of this unknown parameter can be determined either by book keeping experimental data or by using numerical models. Book keeping a data-base that contains information on the pore structure of different types of mixtures is a serious option to achieve an adequate prediction of the pore structure constant "a". Using a numerical model to generate information on the pore structure constant "a" is even more convenient and more challenging. However, it must be born in mind that this is a modelling approach. Therefore, in the next section, it will be elucidated how the pore structure constant "a" can be determined form pore size distribution measurements. In addition, in section 3.3.6, it will be outlined how this constant can be determined by application of a numerical model.

3.2.3.6 Pore structure constant "a" determined from experiments

It is possible to determine the pore structure constant "a" from pore size distribution measurements. The dimension-less parameter "a" can be derived by dividing the pore volume that is intruded in the pore space by the accompanying pore range according to the formula:

$$a = \frac{V_{por}}{\ln(\phi / \phi_0)} \tag{3.3}$$

The diameter of the smallest capillary pore ϕ_0 is equal to 0.002 µm. In equation (3.3), the pore diameter ϕ is equal to the largest pore diameter.

From the literature, it was found that the pore structure constant ranges roughly between 0.05 (coarse cement) and 0.15 (fine cement) [22, 36, 64, 98]. The exact value depends on the type and fineness of the cement that is used. These parameters mainly determine the structure of the pores in a cementitious material. From the results in Fig. 3.8, it can be seen that the relationship between the total pore volume and the corresponding pore size distribution, as it is represented by the pore structure constant, is almost constant throughout the whole hardening process. This permits to apply a constant value for the pore structure constant "a" for the simulations of the pore structure during the whole hardening process.

Therefore, according to the proposed procedure, it is rather easy to determine a pore structure constant "a" from pore size distribution measurements. In Fig. 3.8, pore size distribution measurements (left hand side) [97] are compared with the pore size distribution as modelled according to equation (3.1) (right hand side). From the measurements presented in this example, a pore structure constant "a" of about 0.08 could be calculated. This value has been applied to the model. The simulated pore size distribution (Fig. 3.8, right) shows the reduction of the total pore volume and the maximum pore diameter with progress of the hydration process (see also Fig. 3.7). Whether the pores are filled with water or empty depends on the degree of hydration.

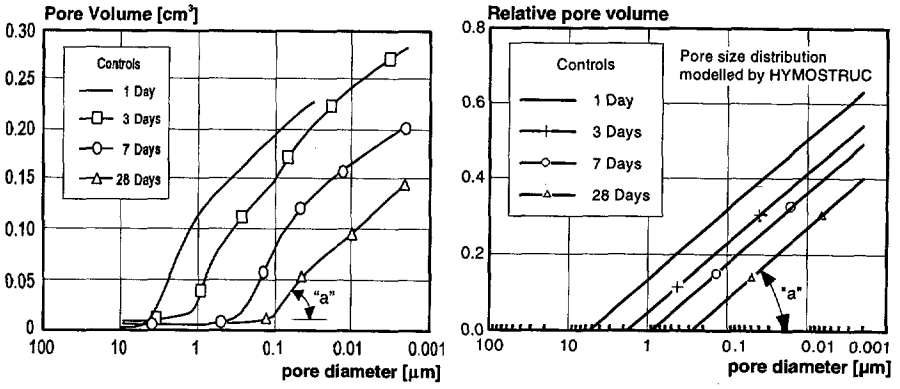

Fig. 3.8. Left: Pore size distribution measured by Whiting [97], Right: Pore size distribution according to HYMOSTRUC (eq. (3.1)).

3.3 Extension of the basic HYMOSTRUC model

3.3.1 General

In the basic HYMOSTRUC model (see section 3.2.3), the distribution of the cement particles in a microstructure is based on a statistical approach. For more advanced research purposes, it is desirable to have information on the validity of this statistical approach. Therefore, application of a hydration model, where the microstructure is based on randomly parked cement particles, will be considered to verify several features of the basic HYMOSTRUC model. On the other hand, a random particle structure can also be used for a more detailed analysis of the interfacial transition zone.

This way of simulating the microstructure is based on a cement grain structure that follows a certain particle size distribution and where the grains are parked randomly in a closed medium. The structure that appears is, in fact, a simulation of the initial stage of the water-cement substance (cement particles in the aqueous phase). For this microstructure, the hydration process can be simulated by "expansion" of the cement grains as modelled by the basic HYMOSTRUC model. This expansion represents the formation of hydration products. Simultaneously, the expansion of cement grains start to form a load bearing microstructure. Simulating the development of a microstructure according to this approach has the advantage that a relative "large" sample can be handled within an acceptable allocation of computation time.
A detailed description on the extension of the HYMOSTRUC model will be elucidated in the next sections. It will also be outlined how the pore structure constant "a" can be deduced from a simulated microstructure.

3.3.2 Random particle structure

The way how a random particle structure can be obtained will be elucidated in this section, briefly. The process starts with the definition of a finite volume in which the cement particles have to be 'thrown'. A spherical shaped volume is a very suitable for this purpose. This type of volume has no singular points, like edges in a rectangular shaped volume. A spherical volume will therefore be considered in this section.
The cement particles which have to be thrown in the sphere follow a certain distribution (see section 2.2.2). The most reliable way to keep to process running is to start with the largest particles, and to continue the particle parking process with the particles smaller than the previously parked particle. The particles can be parked in the sphere randomly. To reach this, two angles and the radius to the position of the particle in the sphere have to be determined. If particles overlap, the current position is erased and a new random position is determined until the particle is placed correctly. If particles cross the boundary surface of the sphere, an additional particle will be placed

at the opposite of the position of the current particle, with respect to the centre of the sphere. In this way, boundary effects at the surface of the sphere will be negligible.
In order to simulated the "wall effect" of the cement particles at the aggregate surface (ITZ), a fictitious boarder plane can be added to the sphere, placed through its centre. For a tubular shaped volume (see Fig. 3.9, left), these wall effects can be also be simulated at both end sides. These type of finite volume is therefore suitable to simulate the random particle structure for the ribbon paste (see chapter 6).

3.3.3 Theoretical background

A random particle structure is defined as:

A closed medium with finite volume V that is filled with n particles that obey a certain particle size distribution G(x).

The random particle structure is a numerical way of simulating the spatial distribution of the cement particles in the aqueous phase. If the water/cement ratio and the particle size distribution G(x) are known, a particle structure can be simulated, with help of an arbitrary shaped volume V. The summation of the mass of all cement particles in the volume V and the mass of the water in the volume are in agreement with the water/cement ratio.
The simulation of a random particle structure starts with the definition of an arbitrary shaped volume V. The number of particles (per fraction) that will be parked in the volume V is governed by the water/cement ratio, the particle size distribution and the finite volume V. The cement particles are considered to be distributed according to the Rosin-Rammler distribution function G(x):

$$G(x) = 1 - \exp(-b_{RR} x^{n_{RR}}) \tag{3.4}$$

where G(x) is the cumulative weight in [g] of the particles with diameter x. The constants n_{RR} and b_{RR} depend on the fineness of the cement. Equation (3.4) is valid for 1 gram of cement. The weight of the particles in a certain fraction can be determined by differentiating the Rosin-Rammler function with respect to the particle diameter x. From this, it can be deduced that the volume V_x of all cement particles in a fraction F_x is equal to the quotient of the weight per fraction and the specific density of the cement ρ_{ce}. To come to the number of particles in a fraction F_x, the volume per fraction V_x must be divided by the volume of a single particle v_x. By doing this, the number of particles in a fraction F_x within one gram of cement becomes:

$$N_x = \frac{V_x}{v_x} = \frac{b_{RR} n_{RR} x^{n_{RR}-1} \exp(-b_{RR} x^{n_{RR}})}{\frac{1}{6}\pi x^3 \rho_{ce}} \tag{3.5}$$

The cement particles are considered to be randomly distributed. This implies that the positions of all cement particles in a certain volume can be determined by a probability density function. The probability of a certain position in the finite volume V is then equal for all particles. Parking the cement particles in this way results in random distances between the cement particles. The probability density function that describes this random particle parking process is equal to:

$$f_x(x) = 1 \tag{3.6}$$

where x is the relative particle size (x_i/x_{max}).
Following the procedure as adopted in this section, a random particle structure can be obtained, representing the microstructure of a hardening cement paste. The volume that represents the size of the sample should be defined. Both a spherical shaped volume and a tubular shaped volume are presented in Fig. 3.9. These volumes are three-dimensional. For this three dimensional approach, several restrictions must be fulfilled in order to obtain a consistent system. Consider a spherically shaped volume with radius R_m that will be used as the physical boundary for the random particle structure. In order to define a unique position in the spherically shaped medium, three parameters are required. These are two 'internal' angles and a radius (see Fig. 3.9). In this figure, φ is the angle between the projection of the vector r_m to the x-y plane and the x-axis. The angle ϑ determines the angle between the z-axis and the vector r_m.

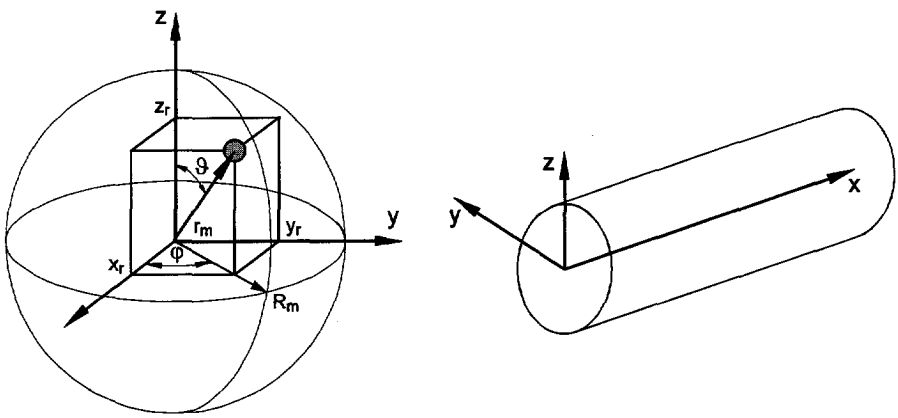

Fig. 3.9. Left: Schematical representation of a position in a spherical volume. Right: Tubular shaped volume representing the physical boundary of the random particle structure (used for ribbon paste, see chapter 6).

In order to get a randomly determined spatial position of a particle in the sphere, the parameters must fulfil the following criteria:

$$\begin{aligned} 0 \le \varphi \le 2\pi \\ -1 \le \cos\vartheta \le 1 \\ 0 \le \frac{1}{3} r_m^3 \le \frac{1}{3} R_m^3 \end{aligned} \tag{3.7}$$

Calculating the random positions according to the distribution function as described in equation (3.6), and meeting the restrictions as given in (3.7), it is possible to determine a random particle structure within a finite volume V for a cement paste of certain water/cement ratio and where the particles follow the particle size distribution G(x) as given in equation (3.4).

In Fig. 3.10, two cross-sections of a three dimensional spherically shaped volume are shown. Both figures represent a random distribution of the cement particles in the aqueous phase (α=0). It concerns the random particle structure for two different water/cement ratios, 0.3 and 0.7 respectively. From these figures, it can be observed that the mean particle spacing strongly depends on the water/cement ratio. This may also be a factor in the strength development of a cement paste mixture since the average distance between two hydrating particles is much larger for the cement paste with a water/cement ratio of 0.7 than for a cement paste with a water/cement ratio of 0.3. For the two different water/cement ratios, a different number of particles will be present in the spherical medium, since particles are parked randomly in an equal medium V which represents the physical boundary of the structure. Different

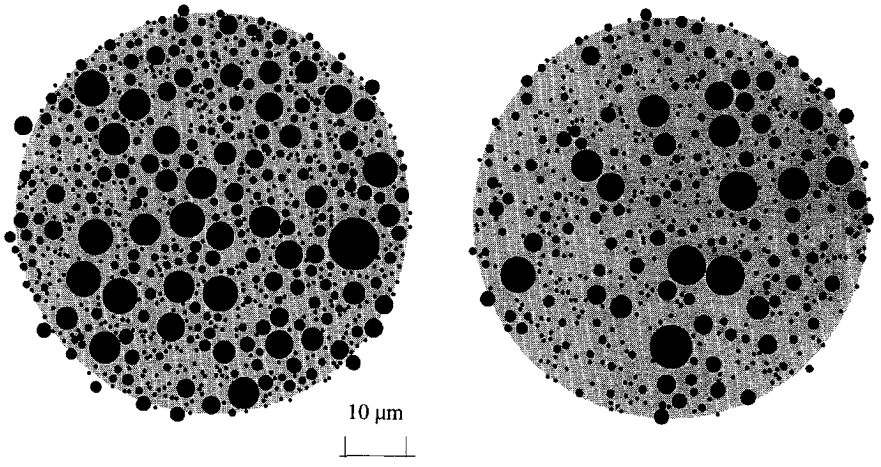

Fig. 3.10. Cross-section of a 3-dimensional random particle structure for two water-cement ratios. (left 0.3 right 0.7). Blaine 420 m^2/kg. For both spheres, radius 100μm.

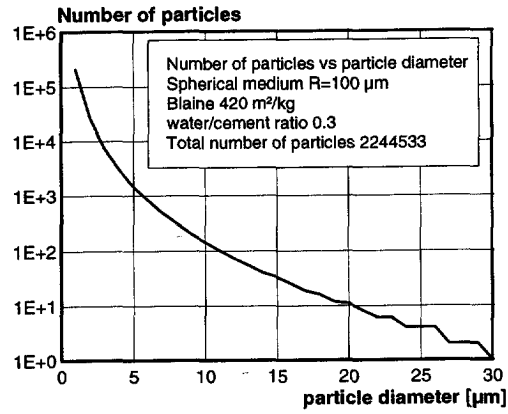

Fig. 3.11. Number of particles versus particle diameter for a spherical shaped medium with a radius of 100 µm, a water/cement ratio of 0.3 and a Blaine value of 420 m^2/kg.

water/cement ratios, then, result in a different number of particles for each simulated random particle structure. For the two structures as given in Fig. 3.10, 224533 particles are parked in the sphere which meet the water/cement ratio of 0.3 (Fig. 3.10, left), whereas 148396 particles are parked in the sphere with a water/cement ratio of 0.7 (Fig. 3.10, right). The distribution of the particles as they were parked in the sphere with a water/cement ratio of 0.3 is presented in Fig. 3.11. From this figure, it can be seen that the large number of particles that have to be parked in the spheres mainly comes from the smaller particle fractions. The large number of small particles claims a lot of memory capacity and increases the computation time substantially. For example, consider a cement paste with a water/cement ratio of 0.3. Disregarding the particle fraction with particles with a diameter of 1 µm leads to a total number of particles to be parked in the sphere of 39644. This is a reduction in number of almost 84%. In volume, ignorance of this particle fraction leads to a reduction of only 2.5% of the total cement volume. Calculations showed negligible differences between the hydration process with and without inclusion of the particles with a diameter of 1 µm. Therefore, accepting this proposed volume reduction makes the simulation model very favourable with respect to the computation time. It makes these types of models for simulation of the microstructure very fast, flexible and convenient to work with.

3.3.4 Mean particle spacing

In the basic HYMOSTRUC model (see section 3.2.3), the distance between two particles of the same fraction is represented by the so called mean particle spacing. This statistically based distance is formulated by making use of the "cell-concept" (see [16]). The cell-concept can be applied for each particle fraction. The mean particle spacing L_x between particles belonging to fraction F_x in a paste with w/c ratio ω_0 can

be estimated by assuming that the particles under discussion are situated in the centre of a "*cell*" (cubed-shaped). Van Breugel [16] defined this cell as follows[2)]:

$$I_x = (V_w + V_{\leq x}) \cdot N_x^{-1} \tag{3.8}$$

where: V_w = initial water volume

$V_{\leq x}$ = cement volume of particles $\leq x$

From this cell concept, the mean centre-to-centre spacing L_x is assumed to be equal to the rib size of the cubic cell with volume I_x:

$$L_x = (I_x)^{\frac{1}{3}} \tag{3.9}$$

Since the cell volume is a function of both the water/cement ratio and the particle size distribution, the particle spacing L_x is a function of these parameters as well. This means that there will be a difference between the mean particle spacing of both a paste with a high water/cement ratio and a low water/cement ratio. In Fig. 3.12, the particle spacing is presented as a function of the particle diameter for a cement paste with a water/cement ratio of 0.3 and 0.4.

In order to validate to what extent the mean particle spacing of the random particle structure is comparable with mean particle spacing based on the statistical approach as defined by van Breugel [16] (eq. (3.9)), these particle spacings are compared with each other (see Fig. 3.12). For a random structure, it is very difficult to determine the mean particle spacing, since there is no "cell" around each particle that determines how many particles are involved in the analysis of this distance. This lack of information makes it very hard to determine the mean particle spacing without making any assumptions. On the other hand, it is possible to determine the minimum particle spacing per fraction of particles in the spherical body (see Fig. 3.10). This information gives an impression about of the general agreement between the particle distance that is based on the random particle structure and the particle spacing that is based on the statistical approach. It must be born in mind that the minimum particle distance that is determined for the random particle structure is, in fact, the lower boundary value for the particle distances. Since the random particle structure is determined for a finite volume, only a relatively small number of large particles may be enclosed. This implies that for these larger particles, the minimum particle distance may show a wider scatter. This can also be observed from Fig. 3.12, where the minimum particle spacing based on the random approach is compared with the mean particle spacing that is based on

---

[2)] Cell definition

A cell I_x is defined as a cubic space in which the largest particle has a diameter x and further consists of 1/N times the original water volume and of 1/N times the volume of all particles with a diameter smaller than that of particle x (after [16]).

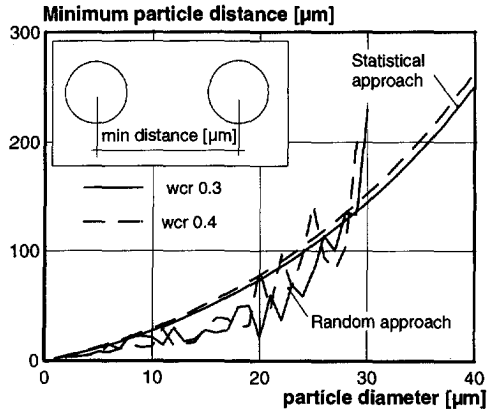

Fig. 3.12. Comparison of minimum particle spacing of random approach with the mean particle spacing of the statistical approach. Cement fines 550 m²/kg, w/c 0.3 and 0.4.

the statistical approach (eq. (3.9)). The results are presented for a cement paste with a water/cement ratio of w/c 0.3 and 0.4 (Blaine 550 m²/kg). For the smaller particles, the minimum particle distance of the random particle structure is smaller than the mean particle spacing as determined according to the statistical approach. Due to the relative small number of large particles, at the larger particle range, the minimum particle distance tend to exceed the mean particle spacing. Nevertheless, the results give a good impression of the relationship between the statistically based particle distance and the particle distance which is based on the actual random distribution.

3.3.5 Formation of microstructure

Hydration of cement generally concerns the formation of hydration products (outer product) and consumption of cement (inner product). This process lasts as long as hydration proceeds. In HYMOSTRUC, the formation of structure is modelled explicitly. The model draws heavily on the work as proposed by Bezjak [13, 14], Pommersheim [66] and Jennings [43]. In the model, distinction is made between the formation of the hydration products that are considered to grow from the original cement grain surface in an outward direction (outer product layer) and hydration products that are considered to grow from the original cement grain surface in an inward direction (inner product layer).

From a modelling point of view, several numerical techniques can be applied to visualise this process [42]. The visualisation of the particle approach model as discussed in section 3.3.1 is presented in Fig. 3.13. From this figure, the formation of a load bearing microstructure can be observed for two stages of the hydration process. Distinction is made between the outer product layer and the inner product layer. Note: The cylindrical shaped anhydrous cement grains are coloured black as well as the background colour. The latter represents the pore space.

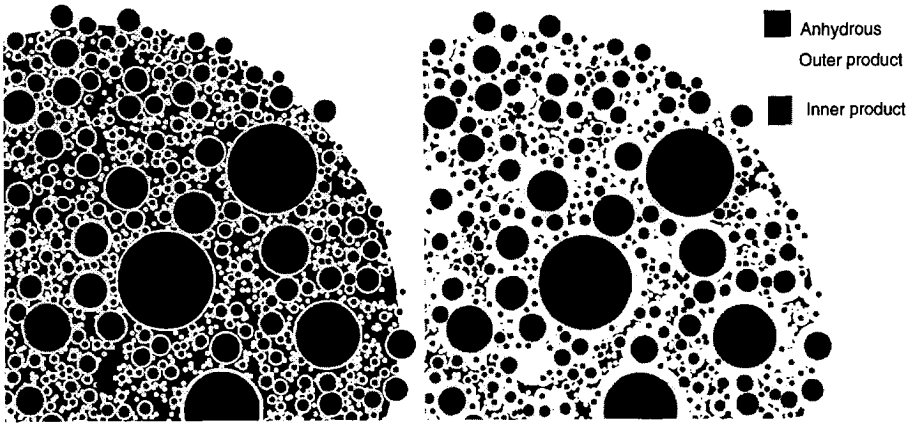

Fig. 3.13. Cross-section of a random particle structure at α=0.1 (left) and α=0.5 (right). Representing a cement paste of medium fineness (Blaine 420 m^2/kg) and a water/cement ratio of 0.3. (background colour black)

From the two stages of the hydration process (α=0.1 and α=0.5) as given in Fig. 3.14, the densification of the microstructure can be observed quite well. The remaining pore space is substantially smaller at a degree of hydration of 0.5 than at a degree of hydration of 0.1. As can be observed from the figure, this is mainly the result of the formation of the hydration products at the periphery of the cement grain surface (outer product). From this, it becomes clear that the development of the pore structure can be related to the degree of hydration, e.g. the formation of hydration products. The way this is done will be discussed in detail in the next section.

3.3.6 Pore structure constant "a" determined from random particle structure

The pore structure constant "a", that determines the pore size distribution in a cement paste microstructure (see eq. (3.1)), can be derived from a random particle structure. Earlier, in section 3.2.3.6, this pore structure constant was determined from experimental results. In this section, it will be elucidated how similar results can be obtained from numerical simulations with the extended HYMOSTRUC model. In the extended version of the HYMOSTRUC model, the formation of structure is modelled by an increase of the radii of the spherical cement particles that are randomly parked in space. During hydration, the cement particles start to "expand" or grow and form a microstructure. Some particles may become embedded in the outer product layer of larger particles. In Fig. 3.14, (a close-up of Fig. 3.13), two stages of the hydration process are presented for a cement of medium fineness (Blaine 420 m^2/kg) and a water/cement ratio of 0.3. Initially, if no hydration has taken place, only unhydrated cement particles exist which are distributed randomly in the water. At a degree of hydration of 0.1, a microstructure with little formation of hydration products can be observed. The distinction between the formed hydration products called: 'outer

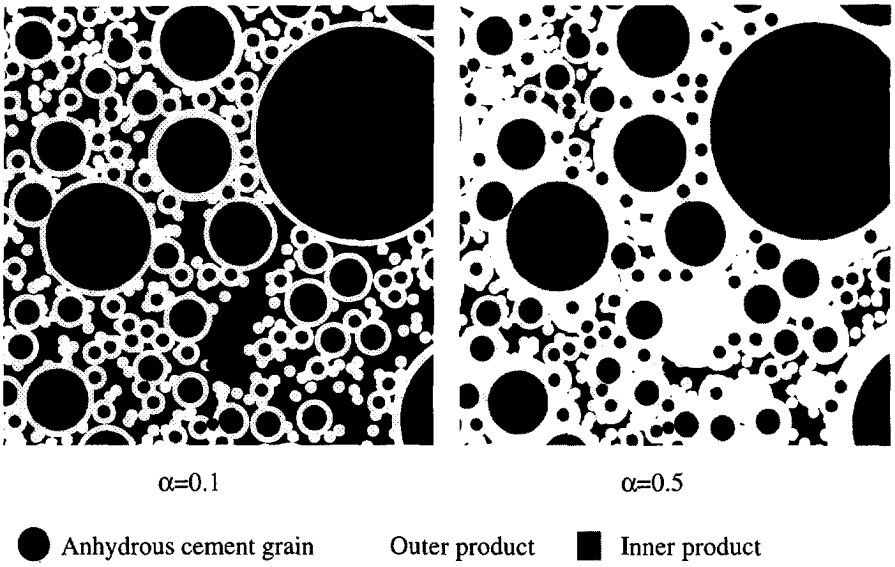

Fig. 3.14. Modelling Formation of structure of a cement paste with a water/cement ratio of 0.3 and a cement fineness of (420 m^2/kg). (Background colour is black!)

product' and the zone at which the water has penetrated into the cement particle called: 'inner product' can be observed in the figure. At a degree of hydration of 0.5, the actual developed hydration products tend to form a dense microstructure. From this structure, the pore space can be recognised (black colour). Most of the pores are closed and surrounded by expanded cement particles. The average dimensions of the pores that can be observed range roughly between 1 and 10 μm. Since the shape of the pores are rather irregular, is it hard to determine a pore size distribution from this microstructural model. To overcome this, use can be made of the weighted average of the total pore volume and total pore wall area. Among others, Setzer [79] proposed a procedure to determine the hydraulic radius from the ratio between the total pore volume V_{por} and the total pore wall area A_{por}. This hydraulic radius R_H, is defined as follows:

$$R_{H=}\frac{V_{por}}{A_{por}} \tag{3.10}$$

For an arbitrary slice of a random particle structure, the pore volume V_{por} can be determined by subtracting the area that is covered by the expanding cement particles A_{solid} from the total cross-sectional area A_{paste} of the slice and multiplied by the thickness of the slice Δx. This can be denoted as:

$$V_{por} = (A_{paste} - A_{solid}) \cdot \Delta x \tag{3.11}$$

For an arbitrary slice with a thickness Δx which is taken from the random particle structure, the pore wall area A_{por} can be determined. The pore wall area can be determined by adding up all those parts of the circumference of the growing cement particles (outer product), which directly border on the pore space l_ϕ and multiply this total pore circumference by the thickness of the slice Δx. In fact, this procedure represents a linear extrapolation of the pore structure. This means that the thickness of the slices which are used in the calculations determine the accuracy of the results. Mathematically, this can be denoted as:

$$A_{por} = \Delta x \sum_{\text{all particles}} l_\phi \tag{3.12}$$

Together with the equations (3.11), (3.12) and (3.10), the hydraulic radius can be determined for the random particle structure (Fig. 3.15, left). The hydraulic radius changes continuously throughout the hardening process. It decreases with increasing degree of hydration. This appears to be true for the three types of cement with different fineness which are considered in Fig. 3.15 (left). The figure shows also that the hydraulic radius is inversely proportional with the fineness of the cement.
Densification of the microstructure due to the formation of hydration products around the hydrating cement particles will reduce the initial pore volume of the hardening cement paste. On the other hand, it will enlarge the pore wall area (Fig. 3.15, right). Assuming that the hydraulic radius represents the weighted pore diameter for the hardening paste, the pore constant "a" can be determined from a random particle structure. From the hydraulic radius R_H and the pore volume V_{por}, the pore structure constant "a" can be calculated from equation (3.3) ($\phi=2R_H$ and $\phi_0=0.002$ µm). In Fig. 3.16, the pore structure constant is shown for two different types of cement paste. It appears that the value differs only slightly for both pastes with progress of the

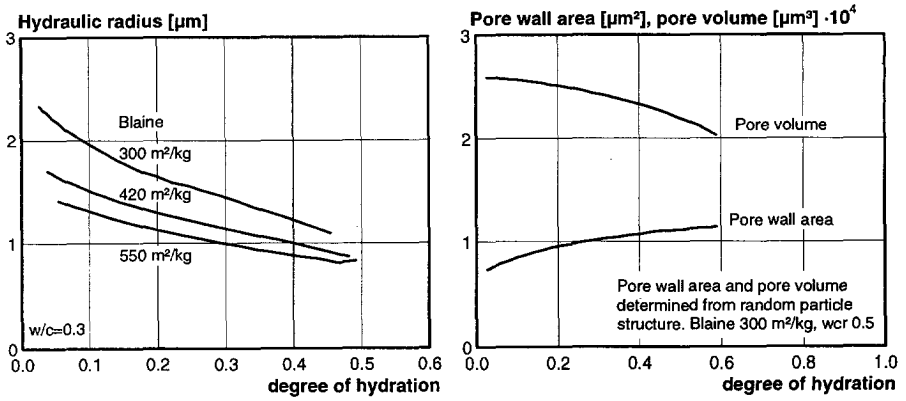

Fig. 3.15. Left: Hydraulic radius (eq. (3.10)) vs degree of hydration, Right: Pore wall area and pore volume vs degree of hydration. Based on random particle structure.

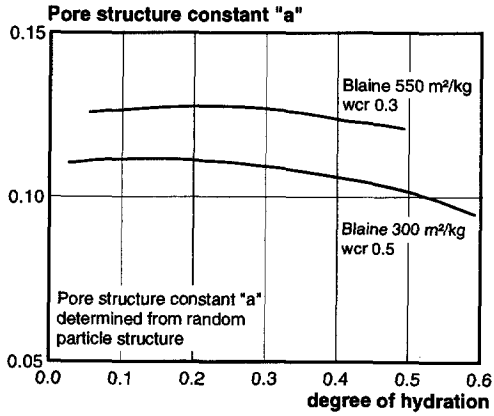

Fig. 3.16. Pore structure constant "a" versus degree of hydration for two different cement pastes determined from the random particle structure.

hydration process. It appears that the value is highest for the cement paste that contains fine cement and a low water/cement ratio. A higher value "a" in equation (3.1) implies that more smaller pores are involved in the microstructure. The same trend is generally found in experimental data [27].

The pore structure constants as shown in Fig. 3.16, represent differences in the fineness of the pores in a hardening cement paste. The inclination angle of the ascending branch of the cumulative pore size distribution of a fine pore structure (high Blaine value) will be larger than the inclination angle of a coarse pore structure (low Blaine value). This effect is schematically shown in Fig. 3.17. This is in agreement with the results as presented in Fig. 3.16. For the paste with a cement fineness of 550 m^2/kg, a higher pore structure content is calculated than for the paste with cement fineness of 300 m^2/kg.

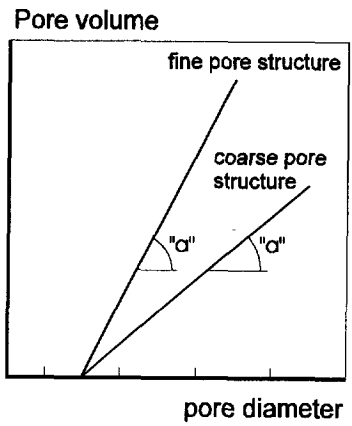

Fig. 3.17. Schematic representation of the different pore structure constants and the associated pore size distribution.

3.4 Discussion

Simulating the development of the microstructure according to the particle approach as outlined in this chapter, turned out to be very useful for the analysis of the microstructural properties. The progress of the hydration process can be visualised with the model quite well. The simulation of the growth of the cement particles and the densification of the microstructure and the associated development of the pore structure form a solid basis to proceed with further development of the modelling of the microstructural behaviour of hardening cement-based material.

A reliable description of the microstructure is also indispensable for the analysis of the volume changes, viz. autogenous shrinkage, which appear during hardening. The way how the autogenous shrinkage can be modelled will be elucidated in detail in the next chapter.

4.

Modelling of autogenous shrinkage

4.1 General

During the hydration process of a low water/cement ratio cement paste (or concrete) a change of the original mix volume is generally observed. If moisture loss to the environment is prevented, the volume reduction of the hardening cement paste can only be the result of the chemical or physical processes that take place during hardening. As has already been outlined earlier, it is assumed that the volume reduction that is the result of the chemical reaction process between the cement and water, causes a pore system in the cement paste.

As hydration proceeds, water will be taken out of the system to form hydration products. For a closed system, this implies that the pressure in the empty pore space will decrease in order to establish thermodynamic equilibrium. A reduction of this pressure implicitly affects the relative humidity in the pore space. A lower relative humidity also affects the thickness of the adsorption layer at the pore wall area. Thermodynamic equilibrium in the pore system requires an increase of the surface tension in the adsorption layer. This process continues as long as hydration proceeds. The stress in the adsorption layer causes a certain deformation which will be restrained by the actual stiffness (elastic modulus) of the microstructure. In the early stage of the hardening process, when the elastic modulus has only partly developed, the deformations which are the result of the stresses in the adsorption layer may cause large macro deformations of the microstructure. This macro deformation is generally known as *autogenous shrinkage*.

In this chapter, it will be described how autogenous shrinkage can be modelled. The hydration process, which is assumed to be the driving force behind the autogenous shrinkage mechanism, is determined numerically with the HYMOSTRUC model. This chapter continues with a thermodynamic analysis of the moisture state in a continuously changing pore system. Thereafter, a constitutive model will be described that relates the stresses in the adsorption layer to the macro deformation, i.e. autogenous shrinkage.

4.2 Thermodynamic analysis of the moisture state in a changing pore system

4.2.1 Literature survey

At this moment, there is a lot of discussion about the autogenous deformation of a hardening concrete or cement paste. Some topics in this discussion concern the definition of autogenous shrinkage and the mechanism behind it, but also the way how to model this phenomenon. Authors agree that a volume change of a cement-based material is the result of a change of the relative humidity [8, 28, 35, 65, 68, 69, 78, 79, 80, 81, 82, 100, 101, 102]. Based on this concept, several authors developed models to predict the volume change of a hardened cement based material. The most well known models in this respect are of Powers and Brunaur [69], of Feldman and Sereda [26] and the Munich model [102] (see later 4.2.3). These models have been used to predict the swelling of a oven-dried hardened cement paste as a function of the relative humidity of the specimen. According to the Munich model, a change of the relative humidity is associated with a change of the surface tension in the adsorption layer. In this model, the surface tension is considered as the "load" which acts from the interior of the hardened microstructure. For the constitutive relation which relates this surface tension to a certain deformation, the Bangham relation is adopted. According to this model, a linear relationship between the surface tension and the swelling deformations can be obtained for a relative humidity below 40%. For a relative humidity higher than 40%, the deformations show a non-linear behaviour. According to the Munich model, the deformations in the relative humidity range between 40 and 100% and are attributed to the so called disjoining pressure. The latter model does not include a constitutive relation for this particular humidity range.

In hardening concrete, the relative humidity differs substantially from what is generally considered in the models as presented before. In [100], Wittmann shows results of the relative humidity of hardening cement pastes for different water/cement ratios. (see Fig. 4.1). These results show that the relative humidity of hardening paste ranges roughly between 80 and 100%. More recently, this order of magnitude of the relative humidity was also shown by Hua et.al. [40]. It was shown that these results could be simulated by application of the Kelvin law. In [40], it was proposed to calculate the autogenous deformation of hardening cement paste from the reduction of the pore pressure which is associated with the decreasing relative humidity. Hua et. al. conclude that the self-desiccation of the hardening microstructure takes place at high values of the relative humidity. In Hua's model, it is proposed to adopt the pressure in the empty pore space as the load that acts on the microstructure from the interior.

In this chapter, a model will be proposed which is in good line with the mechanism as proposed by Hua et.al. The main difference is that, in the model as proposed in this

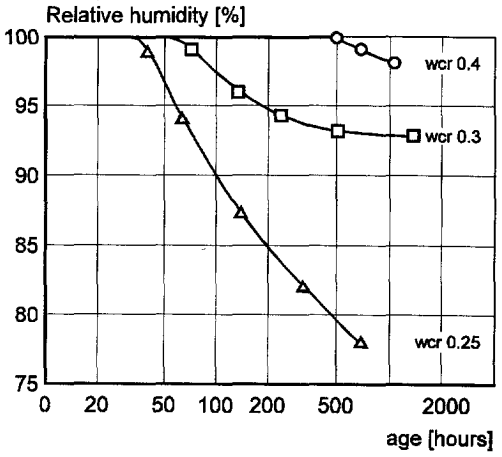

Fig. 4.1. Relative humidity versus hydration period for three different water/cement ratios (taken from Wittmann [100]).

chapter, the surface tension in the adsorption layer which is in balance with the pressure in the pores, is considered to be the load that acts form the interior on the hardening microstructure. The surface tension is calculated by a thermodynamic analysis of the moisture state in the continuously changing pore system. To relate the surface tension to the microstructural deformation, a Bangham-like constitutive equation has been adopted. Based on this approach, deformations can be calculated which are induced by a lowering of the relative humidity in the gradually emptying pores. The process is driven by the degree of hydration which is calculated with the HYMOSTRUC model.

4.2.2 Basic mechanism of thermodynamic analysis

Thermodynamic phenomena in a porous cement-based material, like cement paste or concrete, have been studied by several authors [6, 7, 18, 21, 23, 62, 81]. Most of these authors explain the mechanism which describes the thermodynamic behaviour in a porous system on the basis of the Gibbs theory (1906) [33]. This theory deals with the equilibrium between the gas pressure in an arbitrary volume of a closed system and the product of the stress and area in the adsorption layer against the pore walls. For cement-based systems, this theory can be adopted for the thermodynamic analysis of the moisture state in the changing pore space. It holds that equilibrium between the volume and pressure in the empty pore space (gas pressure) and the surface tension in the adsorption layer at the total pore wall area must be established. This can be obtained by an iterative calculation procedure.

4.2.3 Existing models based on a thermodynamic approach

Since the Gibbs theory has been known for almost one century, many authors have developed models that are able to predict the microstructural deformation of cement-

based material as a function of changes of the relative humidity. The proposed models describe swelling of an oven-dried material on exposure to water. Three models can be distinguished with respect to their special interpretation of the mechanism behind the swelling of the microstructure. In general, these models are classified as [69]:

- the Powers-Brunaur model
- the Feldman-Sereda model
- the Munich model

The models describe the swelling mechanism as a function of the adsorption of the water molecules to the internal surface area. Differences appear in the interpretation of the forces which cause the expansion of the dry microstructure.

The Powers-Brunaur model explains swelling of the microstructure on exposure to water by the separation of individual particles due to the existence of water molecules between them. The chemical bonds between these particles is assumed to limit the swelling of the microstructure.

In the Feldman-Sereda model, the swelling mechanism is considered to be the effect of several mechanisms. These are:

- the reduction of the free surface energy due to water molecule attraction
- the penetration of water molecules between layers
- the menisci effect due to capillary condensation
- the finally the ongoing hydration effect

Some mechanisms dominate within a certain range of the relative humidity. In this respect, the penetration of water molecules between the layers is considered to occur throughout the 0 to 100% range of the relative humidity, whereas the ongoing hardening process is considered to dominate at a relative humidity level higher than 20%.

In the Munich model, swelling of the microstructure is considered to be the result of changes of the free surface energy. This can be considered as a change of the surface tension in the adsorption layer at the pore wall area. For relative humidities lower than 40%, the relationship between the change of the free surface energy and the swelling of the microstructure is considered to be linear (see Fig. 4.2) [35, 102]. For higher values of the relative humidity this relationship becomes non-linear. Swelling deformations in the relative humidity range between 40 and 100% are attributed to the so called disjoining pressure. Water molecules separate the surfaces that are held together by van der Waals forces.

These thermodynamically based models have proved to describe the swelling behaviour of an already hardened and dry microstructure that is placed in a moist environment quite well. This implies that the theory as proposed by Gibbs can also be applied for cement-based materials. Therefore, the model that is discussed in the next sections is based on the similar mechanism as discussed in section 4.2.2. The major difference with the three models as discussed in section 4.2.3 is, that the proposed model is derived to describe the autogenous shrinkage of a hardening microstructure. This means that

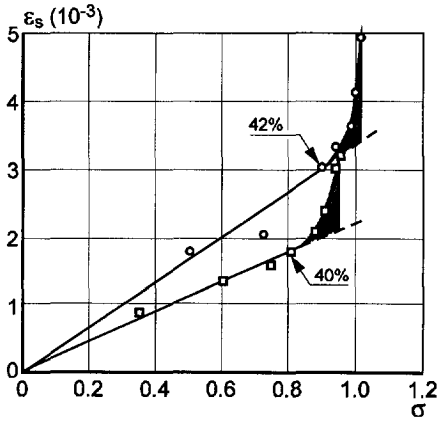

Fig. 4.2. Hygral swelling deformation versus changes of surface tension acc. to Munich model [102].

initially, the relative humidity in the pore system will be 100%. During hydration, this value will drop depending on the degree of hydration. The relationship between the stresses that develop in the adsorption layer at the pore wall area (surface energy) and the deformation of the microstructure is described according to the constitutive equation concept as proposed by Bangham [7]. This is similar to the approach adopted in the Munich model. The main difference is that for a hardening microstructure, all material properties change throughout the hardening process. This requires a step wise treatment of the calculation process.

Since the hardening process of a cement-based system can be considered as semi-static, the thermodynamic approach for the description of the moisture state is adopted. From this approach, thermodynamic equilibrium in the hardening microstructure can be established as well. Some aspects of the thermodynamic approach will be outlined in the next section.

4.2.4 Description of a thermodynamic analysis of a pore system

Volume changes of the hardening cement paste can be determined with help of a change of the associating thermodynamics. Thermodynamic equilibrium in a continuously changing pore volume will be affected by a change of the degree of hydration. As hydration proceeds, the actual state of energy in the paste changes and a new state of equilibrium must be established. Based on first principal of thermodynamics, this can be determined by:

$$dQ = dU + dW \tag{4.1}$$

where dQ is the heat that is produced during an infinitesimal change of a mechanical system, dU is the internal energy in the system and dW the work carried out by the system. For a closed system, an infinitesimal change of the heat increment dQ can be written as dQ=SdT, where dT is the absolute temperature increment of the system and S

the entropy. For isothermal hardening conditions, the temperature remains constant during an infinitesimal phase change. This means that there will be no heat exchange, so that dQ=0.

For a hardening cement paste, the internal energy in the system remains constant (dU=0). It is assumed that there is no internal dissipation of energy. This means that all energy is conserved while hardening. This leads to a more simplified formulation for the description for the conservation of the actual energy level in the system, e.g. dW=0. This concerns only the internal work of the system.

For a hardening cement paste, a incremental change of the hydration process affects several parameters which are in the conservation of the internal work. After mixing, a cement paste consists only of a water-cement dispersion. At this early stage of hardening, no structure has been formed by the hydrating cement grains which are randomly distributed through the paste. This means that all pores in the paste are considered to be completely filled with water.

After setting, at a certain stage of the hydration process, pores are partly filled with water. The empty pore volume is filled with air. A thin layer of water molecules is adsorbed against the pore wall area. There exists a water/vapour interface between the adsorbed water and the air in the empty pores. In general, this system can be considered as a three phase system, e.g. adsorbed water - interface layer - air (gas). The thickness of the adsorption changes during hardening. Therefore, it turned out to be useful to express this adsorption layer in terms of mole or weight fractions. A macroscopic definition of the adsorbed volume can be derived by using the Gibbs theory [23]. This theory is based on a three phase system consisting of a water-vapour layer and two additional phases of homogeneously distributed substances (see Fig. 4.3).

In the Gibbs model, initially the thickness of the interface is taken zero, whereas in a real system, this adsorption layer has a finite thickness. The actual volume of the adsorption layer can be determined with help of the concentration of the actual phase. Assume c_i as the concentration of component i, in moles per unit volume. From this, the number of moles in the water phase and the air (gas) phase can be denoted by $n_i=c_i \cdot V_i$. For the empty pore volume in the cement paste, the number of moles n in the adsorption layer can be determined by:

$$n = n_\sigma + n_{liquid} + n_{gas} \tag{4.2}$$

where n_σ is the number of moles adsorbed to the pore wall area, n is the total number of moles involved in the total system, n_{liquid} is the number of moles in the water phase (capillary water) and n_{gas} is the number of moles present in the gas phase of the system (gas in empty pores). The total thickness of the adsorption layer on the pore walls can be determined by:

$$\Gamma = \frac{n_\sigma}{A_{por}(\alpha)} \tag{4.3}$$

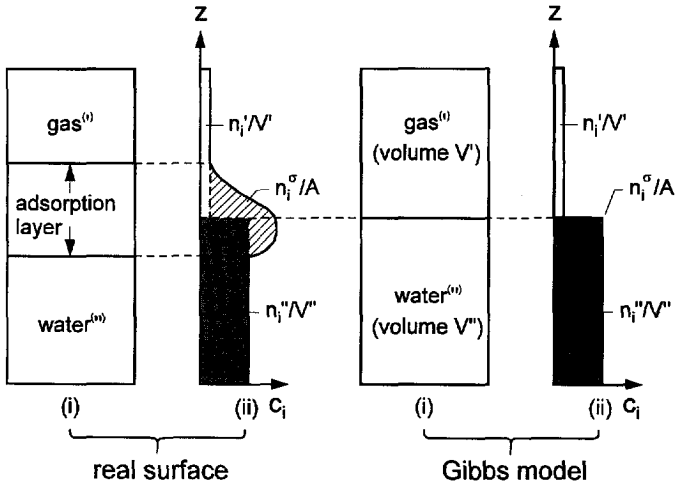

Fig. 4.3. Schematical representation of the liquid-interface-gas system (taken from [23]). Left: Real situation. Right: Gibbs model.

where $A_{por}(\alpha)$ is the total pore wall area (see also Fig 3.6). From this equation, it can be seen that the thickness of the adsorption layer is also a function of the degree of hydration.

Considering the three phase system as described above, an infinitesimal change of the mechanical work dW in the pore system can be formulated as follows:

$$dW = d(p_g V_g) - d(\sigma A_{por}) = 0 \tag{4.4}$$

where p_g is the gas pressure in the empty pores, V_g the volume of the gas in the empty pores, σ the surface tension (free surface energy) and A_{por} the surface area that is submitted to the surface tension. Elaboration of this equation leads to:

$$dp_g V_g + p_g dV_g = d\sigma A_{por} + \sigma dA_{por} \tag{4.5}$$

Within an incremental change of the hardening process, it is considered that the gas volume) as well as the pore wall area A_{por} remains constant (dV_g=0 and dA_{por} =0). Due to these restrictions, equation (4.5) reduces to:

$$\frac{d\sigma}{dp_g} = \frac{V_g}{A_{por}} \tag{4.6}$$

which describes the change of the surface tension in the adsorption layer as a function of the gas pressure in the empty pore volume. The gas volume is considered to be governed by "ideal" gas conditions. According to the ideal gas law, for the volume of the adsorbed it holds that:

$$\frac{p_g V_g}{T} = n_\sigma R \tag{4.7}$$

From this equation, the gas volume can be expressed as a function of the pressure that prevails in the gas. Combining the equations (4.6) and (4.7) leads to the following relationship between the surface tension in the adsorption layer and the gas pressure in the empty pore volume:

$$\frac{d\sigma}{dp_g} = \frac{RTn_\sigma}{p_g A_{por}(\alpha)} \tag{4.8}$$

with R the general gas constant and T the absolute temperature. Substitution of equation (4.3) in (4.8) and integration leads to the basic equation (4.9):

$$\sigma = RT \int_{p_g/p_0}^{p_g/p_0=1} \Gamma \, d\left(\ln(p_g / p_0)\right) \tag{4.9}$$

in which p_g/p_0 is the relative humidity in the empty pore space. The thickness of the adsorption layer $\Gamma=\Gamma(p_g/p_0)$ is considered only to be a function of this relative humidity. For a hardening cement paste, the relative humidity in the gradually emptying pore space decreases as hydration proceeds. From equation (4.9), it can be noticed that the surface tension in the surface layer will increase if the relative humidity in the pore space changes. With this equation, thermodynamic equilibrium in the pore space can be established iteratively.

4.2.5 Adsorption layer at the pore wall area

Due to the existence of adhesion forces [21], vapour molecules tend to be adsorbed on the surface of a pores of a porous material. Generally, the thickness of this adsorption layer is restricted. The adsorbed molecules are in thermodynamic equilibrium with the gas phase in the empty pore space. On the other hand, the amount of adsorbed molecules is determined by the relative pressure in the gas, i.e. the relative humidity, and also by the curvature of the interface. At decreasing pressure, water molecules will desorb from the surface layer. The surface tension σ in the adsorption layer appears to be a function of the thickness of the adsorption layer Γ (see eq. (4.9)) and of the relative pressure in the pore system p_g/p_0. As the thickness of the adsorption layer is a function of the relative pore pressure, a change in pore pressure will affect the thickness of the adsorption layer as well as the surface tension in the adsorption layer. The relationship between the thickness of the adsorption layer and the relative pressure in the pore system has been investigated by several authors [2, 23, 38, 62]. In [38], Hagymassy describes the thickness of the adsorption layer in terms of the number of mono-molecular layers (Fig. 4.4). At a relative pore pressure of 1.0 about 6 mono-molecular layers are adsorbed to the pore wall area. Considering the thickness of one mono-layer to be equal to 3 Å, the thickness of an adsorption layer can reach a maximum thickness up to 18 Å. This order

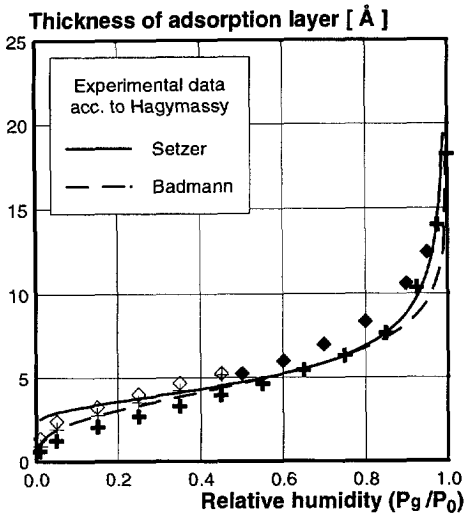

Function proposed by

Setzer: $\Gamma = 3\left(\frac{-c_1}{\ln(p_g / p_0)}\right)$

Badmann:

$\Gamma = \{c_2 - c_3[\ln(-\ln(p_g / p_0)]\}$

where:

c_1=2.7, c_2=3.95 and c_3=1.89

Fig. 4.4 Schematical representation of the state of water in the pore system as measured by Hagymassy [38].

of magnitude of thickness of the adsorption layer has also been found by Badmann et.al. [4]. In [21], Cuperus visualised the adsorption layer by application of ultra filtration technique in combination with SEM scanning. With this techniques he could measure the thickness of the adsorption layers ranging from 20 Å to about 30 Å.

4.2.6 Relative humidity in empty pore space

Directly after setting, the microstructure of a hardening cement paste starts to develop. This is accompanied by the development of a pore structure (see also Fig. 3.6). Initially, the relative humidity in the pore system (space) is equal to 100% and the pressure in the system is equal to the atmospheric pressure. With progress of the hydration process, water is consumed by the anhydrous cement to form new hydration products. Due to this process, parts of the pores remain filled with capillary water and parts of the pores become empty. At this stage of hardening, the relative humidity in the empty pore space will drop below 100%. Implicitly, the reduced pressure in the empty pore space will be lower than the atmospheric pressure. In HYMOSTRUC, the relative humidity RH=p_g/p_0 in the empty pore space is modelled according the Kelvin equation [23, 36] for tubular shaped pores:

$$\ln(RH) = \ln\left(\frac{p_g}{p_0}\right) = \frac{-4\sigma}{RT\gamma_w\phi_{wat}} \qquad (4.10)$$

in which ϕ_{wat} is the widest pore diameter that is still completely filled with water (see Fig 3.6), and σ the actual surface tension in the adsorption layer at the pore wall area (eq. (4.6)). The Kelvin equation describes the variation of the relative humidity as a function

of the pore diameter ϕ_{wat} and also as a function of the actual surface tension σ. Both the pore diameter ϕ_{wat} and the actual surface tension σ will change as hydration proceeds. Both parameters depend on the actual volume of capillary water that is available in the system. A further reduction of the capillary volume caused by progression of the hydration process, will result in a decrease of the pore diameter that is still completely filled with water and an increase of the surface tension in the adsorption layer. Together, they determine the relative humidity in the empty pore space.

4.2.7 Gas pressure in empty pore space

The pressure in the empty capillary pore space can be determined with Boyle's law by considering a closed medium that contains a certain volume of water which is in equilibrium with a certain volume of gas. This pressure in the gradually emptying pore space p_g can be determined by [45, 78, 99]:

$$p_g = \frac{RT}{V_w} \ln(RH) \tag{4.11}$$

where $RH=p_g/p_o$. (p_g=gas pressure, p_0 = atmospheric pressure). Several authors have shown that the relative humidity in the pore system of plain pastes, generally, ranges between 80% and 100%, while under sealed conditions [45, 78, 100]. Powers [67] suggested that there would exist a lower boundary value of 75% for the relative humidity that can minimally be reached. According to equation (4.11), a relative humidity in the pore space that ranges between the 75% and 100% associates with a pressure in the empty pore space that ranges between ca. -35 MPa and 0 MPa, respectively. These relative high values of reduced pressure in the pore space may lead to substantial deformations of the microstructure of cement paste. Since the relative humidity is a function of the degree of hydration, the pressure in the empty pore space will be a function of the degree of hydration as well. Therefore, the proposed microstructural deformations, induced by the pressure, will also be a function of the degree of hydration. The way how this internally induced deformation can be modelled will be discussed in the next section.

4.2.8 Surface tension in the adsorption layer

The surface tension in the adsorption layer will increase if the thickness of this layer decreases. With the HYMOSTRUC model, this relationship is calculated for a hardening cement paste. The result of this calculation is presented in Fig. 4.5. From this figure, it can be seen that the surface tension in the adsorption layer increases form 0 to about 0.04 N/m while the thickness of the adsorption layer drops from 18 Å to about 6 Å.

This tension in the adsorption layer increases if hydration proceeds. This means that this surface tension, which acts on the microstructure from the interior, may be responsible for a certain deformation of the hardening microstructure. The way how this can be modelled will be elucidated in the next section.

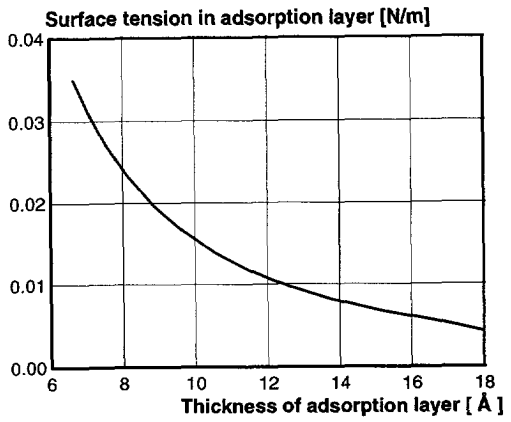

Fig. 4.5. Surface tension in adsorption layer versus thickness of the adsorption layer, calculated with HYMOSTRUC.

4.3 Deformation of the cement paste

4.3.1 General

As hydration proceeds, the relative humidity in the gradually emptying pore space will decrease. From a thermodynamic point of view, the relative humidity can be considered as the main parameter in a system. All parameters that are involved in a thermodynamic system change if the relative humidity, viz. the relative gas pressure, in that system changes. This means that a change of the relative humidity in a closed system goes along with a change of the gas pressure in the empty pore space as well as with a change of the surface tension in the adsorption layer at the pore wall area (see eq. (4.9)).

The surface tension can be considered as a driving force behind the contraction of the hardening system. The surface tension can be determined by combining thermodynamic concept and the HYMOSTRUC concept. In the next sections, the constitutive equation as originally proposed by Bangham, will be adopted to relate the microstructural deformation to the surface tension in the adsorption layer. In this way, the microstructural deformations of a hardening cement-based material are also related to the relative humidity in the gradually emptying pore space (self-desiccation). This mechanism is considered to be responsible for the *autogenous shrinkage* of a hardening cement-based material. According to the constitutive equation of Bangham, microstructural deformation depend on the elastic modulus, the specific mass of the cement paste and the pore wall area of the empty pore space (see appendix D). These parameters as well as the mechanism with which the deformation can be described will be discussed hereafter.

4.3.2 Deformation mechanism

It was Bangham (1937) [5] who related the external deformation of coal to the surface tension in the adsorption layer formed at the pore wall area. In several papers [5, 6, 7] Bangham used the adsorption equation of Gibbs to describe this phenomenon. Bangham used his theory to point out that with solid surfaces, as opposed to liquid surfaces, the surface energy, representing the work spent for the formation of a unit of new surface, must thermodynamically be in equilibrium with the pressure. In his work, he considered a three-phase system as discussed in the previous sections (see section 4.2.4). He found that a change of the expansion of coal could be related linearly to the change of the surface energy in the adsorption layer. This approach has been shown to be valid for hardened cement paste by, among others, Wittmann [100]. For hardened cement paste, the material properties are totally developed. When dealing with hardening cement paste, the material properties change continuously with progress of the hydration process. Therefore, relationship between the external deformation and the surface tension must be considered incrementally and can be formulated as follows:

$$\frac{\partial \varepsilon_a}{\partial \alpha} = \lambda \cdot \frac{\partial \sigma}{\partial \alpha} \tag{4.12}$$

where $\partial\varepsilon_a$ is the strain increment that describes the microstructural deformation of the hardening paste (autogenous shrinkage due to self-desiccation), $\partial\sigma$ the surface tension increment (see eq.(4.9)) and λ a proportionality factor. In fact, this proportionality factor is the compliance modulus of the hardening material, e.g. cement paste.

The proportionality factor λ, that relates the microstructural deformation to the surface tension in the adsorption layer, has been discussed by several authors [7, 39, 69, 103]. Minor differences appear between the relations as proposed by these authors. According to Bangham [7], this constitutive relation has the following shape:

$$\lambda = \frac{\Sigma \cdot \rho}{3\,E} \tag{4.13}$$

where Σ is the pore wall area per unit weight, ρ the density of the material and E the Young's modulus. In [102], Wittmann used a similar relation to model the swelling deformation of hardened cement paste. In his model, the pore wall area Σ, the density ρ and the Youngs modulus are taken as being constant. For hardening cement paste, however, these parameters can not be considered as constant values. The parameters change throughout the hardening process. Therefore, the relation (4.13) has to be adjusted in order to be applicable for modelling volumetric changes of hardening cement-based materials. In this respect, the pore wall area requires due attention. As hydration proceeds, pores will be emptied. This implies that a certain part of the pore wall area borders on the capillary pore water (filled pores) and a remaining part borders on pore gas (empty pores). Since water is assumed to be incompressible, only the empty pores are considered to be able to deform. This implies that only the pore wall area of the

empty pores has to be considered in the description of the volumetric changes. This is also required from a thermodynamic point of view, since the load that acts on the microstructure from the interior, is manifested by the empty pores.
Therefore, the proposed constitutive equation has the following shape.

$$\lambda(\alpha, RH, wcr) = C\frac{(A_{por}(\alpha) - A_{wat}(\alpha, RH))\cdot \rho_{pa}(wcr)}{E_p(\alpha)} \qquad (4.14)$$

where: $A_{por}(\alpha)$-$A_{wat}(\alpha,RH)$ = pore wall area of the empty pores
$\rho_{pa}(wcr)$ = specific mass of the cement paste
$E_p(\alpha)$ = modulus of elasticity of the cement paste
C = constant = 3

What is striking in constitutive relation (4.14) is that, besides the degree of hydration and the water/cement ratio, the proportionality factor λ depends also on the relative humidity in the empty pore space. For the time being, no restrictions apply as regards the relative humidity limits. This means that this constitutive equation therefore also have the potential to determine the swelling of oven-dried hardened cement-based materials that are exposed to moisture. This will be shown in section 4.3.6. As can be noticed from equation (4.14), the changing pore wall area and the development of the modulus of elasticity play an important role in the simulation of the volumetric changes of the microstructure (autogenous shrinkage) during hardening.

4.3.3 Pore wall area of the empty pores

The pore structure of a hardening cement paste is modelled according to the method as was used by van Breugel (see eq. (3.1) and (3.2)) [16]. The pore structure of cement paste consists of narrow gel pores of a diameter up to about 20Å and of wider capillary pores. With an increasing degree of hydration, the pore volume decreases, mainly at the cost of the larger pores. The water available for hydration accumulates in the smaller pore regions and the largest pores are emptied. Depending on the relative humidity in the pores, an adsorption layer of a certain thickness will exist in the pores. Van Breugel proposed to divide the total volume of capillary water in the pore system into a part that is adsorbed to the pore wall area and a remaining part, called "free capillary water" that is available for further hydration (see Fig. 3.6). From this modelling approach it is possible to calculate the total pore wall area of those pores that are still completely filled with water. From geometrical consideration of the pore system it can be derived that for the pore wall area of the empty pores it holds (see also appendix D):

$$A_{por}(\alpha) - A_{wat}(\alpha, RH) = -4\cdot a\left(\frac{1}{\phi_{por}(\alpha)} - \frac{1}{\phi_{wat}(\alpha, RH)}\right) \qquad (4.15)$$

where "a" is the pore structure constant (see section 3.2.3.4 and 3.3.5), $\phi_{por}(\alpha)$ is the maximum pore diameter involved in the pore structure and $\phi_{wat}(\alpha,RH)$ is the pore

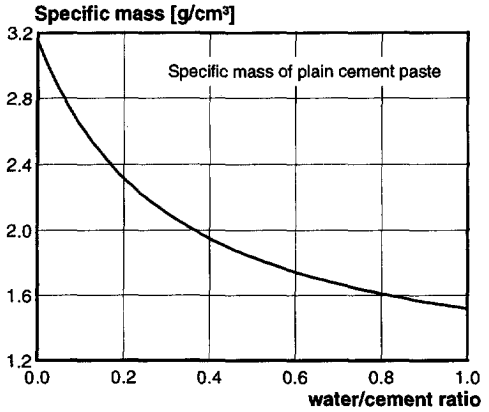

Fig. 4.6. Specific mass ρ_{pa} as a function of the water/cement ratio.

diameter of the pores that are still completely filled with water. If $\phi_{wat}(\alpha,RH)$ is equal to $\phi_{por}(\alpha)$, all pores in the system are filled with water. For that particular situation, the relative humidity is equal to 100%. For this case it can be derived from the equations (4.15) and (4.13), that there will be no contraction of the microstructure. As hydration proceeds, the pores will be emptied, the relative humidity will drop down, the surface tension will increase and the microstructure will deform according to the formulation as given in (4.13).

4.3.4 Specific mass of plain cement paste

In the deformation mechanism as described with equation (4.12) depends also on the specific mass of the cement paste. The specific mass of the cement paste appears to be depending on the water/cement ratio and on the specific density of the cement. The specific mass of cement paste can be calculated with equation (4.16).

$$\rho_{pa} = \frac{\rho_{ce} \cdot (1+\omega_0)}{1+\rho_{ce}\omega_0} \tag{4.16}$$

The relationship between the specific mass and the water/cement ratio is shown in, Fig. 4.6. In this figure, specific density of the cement ρ_{ce}=3.15 g/cm³ was adopted.

4.3.5 Modulus of elasticity of hardening cement paste

Several authors have proposed models to predict the elastic modulus of hardening cement paste as a function of the degree of hydration [37, 56, 58, 94]. In [59], Lokhorst suggested to relate the formation of the microstructure to the amount of contact zones that are formed between the spatially distributed cement grains. In his view, distinction should be made between formation of clusters, represented by a system (group) of hydrating cement particles, and the formation of so called "bridges", which are considered to be able to make contact between the hydrating cluster systems (see Fig. 4.7). For quantification of the bridge volumes and the cluster volumes which are

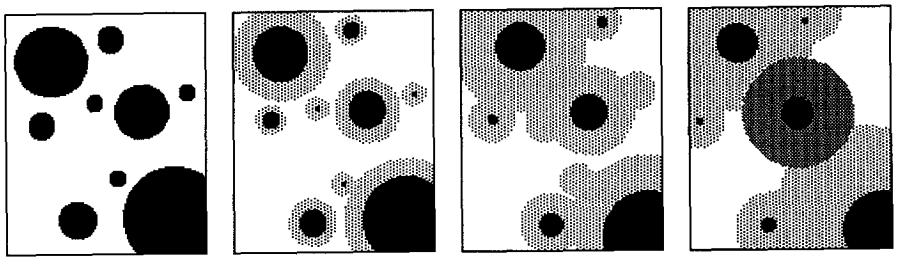

a) initial stage | b) early hydration | c) "clusters" first embedding | d) "bridging" between clusters

Fig. 4.7 Formation of a load-bearing microstructure in hardening cement paste.

involved in this process, the HYMOSTRUC model has been applied.
The stiffness of the microstructure depends on the stiffness of the independent cement particles and on the stiffness of the hydration products. The elastic modulus is determined by considering a series model for the contributions of the anhydrous cement volume, the cluster volume and the bridge volume. The individual contributions change continuously during the hardening process. In Fig. 4.8, the elastic modulus according to the proposed model is compared with experimental results that were published by Ghosh et.al. [31, 32]. Two cement pastes are considered that contain cement of medium fineness (Blaine 477 m²/kg) and a w/c ratio of 0.3 and 0.5. The results show fairly good agreement with the numerical simulations according to Lokhorst's model. The satisfactory results support the interpretation of the mechanism behind the model, e.g. the various volume components and their contribution to the development of the stiffness of the hardening cement-based system.

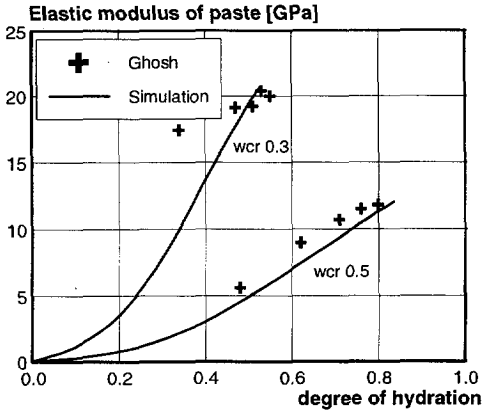

Fig. 4.8. Elastic modulus of cement paste versus the degree of hydration. Numerical simulation compared with experimental results (Simulations with HYMOSTRUC [59]).

4.3.6 Validity range of the thermodynamic approach

Several authors have proposed validity ranges for models that describe the swelling of a hardened oven-dried cement-based material (like cement paste, see section 4.2.3) on the basis of a thermodynamic approach. In [8] Bazant and Wittmann gave boundary limits for the relative humidity and also Setzer [80] gave almost similar ranges within which this thermodynamic approach would be valid. They stated that the Bangham approach for describing swelling of a hardened oven dried cement paste that is exposed to water is only applicable within a relative humidity range of 0% and 40%. Within this range they observed a linear relationship between the stresses in the adsorption water layer at the pore wall area (surface tension) and the external swelling deformation of the sample (Gibbs-Bangham effect) (see also Munich model Fig. 4.2). At a relative humidity higher than 40%, a non-linear relationship between the external swelling deformations and the surface tension in the adsorption layer is observed (see Fig. 4.2). This non-linear swelling is considered to be caused by the so called disjoining pressure. The way how this disjoining pressure is related to the external swelling deformations is not modelled explicitly in the Munich model (see Fig. 4.9).

According to the Munich model, the relationship between the external deformations and the surface tension in the adsorption layer is determined by the proportionality factor λ (see eq. (4.12)). This relationship is assumed to be constant within the relative humidity range of 0 and 40%.

For a hardening cement-based material, the situation is different. The relative humidity changes and is generally larger than 40%. The pore wall area of the empty pores as well

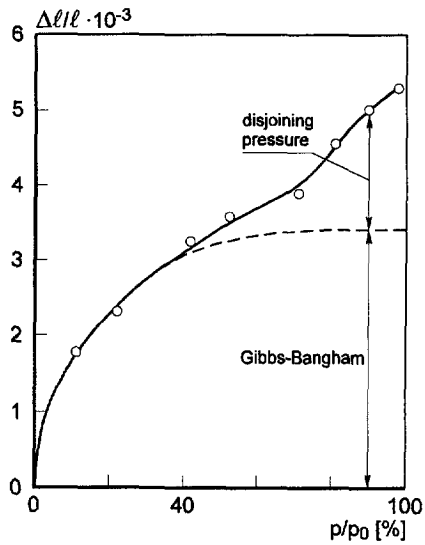

Fig. 4.9. Schematic representation of the different mechanisms which are responsible for swelling of hardened cement paste according to the Munich model.

as the elastic modulus change also continuously as hydration proceeds. This means that the proportionality factor $\lambda=\lambda(\alpha,RH,wcr)$ (see eq. (4.14)) is not a constant, but it depends on the stage of the hardening process as well as on the water/cement ratio and it also depends on the relative humidity in the empty pore space.

Consider the experimental results as were published by Feldman [26] and Klug [46] (see also Wittmann [102]). Feldman determined the length change of an oven-dried hardened cement paste with water/cement ratio of 0.5 which was exposed to different moisture conditions. Klug carried out similar tests for a cement paste with a water/cement ratio of 0.4. In both cases, the specimens experienced a relative humidity that ranged between the 0 and 100%.

According to the proposed calculation procedure as given in the previous paragraphs, a change of the relative humidity is associated with a change of the thickness of the adsorption layer at the pore wall area (Fig. 4.4) and also with a change of the surface tension in the adsorption layer (eq. (4.9)). From equation (4.12), it can be seen that this will also effect the swelling deformation. The degree of saturation of the pore space will increase proportionally to the increase of the relative humidity. This means that, if the relative humidity increases, the pore wall area of the empty pores (A_{por}-A_{wat}) will decrease. This will also affect the swelling behaviour of the hardened cement paste. In equation (4.14), these influences are considered to be dependent on the relative humidity. The elastic modulus and the specific density of the paste are constant.

In Fig. 4.10, the experimental results as published by Feldman and Klug are compared with simulations as obtained with the proposed model. On the left hand side, the swelling deformation is presented as a function of the relative humidity. Over the relative humidity range from 0 - 100%, the simulations agree very well with the experimental results (see appendix D). The results are calculated with the changing proportionality factor $\lambda(\alpha,RH,wcr)$ (see eq. (4.14) and also Fig. 4.11, left). Due to this, the calculation of the

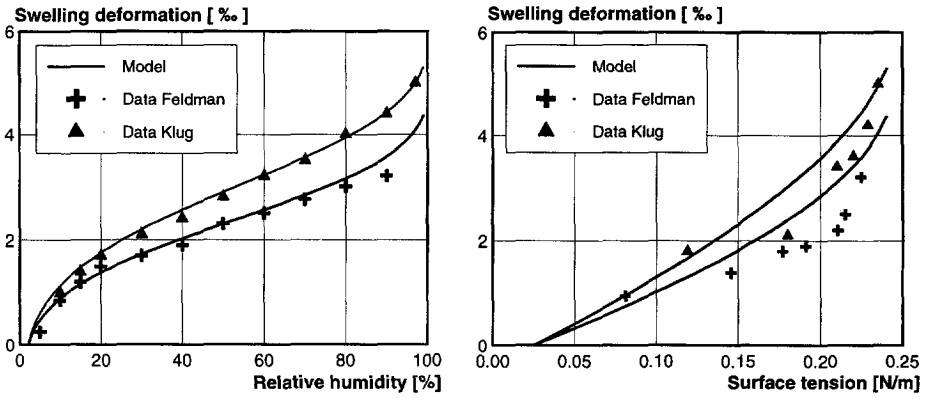

Fig. 4.10. Left: Swelling deformation vs relative humidity. Right: Swelling deformation vs surface tension. Model results compared with experimental data of Feldman and Klug.

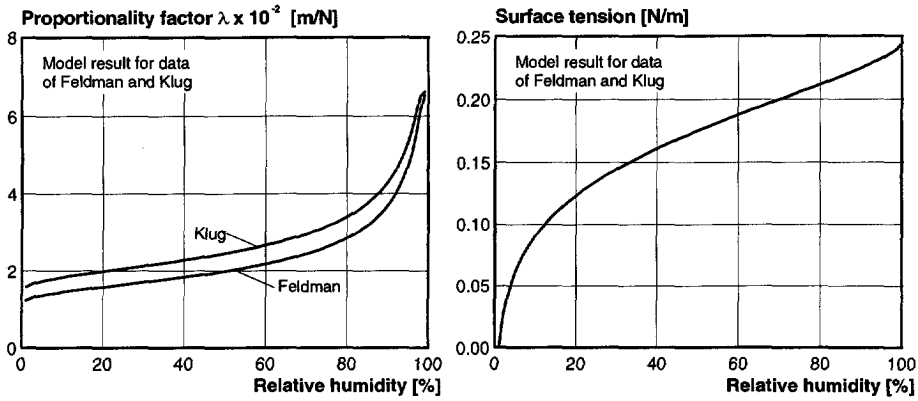

Fig. 4.11. Left: Proportionality factor λ versus the relative humidity. Right: Surface tension in the adsorption layer versus the relative humidity.

Table 4.1. Input values as adopted in the model to calculate the swelling deformation.

Author	wcr	α	E_{paste} [MPa]	"a"	ϕ_0 [μm]
Feldman	0.5	0.8	10	0.1	0.002
Klug	0.4	0.75	18	0.1	0.002

swelling deformation must be executed incrementally. This is in contrast with the Bangham model where the proportionality factor λ is assumed to be constant.

By considering only the empty pore wall are (A_{por}-A_{wat}) in the constitutive equation (4.14), the distinction between the different mechanisms as considered in the Munich model (Gibbs-Bangham and the disjoining pressure) disappears. This also holds true for the surface tension in the adsorption layer. From Fig. 4.10 (right), it can be seen that the model calculates an almost constant rate of swelling with increasing surface tension. However, at higher values of the surface tension (σ >0.2 N/m), a stronger incline of the swelling deformation can be observed.

On the left hand side of Fig. 4.11, the proportionality factor λ is shown as a function of the relative humidity. From this figure it can be seen that the proportionality factor is almost constant up to a relative humidity of 60%. For a relative humidity between 60% and 100%, the proportionality factor increases strongly. This can be attributed to the fact that the growth of the adsorption layer at the pore wall area goes at the cost of the free capillary water in the pore space (see appendix D).

On the right hand side of Fig. 4.11, the development of the surface tension in the adsorption layer is presented as a function of the relative humidity. In fact, this is the integral which is solved for a relative humidity range between the 0 and 100% (eq. (4.9)). The thickness of the adsorption layer is assumed to change according to the data

as given by Hagymassy (see Fig. 4.4). This relation is adopted for both the simulation of the experiment of Feldman and Klug.

From the figure, it can be seen that the surface tension in the adsorption layer increases continuously with increasing relative humidity. This means that the stress that acts from the interior on the microstructure of the hardened cement paste increases with increasing relative humidity. This also affects the swelling deformation (see eq. (4.12)). The swelling deformation increases with increasing surface tension. This seems to conflict with the results as presented in Fig. 4.5, however, from equation (4.10), it can be seen that for hardening cement paste, the diameter of the pores that are still completely filled with water is decreasing with progress of the hydration process. Since for hardened paste the opposite holds, an opposite behaviour of the surface tension with changing thickness of the adsorption layer will be found.

4.3.7 Discussion

From the results given in the previous section, it appears that the proposed model is quite able to simulate the swelling deformation of a hardened oven-dried cement paste which is exposed to a relative humidity range between the 0 and 100%. For this relative humidity range from 0 to 100%, the swelling deformation can be modelled on the basis of one mechanism. This mechanism is based on the surface tension in the adsorption layer. In the proposed model only the empty pores are taken into account in the description of the constitutive equation (A_{por}-A_{wat}) (see eq. (4.14) and appendix D). Due to this, the proportionality factor λ becomes depend on the relative humidity. This makes the model

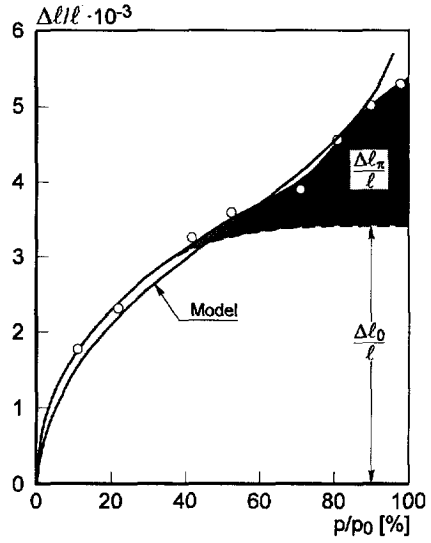

Fig. 4.12. Swelling of a hardened cement paste versus the relative humidity as presented by Wittmann [102]. The model result is also inserted in the figure.

also valid for a relative humidity higher than 40%. The modelling approach turned out to lead to an accurate description of the swelling deformation of a hardened cement paste (see Fig. 4.12).

For hardening cement-based material, besides the relative humidity also the degree of hydration changes throughout the hardening process. The relative humidity in the gradually emptying pore space is an unknown parameter which must be calculated from the actual moisture state of the hardening cement paste. After mixing, the relative humidity will be about 100%. During hydration, this value will drop. This goes along with a so called self-desiccation of the hardening microstructure. Thermodynamic equilibrium requires an increase of the surface tension in the adsorption layer. These stresses act on the interior of the hardening microstructure and introduce autogenous shrinkage. The constitutive relation that relates the autogenous shrinkage to the surface tension in the adsorption layer is similar to the relation which is adopted to describe the swelling deformation (eq. (4.14)). The only difference is that for hardening cement-based material, the elastic modulus also change during hardening.

The way to establish thermodynamic equilibrium in the continuously changing pore space will be outlined and discussed in the next section. After this, a parameter study will be performed where the main parameters which are involved in the thermodynamic analysis will be varied and discussed.

4.4 Flow chart of the iteration procedure

4.4.1 General

Thermodynamic equilibrium in the gradually emptying pore space can only be established iteratively. This is because of the fact that several relationships involved in the proposed model are implicit functions. This means that for these relationships no direct solution can be obtained.

The way how thermodynamic equilibrium is established in the HYMOSTRUC model will be outlined with the help of a flow chart. This chart is shown in Fig. 4.13. In the next section, the steps of the numerical iteration procedure will be discussed briefly.

4.4.2 Description of the flow chart

In Fig. 4.13, the flow chart of the iteration procedure is presented. The procedure starts with the update of the state of the hydration process. After this, the degree of hydration is a known parameter. From this, the total capillary pore volume, the total pore wall area and the actual volume of capillary water can be determined. With this information, the state of the water in the pore system is determined (see Fig. 3.7). The iteration procedure to establish thermodynamic equilibrium starts with the initialisation of the relative humidity, the thickness of the adsorption layer and the surface tension in the adsorption

layer. From this situation, the volume of water that is adsorbed at the pore wall area can be determined as well as the volume of water that is available for further hydration. Together, these contributions must be equal to the actual volume of capillary water in the pore space.

From the capillary water volume that is available for further hydration and the proposed pore size distribution (eq. (3.1)), the maximum pore diameter can be determined of the part of the pores that is still completely filled with water. From this, the accompanying wetted pore wall area can be calculated. At this stage of the iteration procedure, a more accurate approach of the relative humidity in the empty pore space can be calculated (eq. (4.10)). For this, the maximum pore diameter of the filled pores and the surface tension at the pore wall area is required. A change of the relative humidity will also affect the thickness of the adsorption layer at the pore wall area (Fig. 4.4). The new estimation of the thickness of the adsorption layer is necessary to determine the actual surface tension in this layer. Equation (4.9) must be solved for this purpose.

After these calculations, the relative humidity in the empty pore space can be compared with the initial value of the relative humidity. If there is a difference between these values, thermodynamic equilibrium has not yet been established and the iteration process must continue. The newly calculated values for the relative humidity, the thickness of the adsorption layer and the surface tension in the adsorption layer are considered as the initial value for the next calculation loop. This procedure goes on as long as the relative humidity in the empty pore space is not in agreement with the cut-off value of the required accuracy. Then thermodynamic equilibrium has been established.

The next step in the calculation procedure is the calculation of the proportionality factor λ (see eq. (4.14)). Together with the surface tension in the adsorption layer, the autogenous shrinkage increment of the hardening paste can be determined. After this, a new hydration increment can be determine with the HYMOSTRUC model and the iteration procedure will be repeated.

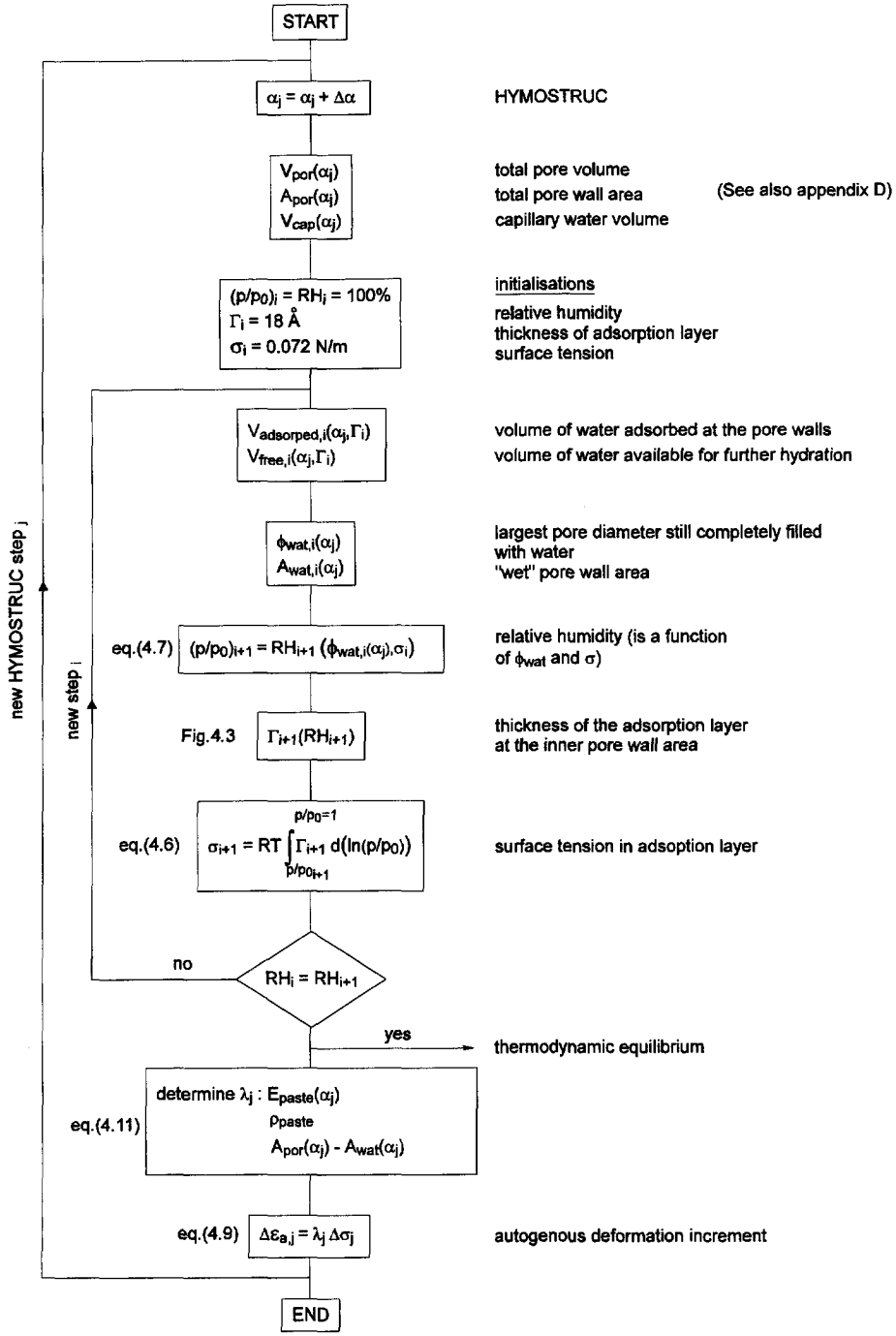

Fig. 4.13. Flow chart of the iteration process to establish thermodynamic equilibrium.

4.5 Parameter study and model features

4.5.1 General

In this section, the parameters that are involved in the proposed model to establish thermodynamic equilibrium in the emptying pore space will be discussed and the model features will be investigated by means of a parameter study. The validation of the model is chosen this way since the parameters that play a role in the model are active on a micro-scale level. It is hard to measure these parameters on that particular level. Therefore, three different water/cement ratios will be considered in the parameter study, for cement pastes of three different finenesses. The proposed parameters are listed in Table 4.2.

It must be noticed that all calculations are performed with the adoption of the same pore structure constant of "a"=0.1, and isothermal curing conditions at 20 °C.

The parameter study starts with a discussion on the evolution of the degree of hydration of the different cement pastes. After that, all parameters involved in the model will be presented and discussed.

4.5.2 Evolution of the degree of hydration

The evolution of the degree of hydration can be simulated numerically with the HYMOSTRUC model. In a systematic calculation procedure, the increase of the overall degree of hydration is determined by adding up the contributions of the individual particle fractions. These contributions are determined from the progress of the reaction front into the individual cement particles. For the rate of penetration of the reaction front in a cement particle, a *basic rate equation* is proposed [16] in which the effects of the formation of microstructure, i.e. of the interaction between hydrating and expanding particles and the rate of hydration, is explicitly accounted for. The basic rate equation comprises five reduction factors. These five factors comprise:

1. Differentiation between a phase-boundary and a diffusion controlled reaction process.
2. Water withdrawal by small particles which are embedded in the outer shell of larger particles.
3. The effect of the distribution of capillary water in the pore system.
4. The amount of capillary water in the pore system.
5. The effect of curing temperature on the rate of penetration of the reaction front.

Table 4.2. Overview of variations for parameter study.

Parameter	Variation
Water/cement ratio:	0.3, 0.4, 0.5
Cement fineness [m^2/kg]:	300, 420, 550

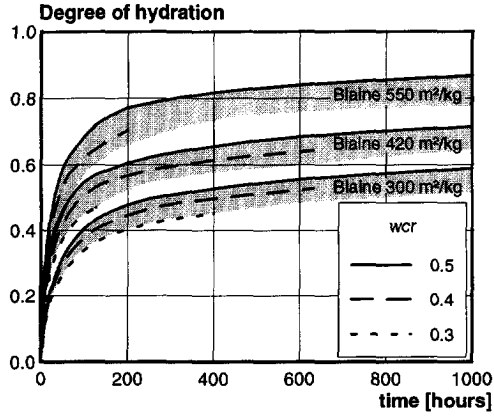

Fig. 4.14. Calculated degree of hydration versus time for pastes with three cements with different fineness and a water/cement ratio of 0.3, 0.4 and 0.5.

With the basic rate equation, the volume of hydration products which are formed on a micro-scale level can be determined. In order to obtain information about the actual state of the hydration process, the volume of hydration products must be related to the total volume of cement that is available in the cement paste. The rate at which the hydration products are formed depends on several parameters. In this respect, two dominant parameters are the particle size distribution and the water/cement ratio. In the HYMOSTRUC model, the influence of these parameters on the rate of the hydration process is dealt with explicitly.

For a plain Portland cement paste, the influence of the fineness of the cement and the water/cement ratios on the degree of hydration is shown in Fig. 4.14. The cement type with the highest fineness shows the highest rate of hydration.

It will be investigated numerically, how the changes in the cement fineness and the water/cement ratio affect the:

- Relative humidity in the empty pore space
- Thickness of the adsorption layer in the pore space
- Gas pressure in the empty pore space
- Surface tension in the adsorption layer

For these parameters, results as calculated with the proposed model will be presented and discussed briefly.

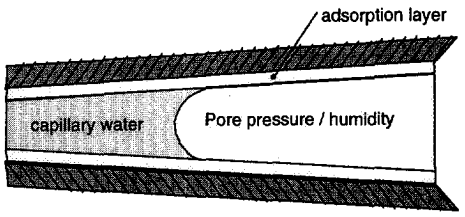

Fig. 4.15. Schematical representation of the capillary pore system.

4.5.3 Relative humidity in the empty pore space

The relative humidity in the gradually emptying pore space can be determined by the equation as proposed by Kelvin (see also section 4.2.4). In this equation, the relative humidity is defined as the ratio between the gas pressure in the empty pore space p_g and the atmospheric pressure p_0 (see also Fig. 4.15). According to Boyle's law, the pressure in the gas is related to the volume of this gas. For the hardening cement paste, the volume of the empty pore space is a measure for the relative humidity that will prevail. Low water/cement ratio pastes will, therefore, show a lower relative humidity in the pore space than a paste with a higher water/cement ratio. This phenomenon can also be observed from Fig. 4.16. On the left hand side, the development of the relative humidity is shown for three different water/cement ratio's (0.3, 0.4 and 0.5). For a water/cement ratio of 0.3, the relative humidity drops from 100% to a level of about 75% after a hardening period of 1000 hours. For the higher water/cement ratio pastes, the relative humidity remains substantially higher. After 1000 hours of hydration process, the pastes with a water/cement ratio of 0.4 and 0.5 reach a relative humidity of about 86% and 95% respectively.

On the right hand side of Fig. 4.16, the relative humidity is presented for a cement paste

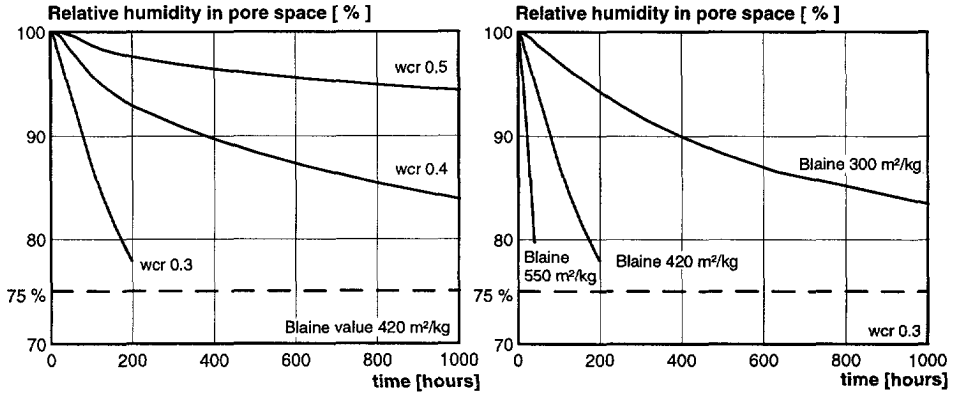

Fig. 4.16. Relative humidity in the empty pore space versus time. Left: Three different water/cement ratios. Right: Three different finenesses of the cement.

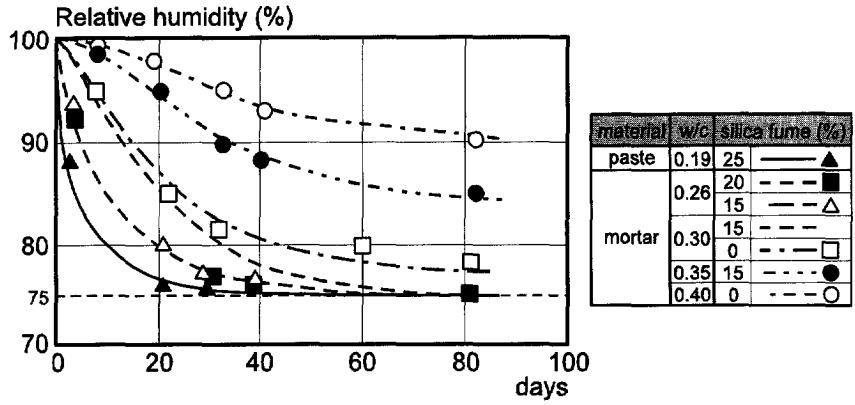

Fig. 4.17. Relative humidity versus time for different water/cement ratios ([44]).

with a water/cement ratio of 0.3 and with cements of different finenesses. A rather coarse type of cement (Blaine 300 m^2/kg), a cement of medium fineness (Blaine 420m^2/kg) and a cement of high fineness (Blaine 550m^2/kg) are used to show the influence of the fineness on the development of the relative humidity of a plain cement paste. The relative humidity of the cement paste with a cement of high fineness drops very rapidly whereas the coarser cements show a more moderate behaviour of the reduction of the relative humidity.

From the calculated results presented in Fig. 4.16 it can be noticed, that the relative humidity varies between 100% and 75%. This is in good agreement with the boundary limits as given by Jensen [44] (see Fig. 4.17). Using a thermodynamical approach, he verified the statement of Powers that the relative humidity in cement pastes could not drop below 75%, without artificial drying and under sealed conditions.

In Fig. 4.18, the results shown in Fig. 4.16 are presented as a function of the degree of hydration. It concerns cement pastes with three different finenesses of cement and three different water/cement ratios. The figure shows that according to the model, the decrease of the relative humidity with respect to an increasing degree of hydration would be almost independent of the fineness of the cement. This is not surprising, since for the cements the same pore structure constant "a" has been adopted. The model shows also that the development of the relative humidity appears to be more sensitive to the water/cement ratio. For a relative high water/cement ratio, the relative humidity in the empty pore space will drop very slowly. The formed pore structure will remain filled with capillary water for a long period of time. Depending on the fineness of the pore structure that is formed, the relative humidity will drop to a certain level, This behaviour is most pronounced for the low water/cement ratio pastes.

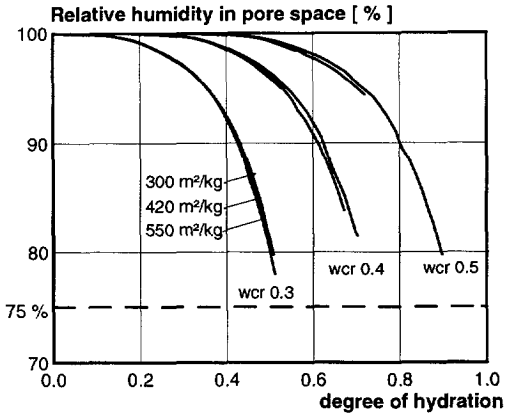

Fig. 4.18. Calculated relative humidity versus the degree of hydration for three different finenesses of the cement and for three different water/ cement ratio's.

4.5.4 Thickness of the adsorption layer in the pore space

As hydration proceeds, capillary water will become consumed by the anhydrous cement. A pore structure will be formed that will be partly filled with water and partly filled with gas. During this process, the under-pressure in the gas may reach substantial values. Due to this, an adsorption layer may be formed to the pore wall area. The thickness of this adsorption layer is a function of the relative humidity in the empty pore space. The relative humidity in the pore space changes continuously during hydration. In Fig. 4.19, the thickness of the adsorption layer is presented as a function of time (left) and also as a function of the degree of hydration (right). Three different finenesses of cement are considered. From the figures it can be seen that the differences which occur in the time domain, disappear if the results are presented in the hydration domain. The thickness of

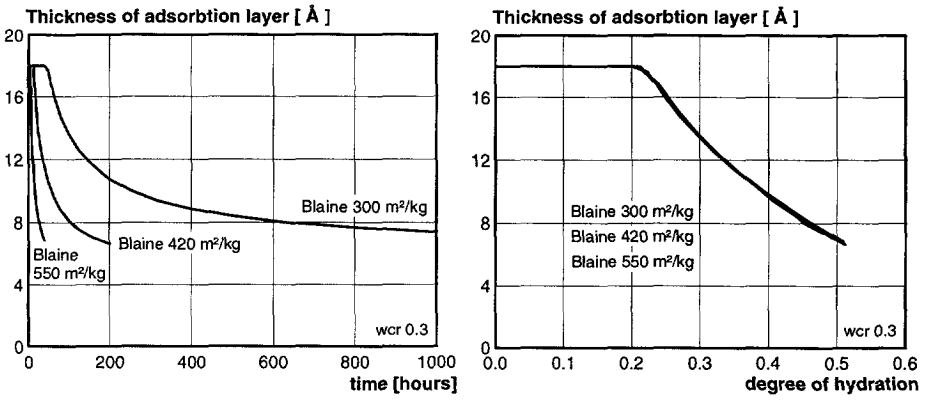

Fig. 4.19. Left: Thickness of the adsorption layer in the capillary pores versus time. Right: Thickness of the adsorption layer versus degree of hydration (different fineness).

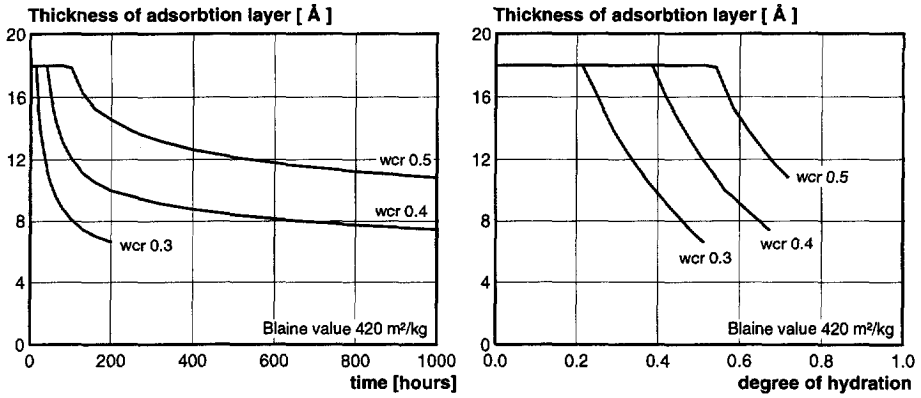

Fig. 4.20. Left: Thickness of the adsorption layer versus time. Right: Thickness of the adsorption layer versus the degree of hydration. Three different water/cement ratio's are considered in both figures.

the adsorption layer follows the same course for each fineness of the cement (at least in the model). In Fig. 4.20, the thickness of the adsorption layer is presented for three different values of the water/cement ratio. It can be seen that the thickness of the layer strongly depends on the water/cement ratio. For low water/cement ratio cement pastes, the thickness of the adsorption layer drops very rapidly to a value of about 6 Å (Fig. 4.20). On the right hand side of Fig. 4.20, the thickness of the adsorption layer is presented as a function of the degree of hydration. For the pastes with a higher water/cement ratio, the thickness of the adsorption layer (see Fig. 4.3) remain constant for a longer period of time. The slope with which the thickness of the adsorption layer reduces, shows to be independent of the water/cement ratio. The cement paste with the lowest water/cement ratio reaches the smallest thickness of the adsorption layer.

4.5.5 Gas pressure in the empty pore space

The balance between the volume of the empty pore space and the gas pressure in this particular space is governed by Boyle's law. At the initial stage of the hardening process, all pores are considered to be filled completely. There will be no gas in the system. At a certain stage of hardening, some pores will be filled with water and some will be filled with gas. This gas appears to be dissolved from the water [91]. The mechanism behind this dissolution process can be described by Henry's law [91, 99].

Establishing thermodynamic equilibrium requires a reduction of the pressure in the empty pore space while the gas volume increases. The gas pressure in the pore system may reach substantial values.

In Fig. 4.21, the gas pressure in the empty pore space is presented for three different finenesses of the cement. The water/ cement ratio of the paste is 0.3. On the left hand

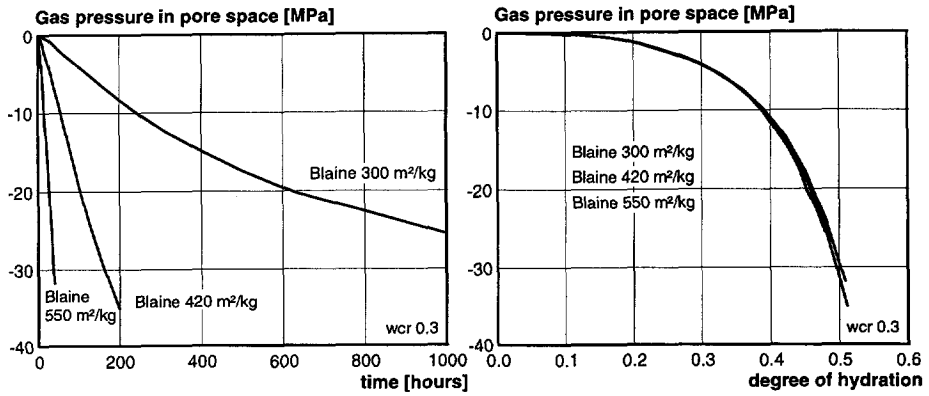

Fig. 4.21. Left: Pressure in capillary pore space versus time. Right: Pressure in capillary pore space versus degree of hydration (different fineness).

side of the figure, the results are given as a function of time, whereas, at the right hand side the results are presented as a function of the degree of hydration. The gas pressure appears to be almost independent on the fineness of the cement. The rate of the hydration process determines the rate at which the gas pressure develops. From the figure it can be seen that the gas pressure in the empty pore space reaches values up to about -35 MPa. This pressure will manifest in the empty pore space of the microstructure. The microstructure may respond by contraction while submitted to this internal pressure.

In Fig. 4.22 the gas pressure in the empty pore space is presented for pastes made with three different water/cement ratio's: 0.3, 0.4 and 0.5. From the results, it can be seen that the water/ cement ratio has a substantial influence on the magnitude of the gas

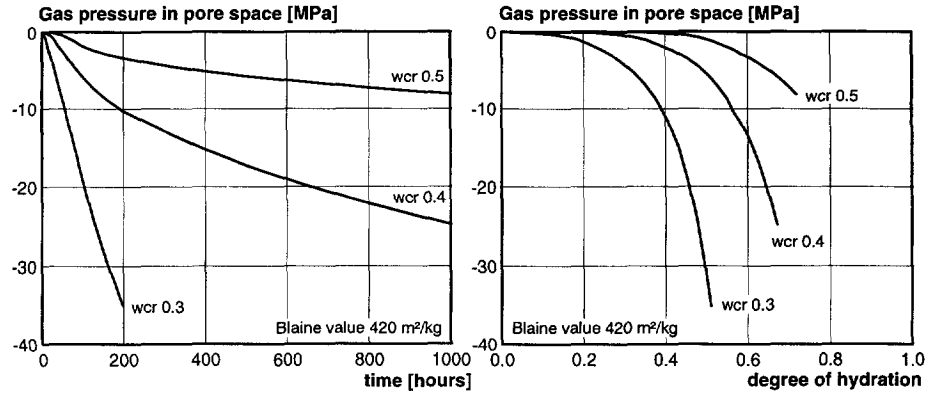

Fig. 4.22. Left: Pressure in capillary pore space versus time. Right: Pressure in capillary pore space versus degree of hydration (different wcr's).

pressure in the empty pore space. The pressure in the pore space in the cement paste with a water/cement ratio of 0.3 is about three times as large as in the cement paste with a water/cement ratio of 0.5, after 1000 hours of hardening. The gas pressure in the low water/cement ratio pastes develops much faster than in high water/cement ratio pastes (e.g. wcr 0.5). This can be attributed to the fact that for high water/cement ratio cement pastes more water must be consumed by the cement hydration before empty pore space is formed.

4.5.6 Surface tension in the adsorption layer

In Fig. 4.23, the surface tension in the adsorption layer is presented for a cement paste made with cement of different finenesses. On the left hand side of the figure the results are presented as a function of time. The surface tension appears to develop faster for the cement with a higher specific surface. On the right hand side the development of the surface tension in the adsorption layer is presented in the hydration domain. From this figure it can be seen that, according to the model, the surface tension is almost independent of the fineness of the cement. This means that the different rates at which the surface tension develops in the time domain are the result of the different rates of the hydration process.

In Fig. 4.24 the surface tension in the adsorption layer is presented for three different water/cement ratios. The results show large differences between the development of the surface tension for the different water/cement ratios. This holds true for the time domain as well as for the degree of hydration domain.

From the relationship between the surface tension and the autogenous shrinkage as given in section 4.3.2 and the specific mass of the cement paste (section 4.3.4), it can also be observed that the water/cement ratio has substantial influence on the volume changes of hardening cementitious material.

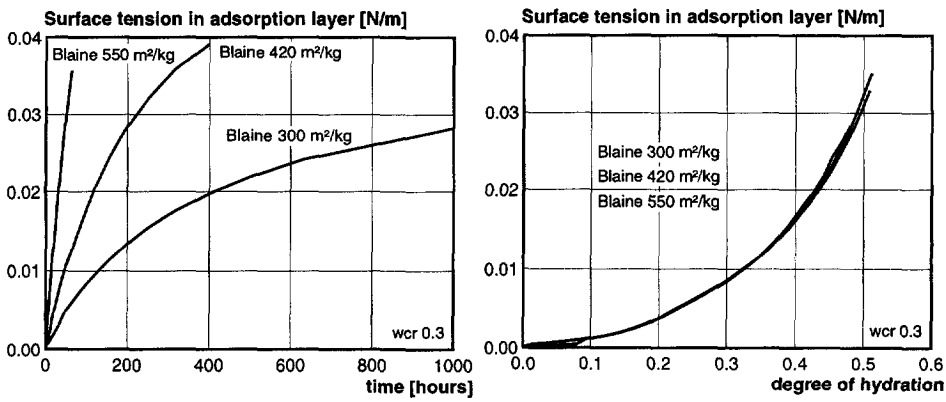

Fig. 4.23. Left: Surface tension in the adsorption layer versus time. Right: Surface tension in the adsorption layer versus degree of hydration (different cement fineness).

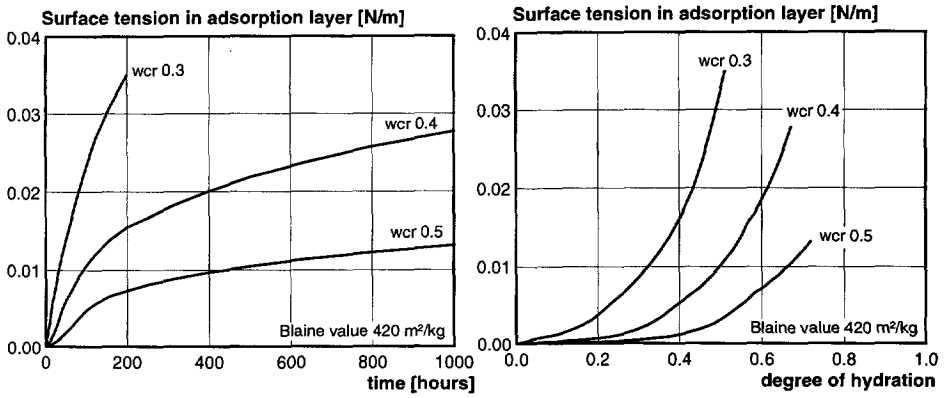

Fig. 4.24. Left: Surface tension in the adsorption layer versus time. Right: Surface tension in the adsorption layer versus degree of hydration (different water/cement ratios).

4.6 Discussion

According to the calculation procedure as presented in Fig. 4.13, thermodynamic equilibrium in the empty pore space can be established iteratively. In this calculation procedure, several parameters are involved that play an important role in the determination of volume changes in hardening cement-based materials.

From the parameter study as shown in section 4.5, a clear picture is obtained on the sensitivity of these parameters with respect to the water/cement ratio and also with respect the fineness of the cement. In general, the results show that the parameters involved in this calculation process depend more on the water/cement ratio than on the fineness of the cement. However, it must be emphasised that this is due to the adoption of the same pore structure constant "a" for all the cement pastes that were considered. From Fig. 3.16, it has already been observed that the pore structure constant "a" depends on the fineness of the cement and on the water/cement ratio. Therefore, small variations in the pore structure constant "a" may influence the model features as presented in section 4.5 some how.

In order to verify whether the proposed model is able to predict the autogenous shrinkage deformations of hardening cement paste well, will be elucidated in the next chapter.

5.

Autogenous shrinkage

Experiments versus numerical simulations

5.1 Introduction

In order to verify the potential of the model (presented in chapter 4) to calculate the autogenous shrinkage of hardening cement-based material, an extensive experimental program was established. Several tests were carried out from which the autogenous deformation (swelling + shrinkage) is measured during hardening. This means that the measured deformations include autogenous shrinkage but they may also experience some influence of the autogenous swelling. Since autogenous swelling is not included in the model as presented in chapter 4, a Portland cement is used in the experiments with a low potential to swell. This cement contains a relatively low percentage of C_3A clinker which is mainly responsible for the swelling [70]. Although the experimental results may include some influence of autogenous swelling, these results are compared by the numerical simulations as calculated with the proposed model.

The experimental program comprises tests on plain cement pastes for different water/cement ratios and also on pastes which are made with cement of different fineness. The autogenous shrinkage is compared in the time domain as well as in the hydration domain. One additional test is carried out on a cement paste with a microfiller to show the influence of this filler on the autogenous shrinkage. These measurements as well as results published by Tazawa [87] are also simulated with the proposed model.

Two different models will de discussed in this chapter with which the autogenous shrinkage of concrete can be calculated from the autogenous shrinkage of cement paste. Firstly, a parallel-series model is adopted to account for the influence of the stiff aggregates on the reduction of the autogenous shrinkage. Secondly, a lattice model is applied to calculate, on the one, hand the reduction of the autogenous shrinkage due to the addition of the aggregates, and on the other, to visualise the local stress zones which are prone to crack. The chapter ends with a discussion.

5.2 Experimental program on autogenous shrinkage of cement paste

An experimental program was established with the aim to validate the numerical model with which the autogenous deformation of hardening cement paste can be calculated (see chapter 4). Experiments carried out by Tazawa et.al [87] have shown that autogenous deformation is especially sensitive to the water/cement ratio and to the fineness of the cement. As far as the water/cement ratio is concerned, values of 0.3, 0.4 and 0.5 are adopted. For the fineness of the cement, Blaine values of 300, 420 and 550 m^2/kg are considered in the experiments. These parameter variations will give a good impression of the sensitivity of autogenous deformation of hardening cement paste to the water/cement ratio and the fineness of the cement. A description of the cement characteristics is enclosed in appendix A.
In addition, an experiment was also carried out on a cement paste with addition of 5% of silica fume (micro-silica powder). The main purpose of this experiment was to verify whether the model is also able to predict the autogenous shrinkage of high strength concrete. A summary of the experimental program is shown in Table 5.1.

All experiments were carried out under isothermal conditions at 20 °C. This temperature was imposed to the specimen with the help of two cryostats. Minor differences between the desired temperature (20 °C) and the measured temperature that appeared during the hardening process were registered. The effect of these temperature differences on the autogenous deformation measurements was compensated afterwards. However, the differences appeared to be almost negligible (± 2°C).

Table 5.1. Overview of the experimental program.

Test series	water/cement ratio	cement fineness Blaine [m^2/kg]	Note:
series 1	0.3 0.4 0.5	550	CEM I 52.5 R (ENCI)
series 2	0.3 0.4	420	CEM I 42.5 R (ENCI)
series 3	0.3	300	CEM I 32.5 R (ENCI)
series 4	0.3	550	CEM I 52.5 R (ENCI) + 5% silica fume

5.3 Description of the experimental set-up

The autogenous deformation is measured from large specimens cast in a temperature controlled mould. The inner dimensions of the mould are 1000 x 150 x 40 mm³ (Fig. 5.1). The mould can be dismantled into several parts. These parts are made of 40 mm foam plastic with a low coefficient of thermal conductivity (λ = 0.03 W/m²K). On one side a 1 mm thick steel plate is glued to the foam to ensure a smooth surface and to cover the "canals" that are cut in the foam. These canals enable cooling or heating of the concrete surface. The canals are connected to a cryostat, one cryostat for the top part of the mould and an other cryostat for the bottom part of the mould. Both cryostats control the water temperature and pump the water through the canals. Before casting, the bottom part and the four side-parts are put together. A wooden frame is used to support the mould during casting and setting of the paste. The inside of the bottom of the mould is covered with a sheet of plastic foil and a sheet of felt. A second sheet of felt covers the bottom and the vertical sides of the mould. Together these three sheets allow the paste to deform without almost any restraint. The latter foil also prevents leakage of paste and it also prevents drying shrinkage of the hardening paste. Thermocouples are placed at five different locations 20 mm above the bottom of the mould. After casting, the topside of the paste is covered by a layer of foil. After that, the top part of the mould is installed. During hardening, the temperature and the load-independent deformation of the paste are measured. The deformations of the cement paste are measured with LVDT's on two sides exterior of the mould, over a length of 750 mm between two steel bars (that pass through the mould) which are embedded in the paste during casting. As soon as the setting period of the paste has ended, measurements can start.
At this moment the paste has built up negligible strength. This is mostly a few hours after casting, depending on the length of the dormant stage of the paste. In this way, the load-independent deformations (autogenous deformation) can be measured soon after the beginning of the hydration process.

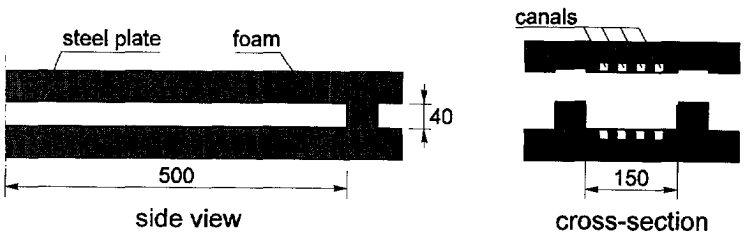

Fig. 5.1. Schematic representation of the thermally insulated mould.

5.4 Experiments on neat Portland cement pastes

For the presentation of the experimental results on the autogenous deformation of the different types of cement paste, a subdivision is made between the fineness of the cements. For a certain fineness, the autogenous deformation will be shown for different water/cement ratios. From the experimental set-up, the autogenous deformation is measured as a function of time. These results are compared with the simulated results calculated with the model proposed in chapter 4. The progress of the hydration process, one of the main parameters in the model, is determined by the HYMOSTRUC model simultaneously. Therefore, it is also possible to relate the measured autogenous deformation to the degree of hydration.

5.4.1 Cement of high fineness (Blaine 550 m²/kg)

On the left hand side of Fig. 5.2, the autogenous deformation is presented as a function of time. It concerns a neat Portland cement paste that contains a cement of high fineness (Blaine 550 m²/kg). The results are shown for three different water/cement ratios. These are 0.3, 0.4 and 0.5. The results show a strong increase of the autogenous deformation with decreasing water/cement ratio. The largest autogenous shrinkage strain, ca. 2‰, is measured after about 80 hours of hardening for a cement paste with a water/cement ratio of 0.3. The measurements show a strong increase of the autogenous deformation directly after setting. For a cement paste with a water/cement ratio of 0.4, less shrinkage is measured. Again, the increase of the autogenous deformation proceeds very rapidly. After 160 hours of hydration a shrinkage of 1‰ is reached. This is a large reduction (≈50%) in comparison with the cement paste with a water/cement ratio of 0.3. A further increase of the water/cement ratio to 0.5 reduces the autogenous shrinkage by another 50%. After 160 hours of hardening, a shrinkage of about 0.5‰ is measured.

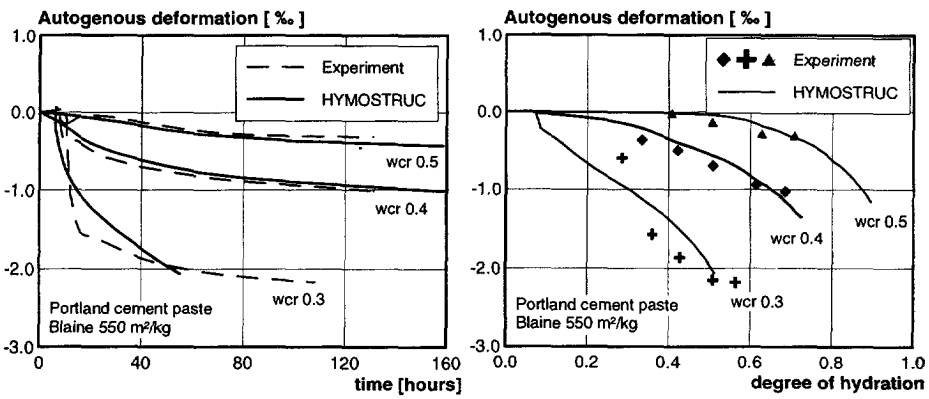

Fig. 5.2. Left: Autogenous shrinkage versus time. Right: Autogenous shrinkage versus degree of hydration. Portland cement paste (different water/cement ratios).

The measured autogenous deformation is simulated by the proposed model as implemented in HYMOSTRUC (see chapter 4). All the calculations are performed with the default model parameters of HYMOSTRUC (appendix A). The results show a good agreement between both the measurements and the numerical simulations. This holds true for all the three water/cement ratio's that are considered.
On the right hand side of Fig. 5.2, the autogenous deformation is presented as a function of the degree of hydration. The results are presented for the same three Portland cement pastes as were considered at the left hand side of Fig. 5.2. From the figure it can be seen that the autogenous deformation of the hardening cement paste is driven by the hydration process. For all three different water/cement ratios, the numerical simulations are in good agreement with the experimentally obtained results (Fig. 5.2, right).
The degree of hydration reached after ceasing of the hydration process is lower for the cement pastes with a lower water/cement ratio. Less water is available to continue the hydration process. However, from the results in Fig. 5.2, it appears that the autogenous deformation is inversely proportional to this effect. For low water/cement ratio pastes (e.g. wcr 0.3), the maximum pore diameter of capillary pores that are still completely filled with water is much smaller than the maximum pore diameter of a cement paste with a higher water/cement ratio (e.g. wcr 0.5). This phenomenon will result in a lower relative humidity (see eq. (4.7)) in the emptied pore space and introduces a higher surface tension in the adsorption layer. This results in larger deformations of the microstructure (eq. 4.9)). The thermodynamic equilibrium in the pore system governs this process.

5.4.2 Cement of medium fineness (Blaine 420 m²/kg)

On the left hand side of Fig. 5.3, the measured autogenous deformation is compared with numerical simulations that were carried out with HYMOSTRUC. It concerns the externally measured deformation versus time for a water/cement ratio of 0.3 and 0.4. Good agreement is reached between the measurements and the numerical simulations. This holds for both water/cement ratios. The experimental measurements, as well as the numerical simulations, show an equal tendency for the relationship between the development of the autogenous deformation and the water/cement ratio. If the water/cement ratio increases, the autogenous deformation decreases. Increasing the water/cement ratio from 0.3 to 0.4 results in a reduction of the autogenous deformation from 1.2 ‰ to 0.38 ‰ after 100 hours of hardening. This absolute difference appears to increase with elapse of time. At the right hand side of Fig. 5.3, the autogenous deformation of the hardening cement paste is presented as a function of the degree of hydration. The experimental results are compared with the numerical simulations as calculated by the proposed model (chapter 4).

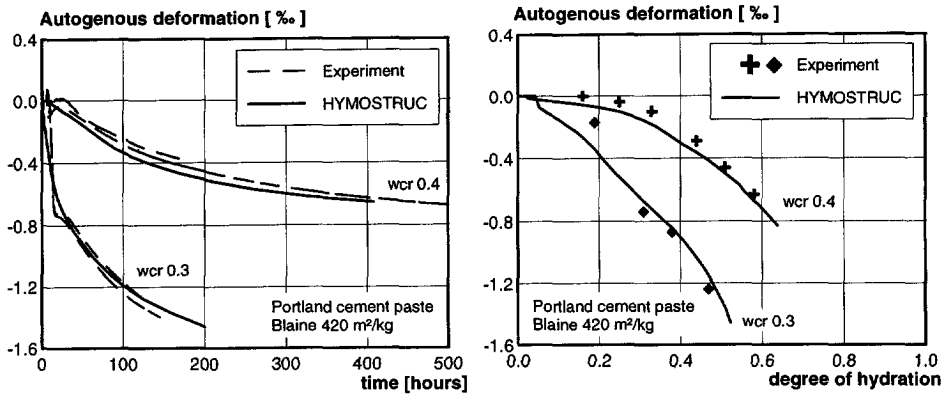

Fig. 5.3. Left: Autogenous shrinkage versus time. Right: Autogenous shrinkage versus degree of hydration. Portland cement paste (different water/cement ratios).

5.4.3 Cement of low fineness (Blaine 300 m²/kg)

The autogenous deformation of a cement paste that contains a relative coarse cement is also measured. It concerns a cement paste made with a Portland cement with a Blaine value of 300 m^2/kg. The experimental results are presented in Fig. 5.4. On the left hand side, the autogenous deformation is presented as a function of time. Good agreement has been reached between the numerical simulations and the experimental results. Due to the relatively coarse type of cement, hydration proceeds rather slowly. The autogenous deformation, therefore, develops slowly as well. From the results in Fig. 5.4 it can be seen that the autogenous deformation is still increasing after more than 1400 hours of hardening, since hydration is still going on.

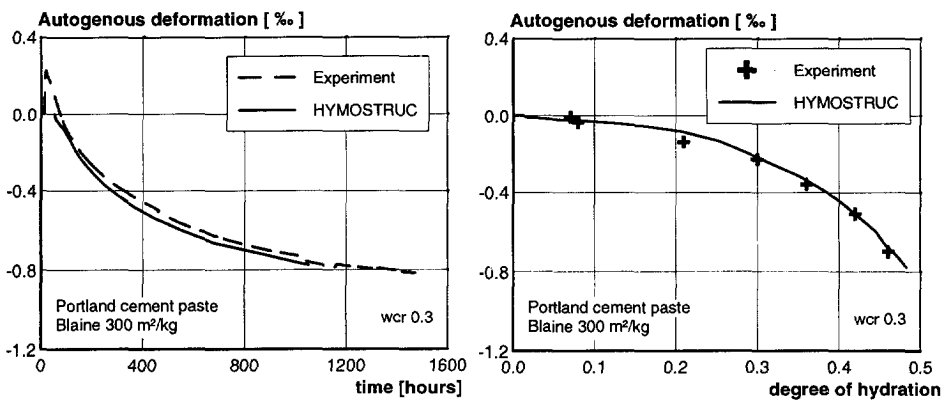

Fig. 5.4. Left: Autogenous shrinkage versus time. Right: Autogenous shrinkage versus degree of hydration. Portland cement paste (water/cement ratio 0.3).

On the right hand side of Fig. 5.4, the development of the autogenous deformation is presented as a function of the degree of hydration. The numerical simulations are compared with experimental results. Also for the very coarse types of cements, the proposed model predicts the autogenous deformation of the hardening cement paste fairly well.
In addition, it must be noticed that mechanisms that cause autogenous swelling is not included in the model. This means that the measured early age swelling can not be simulated with the proposed model (see eq. Fig. 5.4, left).

5.5 Experiment on cement paste with silica fume

To examine the effect of a microfiller (like silica fume) on the development of autogenous shrinkage, an experiment on a Portland cement paste (Blaine 550m^2/kg, wcr 0.3) with 5% percent silica fume has been carried out. Addition of an ultra fine microfiller to cement paste leads to a densification of the microstructure and also to a reduction of the average pore diameter of the microstructure. The reduction of the average pore diameter is a phenomenon which is of paramount importance regarding the development of autogenous shrinkage. The pore radius appears to be inversely proportional to the development of the surface tension in the adsorption layer at the pore wall area. The surface tension in the adsorption layer is considered to be the driving force behind the autogenous shrinkage (eq. (4.9)). Thus, a densification of the microstructure leads to an increase of the autogenous shrinkage.
Modelling the effect of the addition of an ultra fine microfiller to a hardening cement paste requires knowledge on the chemical as well as on the physical behaviour of this substance on the hardening process. Some authors, e.g. [63], have proposed a simple reaction equation that describes the so-called "secondary reaction" which is mainly caused by the chemical reaction between silicon dioxide (enclosed in microfiller like silica fume), calcium hydroxide (additional product from water-cement reaction) and water. At this moment, implementation of this reaction equation into the present hydration model is not a realistic option, due to the ultra fine dimensions of the microfiller particles and also to the uncertainties in the description of this chemical reaction process. For this, it must be born in mind that the formulation of the chemical reaction process between cement and water is in fact a modelling approach of the real situation which conceals already several uncertainties.
Therefore, in order to gain more insight into the present potential of HYMOSTRUC to simulate the autogenous shrinkage of HSC paste, it has been decided to model the effect of silica fume addition on the development of autogenous shrinkage by adjusting the maximum pore diameter which is involved in the pore size distribution (Fig. 3.6). In [27], Feldman published results on the relationship between the maximum pore

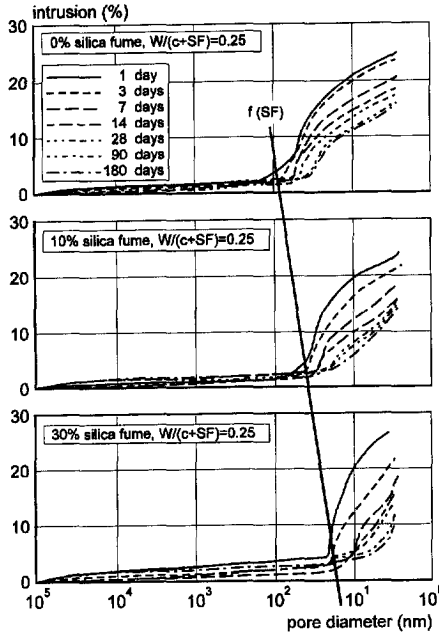

Fig. 5.5. Reduction of the pore diameter as the percentage of silica fume increases, after Feldman [27].

diameter in a hardening cement paste and the percentage of silica fume that is added to this paste. Three different cement pastes were considered which included 0%, 10% and 30% silica fume. Pore size measurements were carried out at various ages of the cement paste. The tests were carried out for two different water/cement ratio's, viz. 0.25 and 0.45. For a water/cement ratio of 0.25, the measurements are presented in Fig. 5.5. From these results, it appears that the largest pore diameter in the cement paste becomes smaller as the percentage of silica fume increases. This relationship can be described mathematically by:

$$f(SF) = a_1 \cdot SF + 1 \tag{5.1}$$

where f(SF) is the correction factor which describes the reduction of the largest pore radius in the paste due to the addition of silica fume, a_1 is a constant and SF the amount of silica fume expressed in percentage of the added cement. For a1, a value of -0.028 was found. This coefficient of inclination turned out to be almost independent of the water/cement ratio. Therefore, this correction function can be applied within a wider range of water/cement ratio's, e.g. 0.2 to 0.5. Multiplication of the largest pore diameter involved in the pore size distribution by the correction factor f(SF) leads to the desired reduction of the maximum pore diameter in the paste, viz. densification of the microstructure. A densification of the microstructure results in a finer "network" of

pores. The capillary water is assumed to be accumulated in these finer pores. Thermodynamic equilibrium in these finer pores will then result in an increase of the surface tension which is induced by the decrease of the average pore diameter in the cement paste system. According to equation (4.9), it will also effect the development of autogenous shrinkage of the hardening paste.

In Fig. 5.6, the autogenous deformation measurements are presented for a Portland cement paste with and without the addition of 5% silica fume (see Fig. 5.2). The water/cement ratio is 0.3. This implies that the water/binder ratio (water/(cement + silica fume)) is 0.285. On the left hand side of Fig. 5.6, the measured autogenous deformations are compared by the numerical simulations of the autogenous shrinkage of the hardening cement paste. The results are shown in time domain. The autogenous deformation measurement showed a very large decline at the very early stage of the hardening process. This decline is followed by a more moderate volume reduction. The paste appeared to reach a contraction of 3‰ after about 100 hours of hardening. This tendency could also be simulated quite well.

On the right hand side of Fig. 5.6, the development of the autogenous deformation is presented as a function of the degree of hydration. The results of the simulation show an almost linear relationship between the autogenous deformation and the degree of hydration. This holds true for the numerical simulations as well as for the experimental results.

A linear relationship between the development of the autogenous deformation and the degree of hydration has also been observed for a HSC mixture [47]. This is in good agreement with the linear relationship as was found for the hardening cement paste with addition of 5% silica fume (Fig. 5.6).

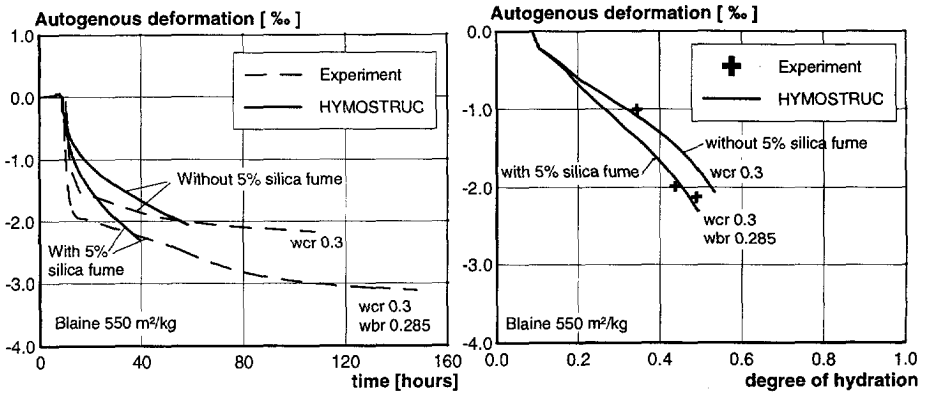

Fig. 5.6. Left: Autogenous deformation versus time. Right: Autogenous deformation versus degree of hydration. Portland cement, paste with and without 5% silica fume. Water/cement ratio 0.3 (water/binder ratio 0.285).

5.6 Numerical simulations versus literature data

In [87], Tazawa et. al. published an extensive experimental study on autogenous deformation of cementitious material. Some of these results are simulated with the HYMOSTRUC model. It concerns a cement paste with a water/cement ratio of 0.23 and another paste with a water/cement ratio of 0.3. The results are shown in Fig. 5.7. Good agreement has been obtained between the measurements and the numerical simulations. This appeared to be true for both the paste with a water/cement ratio of 0.3 and for the paste with a water/cement ratio of 0.23. For the paste with a water/cement ratio of 0.3, the autogenous deformation reaches a value of about 1.5‰ after about 50 days of hardening while for the cement paste with a water/cement ratio of 0.23 the autogenous deformation appeared to reach a value of about 2.5‰. This order of magnitude was also calculated with the HYMOSTRUC model.

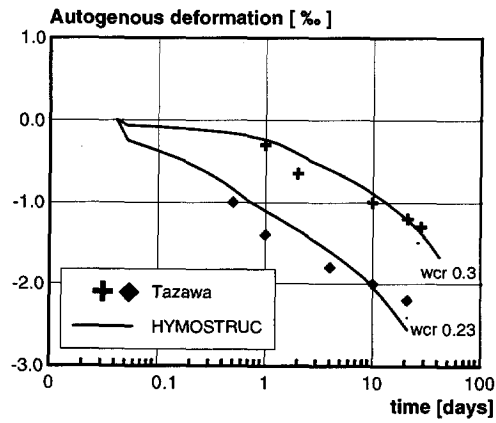

Fig. 5.7. Comparison between experiments on cement paste (Blaine 352 m^2/kg) carried out by Tazawa et.al. and numerical simulations by HYMOSTRUC.

5.7 Autogenous shrinkage of concrete

5.7.1 Internal restraint by aggregates

The autogenous shrinkage of concrete is substantially smaller than the autogenous shrinkage of cement paste. The addition of aggregates to a concrete mix introduces a certain restraint of the cement paste. The level of restraint depends on the percentage of aggregates that is added to the mix. However, it also depends on the particle size distribution, shape and the size of these aggregates. Generally, the stiffness of the aggregates is much larger than the stiffness of the hardening cement paste.

Due to the difference in stiffness, cement paste will be restrained by the aggregate particles. Large stresses may develop in the interfacial transition zone (ITZ) around the aggregates. If the tensile strength at the ITZ is exceeded, micro-cracks may occur in the close vicinity of the aggregate particle. This implies that a certain part of the autogenous shrinkage of the cement paste will be transferred into stresses and may possibly lead into cracks. The stress release in the paste matrix due to cracking will result in a decrease of the autogenous shrinkage of the concrete.

The effect of aggregates on the reduction of autogenous shrinkage can be modelled in different ways. In the next sections, two different models are proposed. The first model concerns a parallel-series model and the second model concerns a so called lattice model [75]. These models will be discussed in detail in the next sections. Finally, the model is verified by a comparison between experimental data and numerical simulations of autogenous deformations.

5.7.2 Parallel-series model

Parallel-series models are commonly used for composite materials. These models simulate the stiffness of the composite material by taking into account the stiffness of the individual components [20]. The stiffness of the different components can be ranked either by a parallel system or by a series system. Authors have also proposed combinations of both these systems. Generally, these types of models are able to give a good approximation of the stiffness of composite materials. Therefore, in order to simulate the effect of the stiff aggregate particles on the reduction of the autogenous shrinkage of the hardening cement paste, a parallel-series model, as presented in Fig. 5.9, is proposed. In this model, the aggregate particles are assumed to be embedded in the cement paste. Equilibrium between the deformation of the different components leads to the following conditions regarding the equilibrium of forces and the compatibility of the

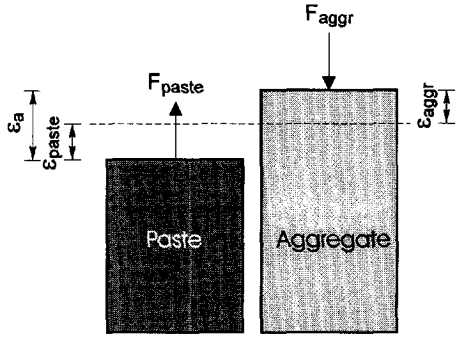

Fig. 5.8. Equilibrium of the parallel-series model.

system:

- Equilibrium of forces: $F=F_{aggr}+F_{paste}=0$ (no external loading)
- System compatibility: $\varepsilon_a=\varepsilon_{aggr}+\varepsilon_{paste}$

where ε_a is the "free" autogenous shrinkage of the hardening cement paste (eq. (4.9)), ε_{aggr} the imposed deformations of the aggregates and ε_{paste} the imposed deformation of the hardening cement paste. F_{aggr} is the load which is experienced by the aggregates and F_{paste} is the load which is experienced by the paste (see Fig. 5.9).

If the parallel-series system is submitted to autogenous shrinkage, compatibility requires an extension of the cement paste and contraction of the aggregates. This goes along with the development of tensile stresses in the cement paste and compressive stresses in the aggregates. The tensile stresses in the paste may exceed the actual paste strength and result in micro-cracks.

From the system compatibility and the equilibrium of forces, the deformation ratio between the imposed autogenous shrinkage and deformation of the two-phase composite system ε_c (concrete, see Fig. 5.9), can be determined according to:

$$\frac{\varepsilon_c}{\varepsilon_a}=(1-x)+\frac{x}{1+\frac{E_a}{E_p}\frac{x}{1-x}} \tag{5.2}$$

where x is assumed to be a "smeared out" measure for the thickness of the layer of paste around the aggregate particle (see left of Fig. 5.9). The relationship is based on a geometrical distribution of the volumetric components in the concrete mixture and also on the stiffness ratio between the aggregates and cement paste. The difference in stiffness is a measure for the internal restraint that is experienced by the cement paste. On the

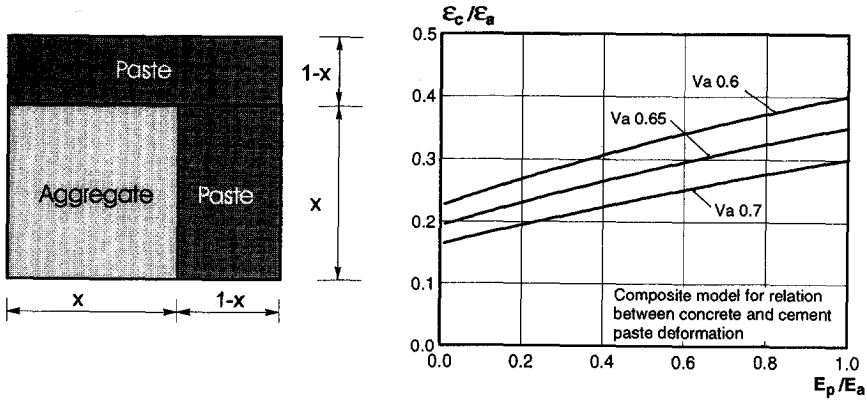

Fig. 5.9. Left: Schematical representation of the proposed parallel-series model for concrete. Right: Relationship between the concrete strain ε_c and paste strain ε_a ratio and the ratio between the elastic modulus of aggregate and paste for different aggregate volumes ($V_a=x^2$ [20]).

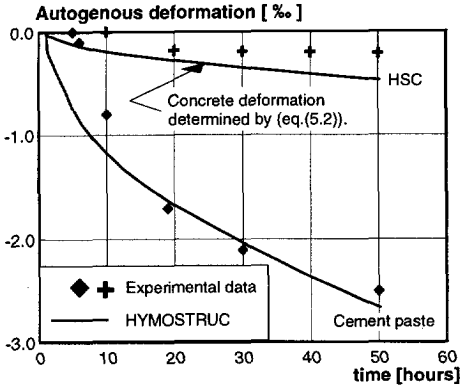

Table 5.2. Mix proportions of HSC mixture and Portland cement paste

Mixture	HSC	Paste
w/c ratio	0.3	0.3
Aggregates	0.7	0
Silica fume	5%	5%
Blaine [m^2/kg]	550	550
$E_{aggregate}$	60 GPa	0

Fig. 5.10. Autogenous shrinkage for HSC and for a cement paste with 5% silica fume.

right hand side of Fig. 5.9, the results are presented of the ratio between the autogenous shrinkage of concrete and paste versus the ratio between the elastic modulus of paste and aggregates. Three different aggregate volumes, e.g. 0.6, 0.65 and 0.7 are considered in the figure. The volumetric part of the aggregates in the parallel-series model is equal to $V_a=x^2$. This relationship can be used in equation (5.2). The results in Fig. 5.9 (right) show that the autogenous shrinkage of the concrete lies roughly between the 15% and 40% of the autogenous shrinkage which is experienced by the hardening cement paste. The exact value depends on the relative aggregate volume and on the relative stiffness ratio (E_p/E_a).

Experimental results from the literature have shown that the autogenous shrinkage of an ordinary HSC is substantially smaller than the autogenous shrinkage of the cement paste (roughly between 10 and 15%) [88]. This order of magnitude has also been observed in tests carried out at the Stevin laboratory in Delft [50, 53].

A large internal restraint of hardening cement paste is accompanied by the development of tensile stresses in the paste and compressive stresses in the aggregates. At certain locations, e.g. around an aggregate particle surface, stress concentrations in the paste may exceed the actual strength and may induce micro-cracking. This may contribute to microstructural damage [54, 77]. For an arbitrary HSC mixture (see Table 5.2), the autogenous shrinkage of the concrete as well as of the cement paste is presented in Fig. 5.10. From this figure it appears, that the internal restraint by the aggregates is very pronounced. For this particular HSC mixture, the ratio between deformation of the concrete and the deformation of the paste is about 10% after cessation of the hydration process. This ratio is smaller than the ratio as determined by the parallel-series model (see Fig. 5.9, right). This can be the result of either the stress relaxation that takes place in the paste during hardening, or it can be the result of the strain release due to the development of micro-cracks which are induced by the internal restraint of the aggregates.

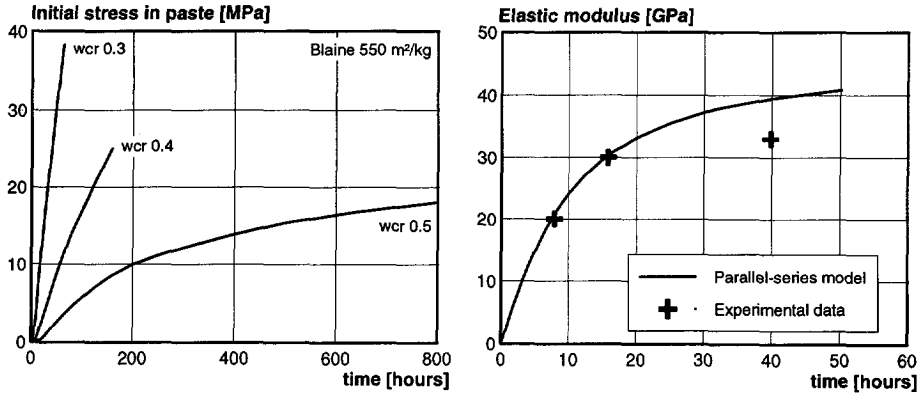

Fig. 5.11. Left: Initial stress in hardening cement paste. Note: Stress relaxation is not taken into account. Right: Elastic modulus of HSC versus time (see Table 5.2). Parallel-series model compared with experimental data.

The tensile stresses in the cement paste which are introduced by the internal restraint of the aggregates can also be determined by the parallel-series model. For this, the actual paste strain ε_{paste} must be multiplied by the actual elastic modulus E_p . In Fig. 5.11, this is carried out for three different water/cement ratios. The tensile stress in the paste increases for decreasing water/cement ratio's. For a water/cement ratio of 0.3 a stress level of almost 40 MPa is reached, disregarding the influence of stress relaxation and microcracking. Under this stress, cracking of the hardening microstructure is very likely to occur. The development of microcracks will reduce the actual stresses in the hardening paste. Microcracking, in turn, will also have a certain influence on the material properties of the hardening concrete. In this respect, the elastic modulus requires due attention.

It turned out that the proposed parallel-series model (Fig. 5.9) overestimates the elastic modulus of a HSC mixture. This can also be observed from Fig. 5.11. According to the proposed parallel-series model, the elastic modulus is overestimated by almost 25% after 40 hours of hardening. This trend is generally found for HSC. From Fig. 5.11, it can also be observed that the overestimation starts after a certain period of hardening ($\approx$ 20 hours). This may be the time at which the microcracks start to develop and damage the microstructure. Before that particular time, the model predicts the development of the elastic modulus of the hardening concrete quite accurate. This suggests the presence of microcracks and their influence on the material properties of low water/cement ratio concretes.

5.7.3 Lattice model approach

Another way to simulate the reduction of autogenous deformation due to internal restraint caused by the aggregates is by application of a lattice model. At Delft University

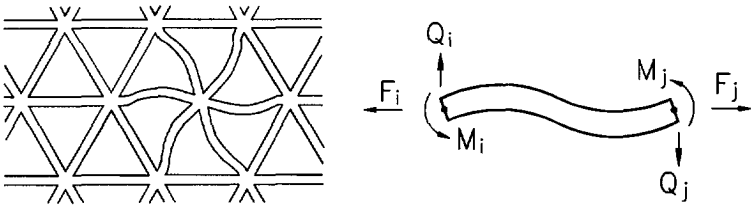

Fig. 5.12. Lattice model [75]

of Technology, a lattice model has been developed by Schlangen [75] (Fig. 5.12). In this meso-level modelling approach, distinction is made between the material properties of the composite material, e.g. aggregates and mortar. The aggregates as well as the hardening mortar are considered to be built of a framework of small beams.

The developing autogenous shrinkage and elastic modulus of the hardening cement paste are assigned to beams which have a length of about 1 mm (1000 μm). These beams represent the mortar of the concrete (sand and cement paste). Together, the spatial framework of beams and the aggregates represents the concrete sample.

To determine the influence of the aggregates on the autogenous shrinkage, a digital image was made of a concrete sample which includes only a few aggregate particles. The image formed the basis of the lattice model. A spatial beam model was made where the different material properties were assigned to the mortar and to the aggregates. The framework is loaded by an internal loading which is caused by autogenous shrinkage. The deformation of the spatial framework can now be determined by a step wise calculation procedure. As hydration proceeds, the beam elements start to deform (shrink). The imposed deformations of the hardening mortar will be restrained by the aggregates. This will result in a lower deformation of the concrete in comparison with the deformation of the mortar. In Fig. 5.13, four subsequent stages of the deformation of the concrete sample (2D) are presented. From this figure, it can be observed that aggregates restrain the hardening mortar. Compressive stress will develop in the aggregates and tensile stresses in the hardening mortar. In the close vicinity of the aggregate surface the mortar is highly restrained, resulting in high stresses. If the actual tensile strength is exceeded, microcracks are very likely to occur. This process will result in a redistribution of the stresses in the sample. It must also be born in mind that the appearing stresses will be submitted to stress relaxation. However, both a redistribution of the stresses and the stress relaxation are not taken into account in the calculation of the deformation of the concrete sample as presented in Fig. 5.13.

The influence of the aggregate particles on the reduction of the autogenous deformation of the hardening mortar is presented in Fig. 5.14. On a macro-scale level, the measured concrete deformation differs from the autogenous deformation that has initially been

t = 0 hour t = 10 hours t = 100 hours t = 1000 hours

Fig. 5.13. Four subsequent stages of the deformation of an arbitrary concrete prism (40x40x160 mm^3) due to autogenous deformation. (2-D image)

assigned to the beams which represented the mortar. For this arbitrary concrete sample, the concrete deformation appeared to be about 40% of the deformation of the hardening mortar. This value lies within the range as was also given by the parallel-series model (see Fig. 5.9, right). However, it must also be born in mind that the concrete sample which is considered in this calculation (Fig. 5.13) does not represent a "real" concrete

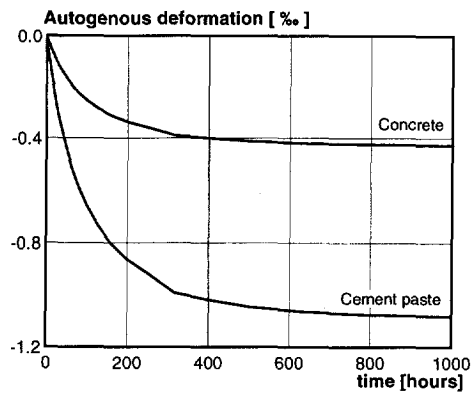

Fig. 5.14. Simulated effect of inclusion of aggregate particles on autogenous shrinkage of concrete. Autogenous shrinkage of the cement paste is imposed to the lattice beams representing the mortar.

mixture. There are only a few aggregates included in the sample that represent influence of the internal restraint. Therefore, it must be emphasised that this numerical test only serves the purpose of gaining insight of the deformations and internal restraint of a concrete sample. For a more representative distribution of the aggregates in the concrete, the internal restraint would be substantially higher. This would certainly affect the deformational behaviour.

5.8 Discussion

To gain more insight in and knowledge of the relationship between the autogenous shrinkage of a hardening concrete and the autogenous shrinkage of paste, it is necessary to look at the material in more detail (microscale level). The way how the aggregate particles influence the geometrical packing of the cement particles is an important issue in this respect. A relatively porous interfacial transition zone (ITZ) will develop at the close vicinity of the aggregate surface. Due to the high porosity, the ITZ will be "water-rich". This will also have consequences for the hydration process at the bulk paste. Pressure differences may develop in the capillary water. Capillary water may become transported from the "water-rich" interfacial zone to the bulk paste or the other way around.

This discussion confirms that the relationship between the volume changes of concrete and paste requires due attention. The hydration processes which develop between two aggregate particles may differ substantially from the hydration process of a plain paste. For this reason, a model is proposed which has the potential to calculate the hydration process of cement paste which is encapsulated by two aggregates (Ribbon paste). This model takes into account the hydration differences that occurs due to packing differences at the close vicinity of the aggregate surface. It also accounts for the transportation of the capillary water through the hardening microstructure.

The derivation of this ribbon model will be elucidated in detail in the next chapter. The hydration process will be calculated with the HYMOSTRUC model. Thermodynamic equilibrium in the empty pore space will be established according to the procedure as outlined in chapter 4.

6.

Ribbon paste hydration

6.1 General

In this chapter, a ribbon model will be proposed with which the hydration process of cement paste which is bordered by two aggregate particles can be analysed (see Fig. 6.1). The ribbon model is considered to give insight in the different processes that play a role during hardening of an arbitrary concrete. It has been observed that the hydration process of concrete differs from the hydration process of plain paste [73]. Generally, these differences are attributed to the differences in the geometrical packing of the cement particles. The aggregate particles in an arbitrary concrete introduce a so called "wall effect". Close to the aggregate surface, the cement particles will have another spatial distribution than in the bulk paste. This may introduce differences in the microstructure. The rate of hydration of the cement particles close to the aggregate surface will be much higher than the rate of hydration of the cement particles which are situated in the bulk paste. These different hydration rates may introduce pressure differences in the capillary water. Capillary water may become transported from the "water-rich" locations to the "water-poor" locations, driven by pressure differences

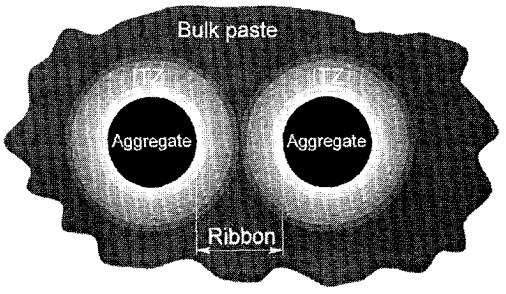

Fig. 6.1. Schematic representation of the ribbon in a concrete.

which are caused by differences in the rate of hydration. This may effect the overall progress of the hydration process of the ribbon paste.
This chapter is outlined as follows: The properties of the ribbon as well as the thickness of the ribbon will be discussed. First, emphasis will be on the determination of the ribbon thickness of an arbitrary concrete mixture. Hereafter, the current potential of the HYMOSTRUC model for evolution of the ribbon paste hydration are presented. In this section, emphasis will be on the possibilities of modelling the variation of the hydration process over the thickness of the ribbon paste analytically. This is used as a basis for the determination of the degree of hydration of the ribbon paste. In the next section, a random particle structure is adopted to determine the variation of the water/cement ratio over the ribbon, and its effect on the hydration process. After this, a detailed outline is given of the derivation of a model that describes the transport of capillary water and gas in the hardening ribbon paste. Finally, the effect of the transport of capillary water and gas on the hydration of the ribbon paste will be presented.

6.2 Interfacial transition zone

The three phase system (see section 2.6.1) is defined as the Aggregate-Interface-Bulk paste structure in an arbitrary concrete mixture (Fig. 6.2). The paste can be distinguished into the bulk paste and the ITZ paste. The material properties of the ITZ are different from the properties of the bulk paste. There exists no clear border between the ITZ and the bulk paste. The material properties change gradually when going from the ITZ to the bulk paste. This can be attributed to the packing differences of the cement particles. Due to the so called "wall effect", the packing density of the cement particles close to the aggregate surface is different from the packing in the bulk paste. The fineness of the cement as well as the water/binder ratio of the concrete mix, affect the width of the ITZ. The ITZ is generally characterised by a high porosity. The poor packing of the cement particles is responsible for a relatively high porosity at the close vicinity of the aggregate surface compared with the porosity in the bulk paste region. Before hydration has started, the porosity near the aggregate surface is mostly about 100% [11]. This holds true for different water/cement ratio's and also for different finenesses of the cement. Precipitation of CH crystals at the aggregate surface may reduce the porosity as hydration proceeds. In the present study, however, the precipitation of CH crystals at the aggregate surface will be disregarded. This means that for proposed ribbon model, emphasis is on the stereological packing effect of the cement particles in the close vicinity of the aggregate surface.
It must be noted that other types of models, which include, among other things, precipitation of CH crystals and the effect the syneresis, are also currently under development at Delft University of Technology (de Rooij et. al. [72]).

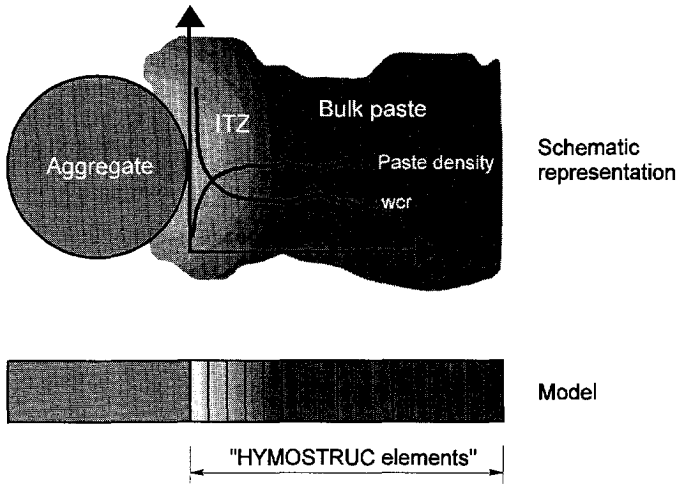

Fig. 6.2. Top: Schematic representation of the three phase system. Inserted are the course of the paste density and water/cement ratio versus distance from the aggregate surface. Bottom: Proposed model for calculation of the material properties versus distance from aggregate surface.

The HYMOSTRUC model is used to calculate the development of the microstructure at different distances from the aggregate surface. For this purpose, the cement paste is subdivided into several elements. This model is shown in Fig. 6.2. For each element, a HYMOSTRUC calculation can be performed. For the determination of the value of the local water/cement ratio and the paste density as a function of the distance from the aggregate surface, a random cement particle structure is used. An analytical function can also be used [16]. The application of a random particle structure is mostly encouraged, since with this method the variations of the paste density are determined geometrically. For this purpose, the random particle structure as outlined earlier in chapter 3 will be applied.

6.3 Concrete RIBBON model

6.3.1 General

A welcome extension of the model as proposed in Fig. 6.2, is a two aggregate particle system which can be applied to simulate the *ribbon* of a concrete (see Fig. 6.3). With this system, it is possible to describe the hydration process in the cement paste between two aggregate particles.

In order to develop a realistic model which is able to describe the hydration process between two aggregate particles, all components within the ribbon must be considered. This means that both the two ITZ regions as well as the bulk paste have to be taken into account in the model. Due to the lower local density of the paste, the ITZ's are considered to be the water-rich zones in the ribbon. These zones have the potential to serve as "storage tanks" with capillary water for the bulk paste. In other words, these water-rich regions may serve as an additional water supply for the hydration of the bulk paste. The latter phenomenon will take place if the gas pressure in the bulk paste is lower than the gas pressure in the ITZ's. This may move capillary water from the water-rich zones into the bulk paste resulting in further hydration and, even more important, less potential of the hardening microstructure to contract [51]. This mechanism can also be enhanced [51] by replacing a certain percentage of the aggregates by fully saturated porous light weight aggregate particles (e.g. Lytag).
In order to be able to describe the variations of the material properties over the ribbon paste accurately, the ribbon paste must be subdivided into several elements (see Fig. 6.3).

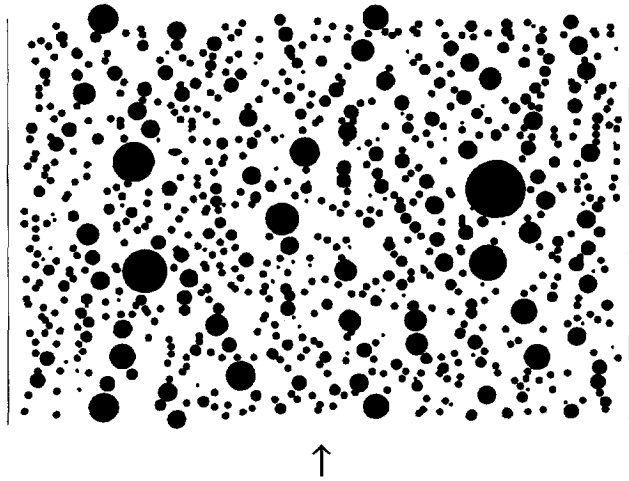

Fig. 6.3. Proposed model for calculation of the material properties and interaction mechanism between two aggregate particles.

Each element represents a certain part of the hardening cement paste with a unique hydration process and with unique material properties. For each element, the hydration process can be determined with the HYMOSTRUC model. In this way, the variation of the degree of hydration over the ribbon can be simulated. However, the transport mechanism which describes the movement of capillary water and gas requires an "interaction" between the "HYMOSTRUC elements" (see Fig. 6.3). This interaction mechanism will be outlined in section 6.7.

For the analysis of the ribbon paste, the distance between the aggregate particles has to be known. This distance is commonly called the *Ribbon thickness*. It would be very convenient to relate this distance to the mix composition of the concrete. In this way, the model results can be assigned to a concrete mixture.

6.3.2 Ribbon thickness

Consider concrete as a composite material which consists of cement paste and aggregate particles. A ratio between the volumetric contributions of these phases can be applied to define material properties. Here, it is wishful to have a measure for the average distance between neighbouring aggregate particles. This average thickness is called the *ribbon thickness* R_t. This distance can be represented by the ratio between the total paste volume and the total surface area of the aggregate particles in a concrete mixture.

Therefore, the ribbon thickness R_t of an arbitrary concrete is defined as the ratio between the paste volume V_p and the total specific surface of the aggregates particles S_a in the concrete mix (see also Fig. 6.1). This can be denoted as follows:

$$R_t = \frac{2V_p}{S_a} \qquad (6.1)$$

For this definition, it is assumed that the total paste volume is smeared out over the total area of the aggregates. The paste will cover the area of the aggregates with a layer of a certain thickness. For a single aggregate particle, this approach gives an average thickness of V_p/S_a for the layer of paste around the aggregate. The distance between the two aggregate particles (see Fig. 6.3) can be represented by two times the average thickness of the paste layer around the aggregate particle. This leads to the definition as given in (6.1).

The ribbon thickness strongly depends on the particle size distribution of the aggregates. The volume of paste in a concrete is determined by the mix composition. From this, it is possible to determine the relationship between the relative amount of aggregates in a concrete mix and the cement content. This relationship is presented in Fig. 6.4 (no admixtures, air 1%). For a certain cement content at a certain water/cement ratio, the relative amount of aggregates in a concrete mix can be obtained directly from Fig. 6.4. In this figure, the area that is of interest for HSC is marked grey. For a water/cement ratio of 0.3, a cement content between 450 to 550 kg/m^3 this results in a relative aggregate

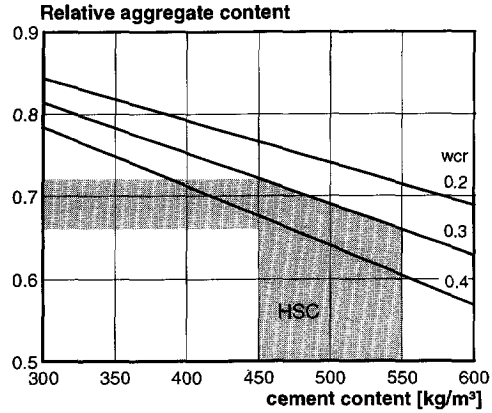

Fig. 6.4. Relationship between the cement content and the relative aggregate volume at three different water cement ratio's (0.2, 0.3 and 0.4).

volume that ranges between 0.65 and 0.72. The total surface area of the aggregate particles can be determined by assuming that the particles are spherically shaped. For the particle size distribution of the aggregates, the Fuller curve can be adopted. The Fuller distribution function can be denoted by:

$$P(x) = \sqrt{\frac{x}{D}} \tag{6.2}$$

where P(x) is the cumulative aggregate volume, x the aggregate diameter and D the maximum particle diameter involved. It is now possible to calculate the surface area of a certain volume of aggregates that are distributed according to eq. (6.2). The weight of the aggregate particles per fraction can be determined by differentiating the Fuller function (6.2) with respect the particle diameter. From this, the volume of the particles per fraction can be determined by dividing the weight per fraction by the specific density of the aggregate particles. The number of particles per fraction can be determined by dividing the aggregate volume of a fraction by the volume of one aggregate particle of that particular fraction (see also eq. (3.5)). The specific surface can be found by multiplication of the number of aggregate particles per fraction by the surface area of one aggregate particle.

If the aggregate volume is known and the volume of cement paste in a concrete mixture is also known, it is possible to determine the ribbon thickness for different aggregate ratio's. However, from eq. (6.2) it can be seen that the specific surface of the aggregates also depends on the maximum diameter of the aggregate particle that is involved in the concrete mixture. More smaller particles will lead to a larger specific surface. For HSC generally a maximum aggregate size of 16 mm is applied. However, other maximum diameters can also be applied. Therefore, in Fig. 6.5 (left), for three different aggregate

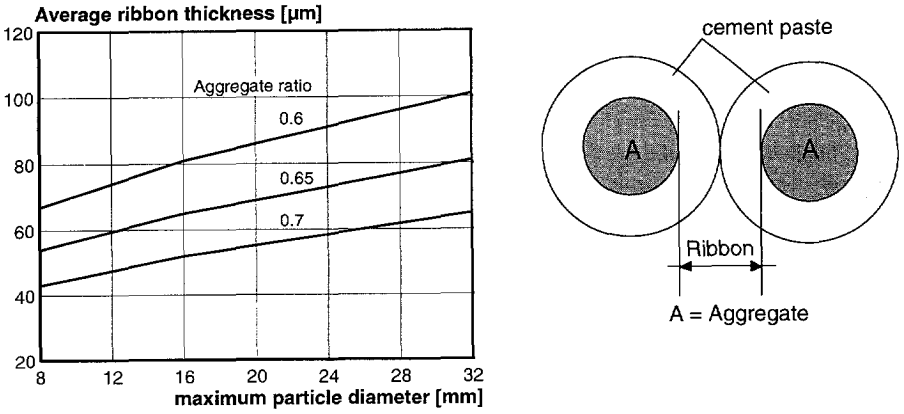

Fig. 6.5. Left: Average ribbon thickness versus maximum aggregate diameter. Right: Schematical representation of ribbon thickness between two aggregate particles (A).

percentages, the ribbon thickness R_t is described as a function of the maximum diameter of the aggregate particle involved. The numerical data behind this figure is listed in Table 6.1. It must be noted that the minimum aggregate particle involved is assumed to be equal to 0.125 mm. This is considered to be the diameter of the smallest sand particle.
From Table 6.1, as well as from Fig. 6.5, it can be observed that the average ribbon thickness of an HSC varies roughly between the 40 and 100 µm, depending on the aggregate content. This is in good agreement with the values that are found by Diamond [24]. On the right hand side of Fig. 6.5, the ribbon thickness is shown schematically, being the average distance between two aggregate particles.

Table 6.1. Calculated ribbon thickness for different aggregate content and different maximum aggregate sizes.

	aggregate ratio: 0.7		aggregate ratio: 0.65		aggregate ratio: 0.6	
D_{max}	S_a [m^2]	R_t [µm]	S_a [m^2]	R_t [µm]	S_a [m^2]	R_t [µm]
32	9269	65	8607	81	7950	101
16	11577	52	10750	65	9923	81
8	14001	43	13000	54	12001	67

6.4 Pore system properties

For a paste volume V, the volume that is initially occupied by the cement V_{c0} can be determined by a volumetric consideration. This results in:

$$V_{c0} = \left(\frac{\rho_w}{\rho_w + \rho_{ce}\omega_0} \right) V \tag{6.3}$$

The accompanying water volume V_{w0} that is initially available in the system can be determined by subtracting the cement volume V_{c0} from the total volume V (*ignoring air bubbles*).

The porosity of the hardening cement paste is determined by the actual pore volume V_{por}. From this actual pore volume the porosity $n(\alpha)$ in a hardening microstructure can be defined as:

$$n(\alpha) = \frac{V_{por}(\alpha)}{V} \tag{6.4}$$

where $V_{por}(\alpha)$ is the total pore volume at a certain degree of hydration α. Subdividing the total porosity in pores that are occupied by the capillary pore water and by pores that are the result of chemical shrinkage leads to (see [16]):

$$V_{por}(\alpha) = V_{cap}(\alpha) + V_{chsh}(\alpha) \tag{6.5}$$

where $V_{cap}(\alpha)$ is the actual capillary volume in the system and $V_{chsh}(\alpha)$ the pore volume caused by chemical shrinkage. Both effects are a function of the degree of hydration. From this, it can be noticed that the total pore volume changes continuously throughout the hardening process. The variation of the total pore volume with the degree of hydration is proposed as follows [16]:

$$V_{por}(\alpha) = \frac{\rho_{ce}}{\rho_w + \rho_{ce}\omega_0} \cdot (\omega_0 - 0.3375\alpha)V \tag{6.6}$$

The volume of the solid material can be determined by subtracting the volume which is occupied by the porosity from the total volume involved. The volume of the solid material can now be determined by:

$$V_s(\alpha) = (1 - n(\alpha))V \tag{6.7}$$

Initially (α=0), the total pore volume $V_{por}(\alpha)$ is equal to the volume which is occupied by the capillary water (aqueous phase). When hydration proceeds, capillary water will be consumed by the hydration process and, due to this, the capillary pores will be emptied. The pores can be emptied partly or completely. The relationship which describes the volume of capillary water that is actually available in the system is proposed as follows:

$$V_{cap}(\alpha) = \frac{\rho_{ce}}{\rho_w + \rho_{ce}\omega_0} \cdot (\omega_0 - 0.4\alpha)V \tag{6.8}$$

A different notation is introduced to obtain the degree of saturation of the pore structure. The degree of saturation s(α) describes the ratio between the volume of capillary water in the pore structure and the total pore volume as follows [92]:

$$s(\alpha) = \frac{V_{cap}(\alpha)}{V_{por}(\alpha)} \tag{6.9}$$

With the degree of saturation (eq.(6.9)) and the porosity (eq. (6.4)), it is possible to describe the volume of the capillary pore water which is actually available in the microstructure. This can be denoted by:

$$V_w(\alpha) = s(\alpha) \cdot n(\alpha) \cdot V \tag{6.10}$$

Implicitly, with the definition of the porosity n(α) and the degree of saturation s(α), the volume of gas in the system is also defined. For instance, if all pore space is filled with water (s(α=0)=1), there will be no gas in the system (ignoring dissolved gas). If hydration proceeds, capillary water will be taken out of the system. This means for the degree of saturation that s≤1. On the other hand, if all water is used up by the cement hydration, the pores would be completely empty (s=0). At that particular time, there will be only gas in the system. This elucidates that the degree of saturation ranges between zero and one (0≤s<1). The actual value depends on the state of the hardening process. At a certain degree of saturation, somewhere in the range between 0 and 1, the pore space is occupied partly with water and partly with gas. This gas volume $V_g(\alpha)$ can be defined by:

$$V_g(\alpha) = (1 - s(\alpha)) \cdot n(\alpha) \cdot V \tag{6.11}$$

The individual contributions as well as a change of one of the contributions in the cement paste system can now be described completely with the three equations (6.7), (6.10) and (6.11). These three contributions change constantly throughout the hydration process. In

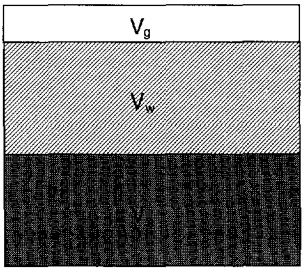

Volume parts

$V_s=(1-n)V$

$V_w=snV$

$V_g=(1-s)nV$

where:

n = porosity

s = saturation

V=elementary volume

Fig. 6.6. Schematical representation of the cement-water-gas system.

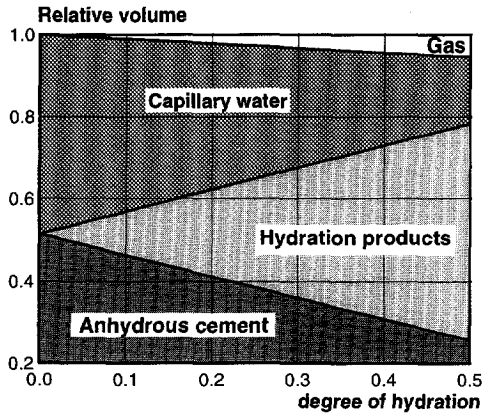

Fig. 6.7. Development of the volume components versus degree of hydration for a Portland cement (Blaine 550 m^2/kg) with a water/cement ratio of 0.3. (External volume constant).

Fig. 6.6, for an arbitrary state of the hardening process, the volume components involved in the system are shown schematically. In Fig. 6.7, the variation of the different volumetric components are presented as a function of the degree of hydration (see also Table 6.2). In this figure, the volume of the solid material is considered to be built-up from anhydrous cement and hydration products (e.g. gel). Furthermore, the decreasing volume of the capillary water and the increasing volume of gas can be observed clearly. Together, the contributions of all volumes, viz. volume of solid, water and gas, correspond with the total volume of the sample V (the external deformation of the paste volume is disregarded in this figure). This means that conservation of volume is accounted for, i.e. $V_s+V_w+V_g=V$. The conservation of volume must be satisfied continuously throughout the hardening process.

Table 6.2. Components in the cement-water-gas system.

Original components before hydration	Components at a certain degree of hydration
anhydrous cement	anhydrous cement
capillary water	hydration products
dissolved gas	capillary water
	dissolved gas
	pore space filled with gas

6.5 Current HYMOSTRUC potential on ribbon hydration

6.5.1 Paste density and water/cement ratio

In the present stage of the development of the HYMOSTRUC model it is already possible to calculate several material properties of the ribbon paste. For the calculation of these material properties, the ribbon model as proposed in section 6.3 (two aggregate particle system) will be applied. However, it is not possible the take into account the effect of transport of capillary water and gas on the hydration process. The necessary extension of the model with this feature will be outlined later in section 6.7. The current approach concerning the hydration of the ribbon paste starts with a description of the "paste density" of the microstructure. This presumed description of the local paste density between the two aggregates (ribbon) is based on a chosen analytical function [16]. This function yields as follows:

$$\zeta_{pa}(x) = \zeta_{pa}\left[1-(1-(x/C_0)\cdot e^{-\frac{x}{C_0}}\right] \quad \forall \quad 0 \le x \le \frac{1}{2}R_t \tag{6.12}$$

where is C_0 a constant that determines the shape of the declining paste density curve at the ITZ, x is the ribbon width co-ordinate and ζ_{pa} is the initial volumetric paste density. This paste density is defined as the cement volume relative to the volume of fresh paste:

$$\zeta_{pa} = [1+(\rho_{ce}/\rho_w)\omega_0]^{-1} \tag{6.13}$$

The analytical function (6.12) is defined for half the ribbon length ($R_t/2$). The symmetrical part can be obtained by the mirror of this function. The major disadvantage of the application of an analytical function instead of a "real" particle structure is the fact that the analytical function is just a phenomenological description of the real situation. It describes only the change of the paste density in outward direction. As mentioned before, with this function, the thickness of the ITZ for an arbitrary ribbon paste can be adjusted by the factor C_0. This analytical function, however, does not relate the thickness of the ITZ, to the spatial distribution of the cement particles in that particular region. The distribution of the paste density determined for a random particle structure, can be considered as an extension of this analytical function. This will be discussed later, in section 6.6.

With the equations (6.12) and (6.13), a description for the distribution of the local paste density of the ribbon paste can be obtained. From this formulation, the distribution of the water/cement ratio can also be obtained according to (6.13). As an example, for a regular HSC with a water/cement ratio of 0.3, the distribution of the local paste density and the local water/cement ratio for a ribbon length of R_t=100 μm, is presented in Fig. 6.8. From this figure, it can be seen that the analytical function describes the distribution of the local paste density and also the local water/cement ratio well.

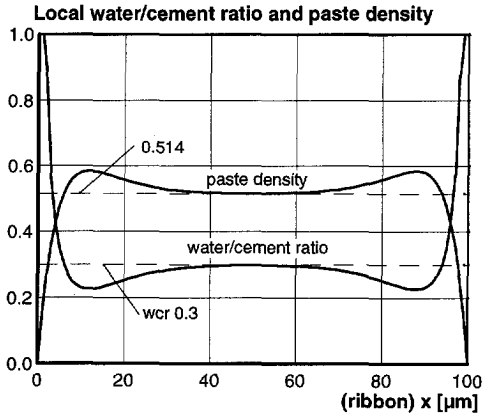

Fig. 6.8. Distribution of local paste density and local water/cement ratio for a ribbon paste with a thickness of 100 μm. (C_0=6).

At the close vicinity of the aggregate surface, the local paste density is almost zero. When going from the aggregate surface to the bulk paste, the local paste density increases and exceeds the mean paste density. After reaching its maximum, the local paste density reduces and approaches the mean paste density. The local water/cement ratio follows almost the opposite course. Close to the aggregate surface, the local water/cement ratio is substantially higher than the mean water/cement ratio. At the bulk paste region, the local water/cement ratio approaches the mean water/cement ratio.

6.5.2 Degree of hydration

The development of the degree of hydration for a certain position in the ribbon paste can be determined by application of the local paste density and the local water/cement ratio profiles as given in Fig. 6.8. For this calculation, the current HYMOSTRUC model can be applied. In, the degree of hydration for the ribbon paste is presented for three different periods of time. Due to the existence of relatively more smaller particles close to the aggregate surface (ITZ) in combination with the high water/cement ratio, high values for the degree of hydration develop in that particular region. The smaller particles (in ITZ) will hydrate (dissolve) faster than the larger particles which are situated more frequently in the bulk paste region. From Fig. 6.9, it can be seen that close to the aggregate surface, the cement hydrates almost completely ($\alpha \approx 1$) whereas the cement at the bulk paste hydrates only for about 40%. This will result in large gradients of the properties in the ribbon paste.

6.5.3 Porosity

Despite the higher degree of hydration at the ITZ, the porosity $n(\alpha)$ in that particular region will be higher than the porosity of the bulk paste. This phenomenon can be

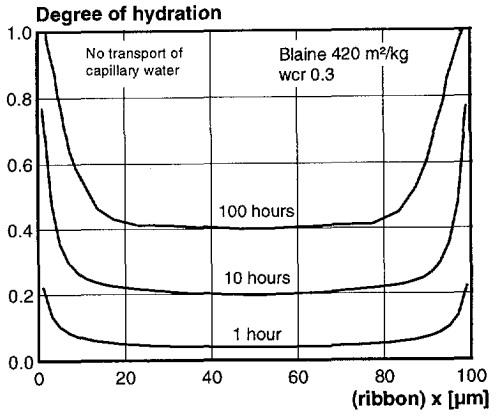

Fig. 6.9. Degree of hydration of ribbon paste for different periods of time (T=20°C).

attributed to the "wall effect" of the cement particles close to the aggregate surface. The variation of the porosity over the ribbon paste is presented in Fig. 6.10 (left). After 10 hours of hardening, the porosity at the ITZ appears to be about 60% whereas the porosity in the bulk paste reaches a value of about 30%. At the bulk paste, the porosity drops from about 50% to almost 30 % after 100 hours of hydration. The differences in porosity are mainly caused by the different volumes of hydration products that are formed at the particular regions. On the right hand side of Fig. 6.10, the porosity is shown as a function of time. The different porosity between the ITZ and the bulk paste are very pronounced. In comparison with the bulk paste, the porosity at the ITZ remains higher with the elapse of time.

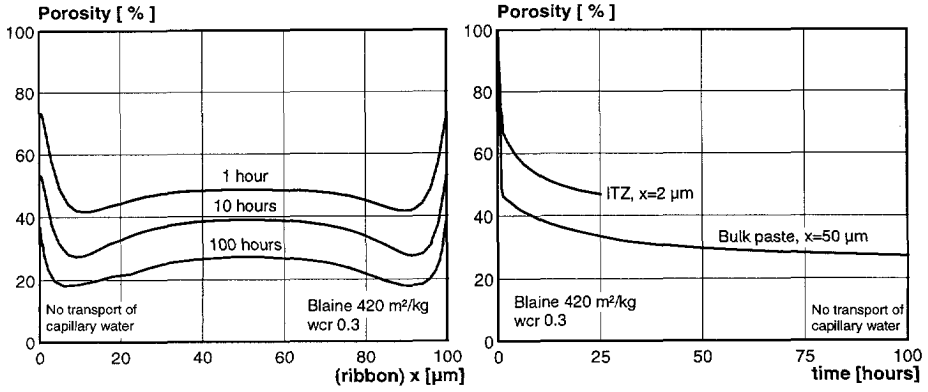

Fig. 6.10. Calculated porosity over the ribbon. Left: Porosity after 1, 10 and 100 hours of hydration. Right: Development of the porosity versus time in ITZ and bulk paste.

6.5.4 Degree of saturation

The pore structure in a hardening cement paste consists of pores of various diameters. Depending on the state of the hydration process, pores can be filled with water or can be empty. In order to know to what extent the pores are filled with water, the degree of saturation can be adopted, as defined earlier (eq. (6.9)). It describes the ratio between the volume of capillary water and the total pore volume. The evolution of this parameter during the hardening process depends on the development of the pore structure as well as on the rate of the consumption of capillary water by the cement-water reaction. It is emphasised that these processes are correlated to each other. The pore volume decreases while water is also consumed by the hydration process. This means that the degree of saturation is almost constant during hydration. In Fig. 6.11, the degree of saturation is presented as a function of time. It concerns the cement paste with a water/cement ratio of 0.3 and a cement fineness of 420 m^2/kg (see also Fig. 6.8). On the left hand side of this figure, the degree of saturation is presented for three different stages of the hardening process, viz. 1, 10 and 100 hours. At the bulk paste region, the degree of saturation decrease from about 100% after 1 hour of hydration to about 85 % after 100 hours of hardening. At the region where the local paste density reaches its minimum, there is not enough water to proceed the hydration process. The low water/cement ratio (see Fig. 6.8) causes a shortage of capillary water in that particular region.

On the right hand side of Fig. 6.11, the degree of saturation is presented for the interfacial transition zone as well as for the bulk paste. From this figure, it can be observed that the degree of saturation in the bulk paste is higher than at little distance from the ITZ. This is due to the shape of the analytical function that describes the local water/cement ratio. The function describes a local minimum between the ITZ and the bulk paste (see Fig. 6.8).

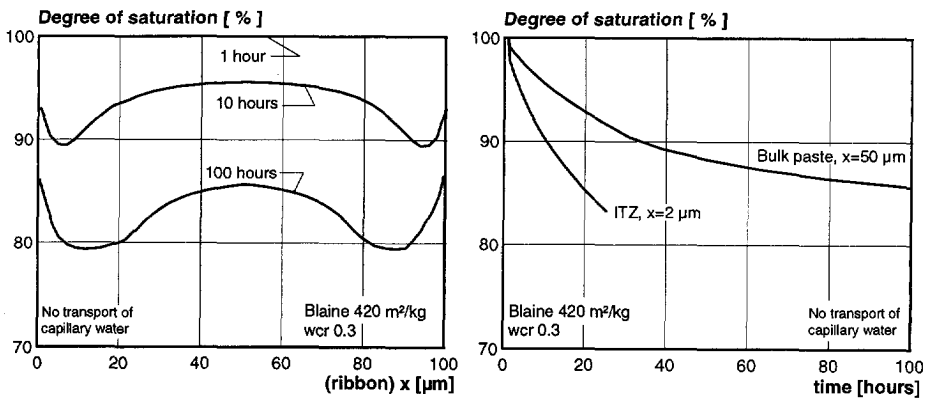

Fig. 6.11. Calculated variation of the degree of saturation over the ribbon. Left: Degree of saturation after 1, 10 and 100 hours of hardening. Right: Degree of saturation versus time at the ITZ and bulk paste.

6.6 Ribbon hydration of random particle structures

6.6.1 General

In order to get a more realistic description of the development of the local water/cement ratio and the local paste density of the ribbon paste, a random particle structure will be applied. The background of this particle structure was discussed earlier in chapter 3. For this approach, a similar the composition will be adopted to the cement paste that was adopted in the previous section, i.e. a paste with a water/cement ratio of 0.3 and a cement of medium fineness (Blaine 420m^2/kg). However, to elucidate some trends, also a water/cement ratio of 0.5 will be considered in this section. The development of the degree of hydration of the ribbon paste, as well as the value of the local water/cement ratio over the thickness of the ribbon, are both based on the "real" random particle structure. This particle structure is based on randomly parked cement grains which are distributed according to the Rosin-Rammler distribution function [16]. The influence of the so called "wall effect" at the ITZ is also taken into account in this structure. In this way, the description of the fresh paste is geometrically more realistic.

6.6.2 Random particle size distribution in sphere

In Fig. 6.12, two cross-sections of a particle structure are presented, representing the packing of cement particles near the aggregate surface. The spatial distribution of the particles is based on a 3-dimensional particle structure (see chapter 3). The aggregate surface is simulated by a fictitious border plane as was discussed in section 3.3.2. The particle structure concerns two different cement pastes with a cement of medium fineness (420 m^2/kg). On the left hand side of the figure, the paste with a water/cement ratio of 0.3 is presented while on the right hand side a paste with a water/cement ratio of 0.5 is shown. The figure shows that the mean particle spacing for the cement paste with a water/cement ratio of 0.3 is much smaller than for the cement paste with a water/cement ratio of 0.5. From the figure, it can be seen that packing of the cement particles in the close vicinity of the aggregate surface is mainly determined by the fineness of the cement and the water/cement ratio. Close to the aggregate surface, particles of high fineness show a denser packing than the particles of low fineness. A denser packing also exists at locations where the local water/cement ratio is relatively low. Different packing of the particles results in different porosities in the transition zones.

6.6.2.1 Paste density and water/cement ratio

The paste density is inversely proportional to the water/cement ratio (eq. (6.13)). The variation of the paste density over the ribbon thickness is directly related to the spatial distribution of the cement particles. In Fig. 6.13, the variation of the local paste density is presented for two different water/cement ratio's (see Fig. 6.12). The results show the course of the paste density as a function of the distance from the aggregate surface.

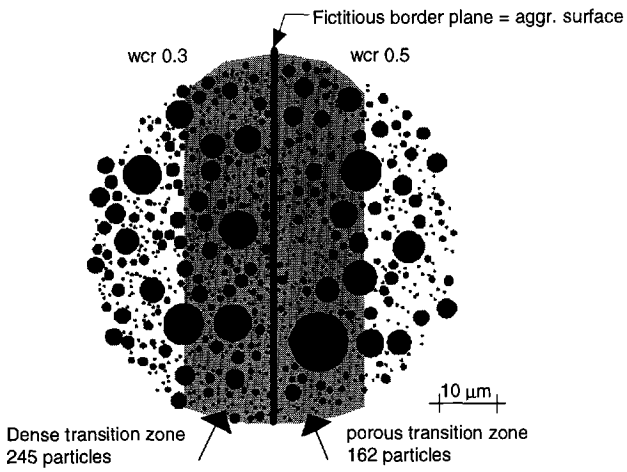

Fig. 6.12. Impression of the difference in particle packing in the transition zone for a water cement ratio of 0.3 and 0.5 (Blaine 420 m^2/kg).

Three different cement finenesses are considered. The initial paste density is also inserted in the figure (eq.(6.13)). The paste with a water/cement ratio of 0.3 has an initial paste density of 0.514 and the paste with a water/cement ratio of 0.5 has an initial density of 0.388.

For a random particle structure, it appears that the local paste density deviates strongly from the initial value when approaching the aggregate surface. This phenomenon is determined geometrically by the packing of the cement particles close to the aggregate surface. The thickness of the interfacial transition zone depends on the fineness of the

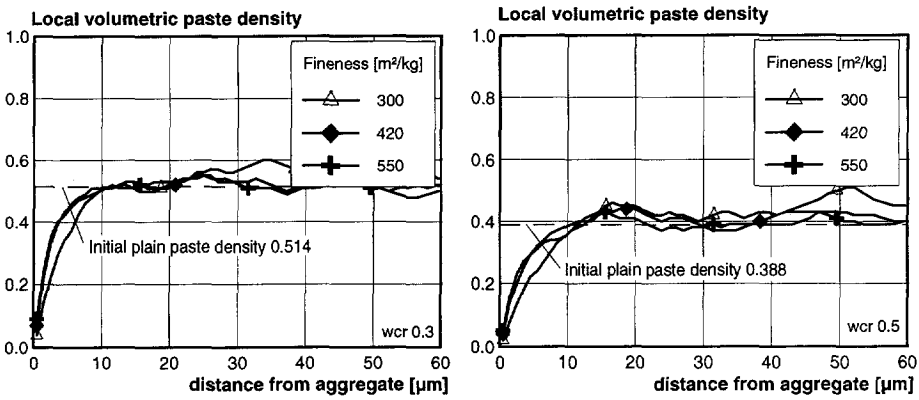

Fig. 6.13. Local volumetric paste density versus distance from the aggregate surface. Left wcr 0.3, right wcr 0.5.

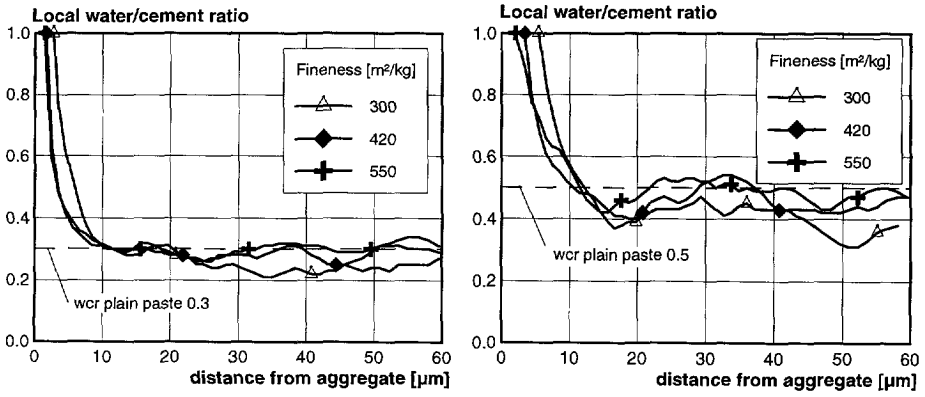

Fig. 6.14. Local water/cement ratio versus distance from aggregate surface. Left wcr 0.3, right wcr 0.5 (global).

cement and on the water/cement ratio. The finer the cement, the thinner the transition zone will be. In Fig. 6.14, the local water/cement ratio is presented versus the distance of the aggregate surface. The results are calculated from the local paste densities as presented in Fig. 6.13. From this figure it can be seen that the discontinuity of the water/cement ratio is determined geometrically. The thickness of the interfacial zone can be influenced by changing either the cement fineness or the water/cement ratio. However, from Fig. 6.14 it can be seen that the thickness of the interfacial zone is more sensitive to variations of the water/cement ratio than to variations of the fineness of the cement. For a coarser cement, the variation of the local water/cement ratio increases with the distance from the aggregate surface. The results show a bigger scatter. Initially, this will also effect the hydration process. However, if transport of capillary water is able to take place, these differences may vanish. This effect will be discussed in more detail in the following sections.

6.6.3 Random particle size distribution in tube

The local paste density and the local water/cement ratio is also determined for a ribbon paste. The ribbon paste is based on the random particle structure where the particles are parked randomly in a tube structure (see Fig. 3.9 and Fig. 6.3). In Fig. 6.15, for a similar ribbon thickness of R_t=100 µm, the variation of the local water/cement ratio and the local paste density is presented.

6.6.3.1 Evolution of the degree of hydration over the ribbon thickness

The evolution of the degree of hydration at the interfacial zone (ITZ) differs substantially from the bulk paste. The relatively large amount of fine cement particles in a water-rich region (ITZ) will lead to a faster development of the degree of hydration in that region (ITZ). The thickness of the zone where the degree of hydration is relatively higher

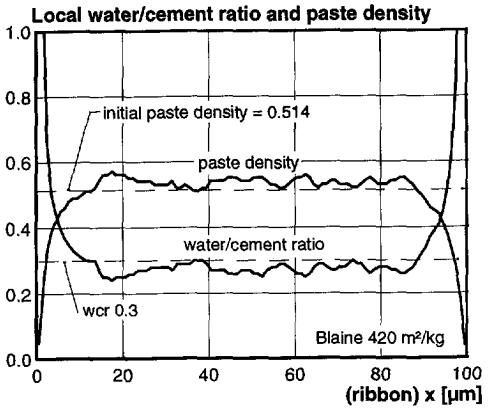

Fig. 6.15. Distribution of the paste density and the water/cement ratio for ribbon paste.

depends on the geometrical packing of the particles. From literature data, it appears that this distance ranges roughly between 0 and 20 µm [16]. In addition, this order of magnitude of the extension of the ITZ is also found numerical simulations with a random particle structure (see also section 6.6.2.1). The evolution of the degree of hydration of the ribbon paste is presented in Fig. 6.16. For this, the distribution of the water/cement ratio over the ribbon has been adopted, as was shown earlier in Fig. 6.15. It must be noticed that no interaction regarding the transportation of capillary water and gas has been taken into account. The influence of this phenomenon on the hydration process will be discussed in more detail in section 6.7.

The development of the degree of hydration as shown in Fig. 6.16 shows the same tendency as the degree of hydration as shown earlier in Fig. 6.9. The main difference in the degree of hydration shown in these figures is caused by the different courses of the local water/cement ratio over the ribbon paste. In Fig. 6.16, the water/cement ratio is based on the random particle structure whereas in Fig. 6.9, the distribution of the water/cement ratio was based on the analytical function (eq. (6.12)).

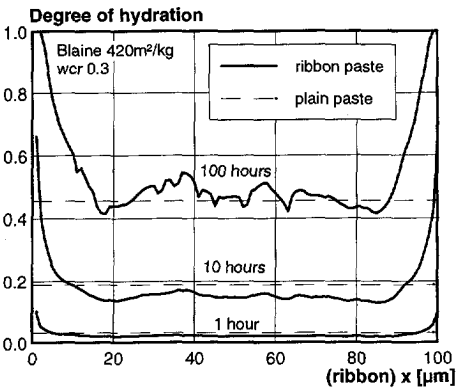

Fig. 6.16. Degree of hydration of ribbon paste based on random particle structure.

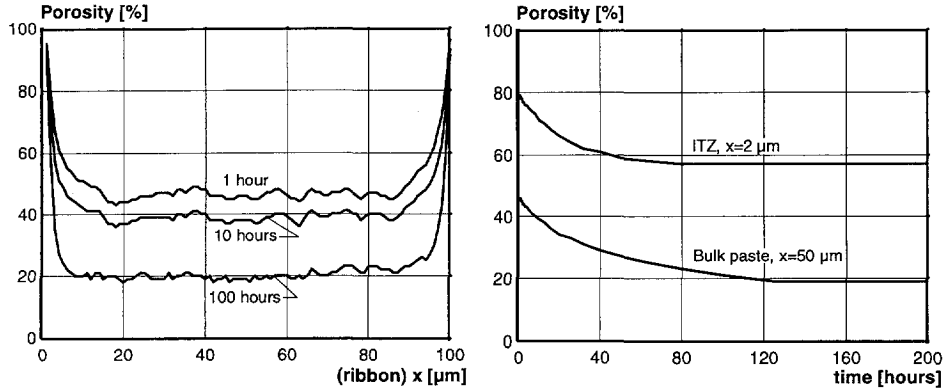

Fig. 6.17. Variation of porosity over the ribbon. Left: Porosity after 1,10 and 100 hours of hardening. Right: Development of porosity versus time at ITZ and bulk paste.

6.6.3.2 Porosity

Fig. 6.10 shows that the porosity ranges roughly between the 100 % at the close vicinity of the aggregate surface (ITZ), to about 20% for the bulk paste. The exact value depends on the degree of hydration. The porosity is decreases with increasing degree of hydration. As hydration proceeds, more hydration products will be formed that fill-up the capillary pore space. This process will reduce the porosity. However, the high water/cement ratio dominates the porosity in the ITZ. The development of the porosity of the ribbon paste that corresponds with a water/cement ratio as presented in Fig. 6.15, is given in Fig. 6.17. Despite the higher degree of hydration at the ITZ, the porosity of the paste near the aggregate surface is high. From this, it can be deduced that the high porosity near the aggregate surface can be attributed directly to the particle packing in that area, i.e. the spatial distribution of the cement grains in the aqueous phase (see Fig. 6.12). The results of Fig. 6.17 can be compared with the results of Fig. 6.10, where Fig. 6.10 represents the porosity of the ribbon paste based on an analytical formulation for the water/cement ratio. Differences in the results of the porosity can be attributed to differences in the course of the local water/cement ratio as considered in the different approaches.

6.6.3.3 Degree of saturation

It is also possible to determine the development of the degree of saturation for the random particle structure as was presented in this section (see also Fig. 6.3 and Fig. 6.15). The results show a similar tendency as the results that were shown in
Fig. 6.11 (mathematical description of water/cement ratio). However, after 100 hours of hardening, the degree of saturation of the random particle structure is lower (≈80%) than the degree of saturation as presented in Fig. 6.11 (≈84%). This can be related to the fact

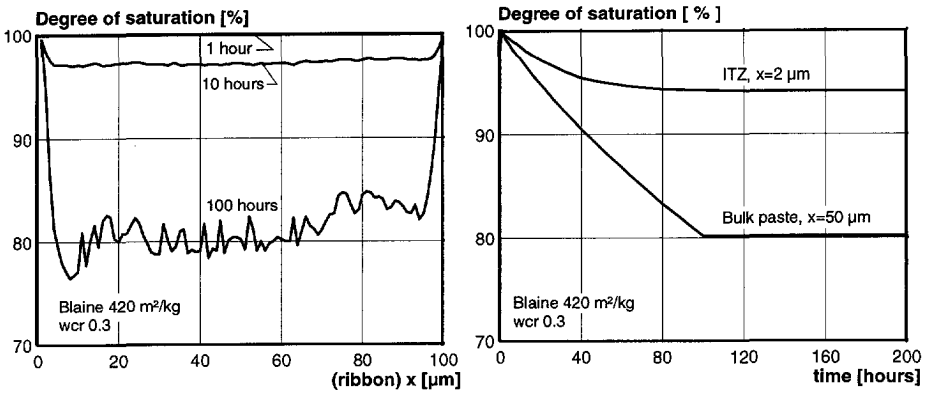

Fig. 6.18. Variation of the degree of saturation over the ribbon. Left: degree of saturation after 1, 10 and 100 hours of hardening. Right: degree of saturation versus time at ITZ and bulk paste

that conservation of volume for the random particle structure is dealt with accurately, whereas for the mathematical description of the water/cement ratio, conservation of volume may not satisfied. This leads to differences in the state of the capillary water of the hardening cement paste.

6.7 Towards the effect of modelling of moisture transport on ribbon paste hydration

6.7.1 General

In order to allow for transport of capillary water and gas through the hardening microstructure, in this section a model will be derived with which this phenomenon can be described. It will be shown how the transport of capillary water and gas between the subsequent HYMOSTRUC elements that are considered in this ribbon can be established.

Transport of capillary water and gas in hardening cement paste can be modelled by considering the capillary pores of an arbitrary pore structure as the transport medium. Cement paste contains pores of different sizes. The size of the pores changes continuously throughout the hydration process. In general, a distinction can be made between three different classes of pores, viz. *gel pores, capillary pores and air voids* (see section 3.2.3.5). The gel pores are the smallest pores and are considered to be unable to transport water through the microstructure. Since the air voids are closed volumes, they are also not able to transport the water throughout the matrix. Only capillary pores, with a minimum pore diameter of 0.002 µm, are considered to be able to

transport the water through the developing pore system. The maximum pore diameter can be determined by assuming a pore size distribution as presented with equation (3.1) (see also appendix D).

At the start of the hydration process, all pores are filled with water. With increasing degree of hydration the pore water volume reduces mainly at the cost of the larger pores. This also means that the relative cross-section of the pores that are able to transport capillary pore water becomes smaller as hydration proceeds. This phenomenon is taken into account in the model and is represented by the effective permeability of the hardening paste.

Thermodynamic equilibrium in the pore-system associates with a reduction of the pressure in the gradually emptying pores space. (see chapter 4). Differences in the pore pressure in the ribbon paste will cause a movement of capillary water through the (partly) filled capillary pores. The gas pressure in the gradually emptying pore space can be considered as being one of the driving forces behind the transport of capillary water and gas. Changes in the gas pressure, on their turn, are caused by progressive hydration.

The proposed model describes the transport of the capillary water and gas as a function of the pressure differences and microstructural changes. A similar kind of approach has also been followed by Verruijt [91]. He derived a model for groundwater flow in partially saturated sand. In his analysis, the pressure difference which develops in the ground water is considered to be the driving force behind the transport of the ground water through the porous medium (sand). This mechanism is comparable with the mechanism in hardening cement paste. However, as far as hardening cement paste is

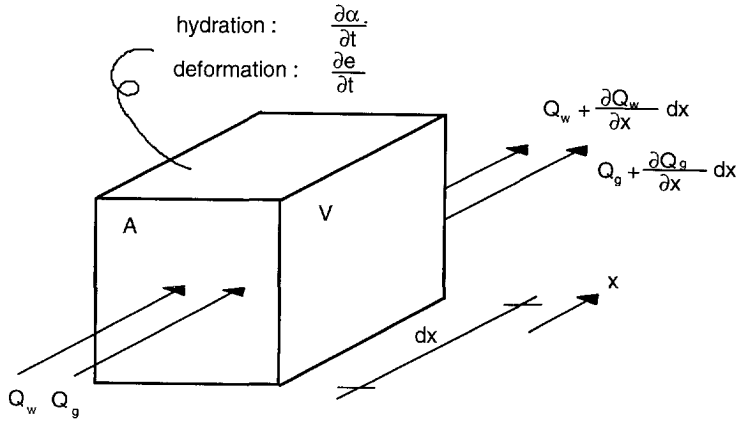

Fig. 6.19 Elementary volume V

concerned, water will also be consumed due to the cement hydration. Consumption of capillary water due to cement hydration is also accompanied by the deformation of the microstructure (autogenous deformation). This may be a dominant effect and must therefore also be taken into account in the formulation of the transport mechanism.

6.7.2 Derivation of a differential equation for moisture transport

The partial differential equation will be derived for the ribbon paste model as presented earlier in Fig. 6.3. The ribbon is subdivided into several (used is 100) elements. All these elements are considered to be built-up from three components viz. cement, water and gas. The hydration process of each element is calculated independently with the HYMOSTRUC model.

Consider an elementary volume V that is built-up from cement, water and gas. The volumetric contributions of these contributions change as hydration proceeds. During this process, the contributions may become affected by several mechanisms. At the initial state of hardening, the volume of cement V_s, water V_w and gas V_g are equal to the volume V. This can be denoted by:

$$V_s + V_w + V_g = V \tag{6.14}$$

Hydration will affect all three components in the system. Consider an infinitesimal small period of time ∂t. During this period, the three volumetric contributions will change according to:

$$\frac{\partial V_s}{\partial t} + \frac{\partial V_w}{\partial t} + \frac{\partial V_g}{\partial t} = \frac{\partial V}{\partial t} \tag{6.15}$$

The change of the different volumetric contributions is driven by the degree of hydration. Each contribution follows a unique rate (see Fig. 6.7). For the change of the volume of the solid material, the following relation can be derived using equation (6.7). Disregarding the notation (α), it holds that:

$$\frac{\partial V_s}{\partial t} = -V\frac{\partial n}{\partial t} \tag{6.16}$$

From this relationship it can be noticed that the volume of the solid material changes when the porosity changes. This can be the result of either a change of the capillary pore volume or by a change of the pore volume which is introduced by the chemical shrinkage.

The water volume in the system is considered to change if either transport of the water takes place, or the available water is compressed or the water is taken out of the system due to hydration. These three contributions are responsible for a change of the capillary water volume in a certain "slice" in the ribbon (see Fig. 6.3). The three contributions can be described mathematically in the following way (for notations also see appendix B):

$$\frac{1}{V}\frac{\partial V_w}{\partial t} = \frac{\partial}{\partial x}\left(\frac{k_w}{\gamma_w}\frac{\partial p_w}{\partial x}\right) \qquad \text{transport of water} \qquad (6.17)$$

$$\frac{1}{V}\frac{\partial V_w}{\partial t} = -ns\beta\frac{\partial p_w}{\partial t} \qquad \text{compression of water}$$

$$\frac{1}{V}\frac{\partial V_w}{\partial t} = -\frac{0.4\rho_{ce}}{\rho_w + \rho_{ce}\omega_0}\frac{\partial \alpha}{\partial t} \qquad \text{consumption due to hydration}$$

Together these contributions describe the change of the water volume in the ribbon during a small time step ∂t.

The gas volume also changes during the hydration process. During a small time step ∂t, the gas volume may change due to transport of gas through the emptied pore volume or it may change due to compression of the gas (see [91]). If hydration proceeds, the consumed capillary water becomes replaced partly by gas and partly by solid. These influences can be denoted as follows:

$$\frac{1}{V}\frac{\partial V_g}{\partial t} = \frac{k_g}{2\gamma_g p_g}\frac{\partial^2 p_g^2}{\partial x^2} \qquad \text{transport of gas} \qquad (6.18)$$

$$\frac{1}{V}\frac{\partial V_g}{\partial t} = -\frac{(1-s)n}{p_g}\frac{\partial p_g}{\partial t} \qquad \text{compression of gas}$$

$$\frac{1}{V}\frac{\partial V_g}{\partial t} = \frac{0.0625\rho_{ce}}{\rho_w + \rho_{ce}\omega_0}\frac{\partial \alpha}{\partial t} \qquad \text{contribution due to hydration}$$

These three contributions, see equations (6.16), (6.17) and (6.18), describe the changes of the three different components in the cement paste system. According to the volume balance in equation (6.15), the summation of a change of the solid volume, the water volume or the gas volume must be equal to the change of the elementary volume V. The change of the elementary volume V is in fact a macro deformation of the developing microstructure. This can be the result of e.g. autogenous deformation. For this volumetric deformation of the elementary volume V, it can be denoted that:

$$\frac{1}{V}\frac{\partial V}{\partial t} = \frac{\partial e}{\partial t} \qquad (6.19)$$

where e is the volume strain. Substitution of the equations (6.16), (6.17), (6.18) and (6.19) into the balance equation (6.15), leads to the partial differential equation which describes the transport of capillary water and gas through the developing microstructure. As a first approach it is assumed that the porosity n, the gas volume V_g and the external

deformations are constant during a time step ∂t ($\partial V_s/\partial t=0$, $\partial V_g/\partial t=0$ and ($\partial V/\partial t=0$). Disregarding these effects leads to the following differential equation:

$$\frac{\partial p_w}{\partial t} = \frac{1}{n\beta}\frac{\partial}{\partial x}\left(\frac{k_w}{\gamma_w}\frac{\partial p_w}{\partial x}\right) - \frac{0.4\rho_{ce}}{n\beta(\rho_w + \rho_{ce}\omega_0)}\frac{\partial \alpha}{\partial t} \qquad (6.20)$$

This simplified equation describes the change of the pressure in the capillary water due to a differences in the consumption of the capillary water by cement hydration. The capillary water in the ribbon paste may start to flow due to pressure gradients in the capillary water.

Equation (6.20) can be solved implicitly. The way how this has been performed is described in detail in appendix B.

6.7.3 Permeability of hardening cement paste for water and gas

Modelling the permeability of hardening cement paste in a complex issue. Several authors proposed to schematisize the permeability by assuming the pores to be cylindrically shaped [9, 30, 79]. In [9], Bear suggested to model the pore-system by tubes. This approach has also been followed by Setzer [79]. The theory is based on the Hagen-Poisseuille law and leads to a linear relationship between the transport flux and the pressure gradient. This flow mechanism is based on Darcy's law. The Hagen-Poisseuille approach is only valid for laminar flow. This means that the Reynolds number ($Re=u\phi/\nu$, ϕ diameter, u flow rate and ν the kinematic viscosity) must be smaller than 2300. This was also investigated by Gertis et. al. [30]. Accepting the pore-system as being built-up of tubular shaped pores, it can be derived that the total discharge Q_{cap} of capillary water transported through one arbitrary pore with diameter ϕ is equal to:

$$Q_{cap} = -\frac{\pi\phi^4}{128\rho\nu}\frac{\partial p}{\partial x} \qquad (6.21)$$

where ρ is the density of the fluid or gas that will be transported. As far as hardening cement paste is concerned, the sizes of the pores involved in the transport of capillary water, follow a certain distribution. This means that in order to get the total discharge for the capillary water through all the capillary pores, the pore size distribution, as was earlier presented in chapter 3, must be considered. For this, it must be assumed that the pores are normally directed to the flow. From the pore size distribution, it can be derived that for the relative weight factor (dV/V) that determines the number pores of a certain pore diameter per fraction it holds:

$$\frac{dV}{V} = \frac{a}{\phi}\frac{d\phi}{V} \qquad (6.22)$$

In order to get the weighted specific discharge q for a pore size distribution of a developing pore structure, the discharge of one single tubular pore (eq. (6.21)) as well as the water or gas driving area of one single pore must be multiplied by the weight factor

(eq. (6.22)). Division of the discharge by the water or gas driving area leads to the weighted specific discharge for the pore size distribution as proposed in equation (3.1). This can be denoted by:

$$q = \frac{\frac{1}{V}\int_{\phi_0}^{\phi} \frac{a}{\phi} \frac{\pi\phi^4}{128\rho\nu} \frac{\partial p}{\partial x} d\phi}{\frac{1}{V}\int_{\phi_0}^{\phi} \frac{a}{\phi} \frac{1}{4} \pi\phi^2 d\phi} \tag{6.23}$$

Elaboration of this equation leads to the relationship between the pressure gradient and the specific discharge for the developing pore structure:

$$q = \frac{(\phi^2 + \phi_0^2)}{64\rho\nu} \frac{\partial p}{\partial x} \tag{6.24}$$

From this, the water permeability and also the gas permeability can be deduced. For this, the actual border limits of the capillary pores must be applied to equation (6.24) (see Fig. 6.20). These can be deduced from the pore size distribution. For the water permeability it is defined that:

$$k_w = \frac{\kappa_w \gamma_w}{\mu_w} = \frac{(\phi_0^2 + \phi_{wat}^2)\gamma_w}{64\mu_w} = \frac{(\phi_0^2 + \phi_{wat}^2)g}{64\nu_w} \tag{6.25}$$

and for the gas permeability it is defined that:

$$k_g = \frac{\kappa_g \gamma_g}{\mu_g} = \frac{(\phi_{wat}^2 + \phi_{por}^2)\gamma_g}{64\mu_g} = \frac{(\phi_{wat}^2 + \phi_{por}^2)g}{64\nu_g} \tag{6.26}$$

In these equations, κ_w is the intrinsic permeability of the driving part of the pore structure and κ_g the intrinsic permeability of gas driving part. This parameter only depends on the geometry of the pore structure (see Fig. 6.20). In the equations (6.25) and (6.26) the relationship between the dynamic viscosity of a fluid μ and the kinematic viscosity ν is used. These are related according to $\nu\rho=\mu$. The permeability for water and gas differ from each other due to the different viscosity, different density and also due

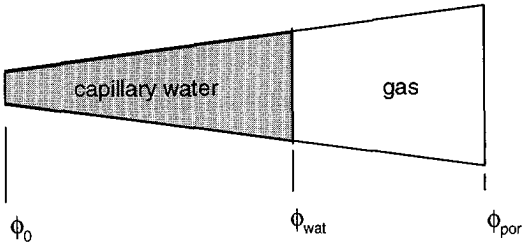

Fig. 6.20. Schematical representation of the border limits for the water permeability (between ϕ_0 and ϕ_{wat}) and gas permeability (between ϕ_{wat} and ϕ_{por}).

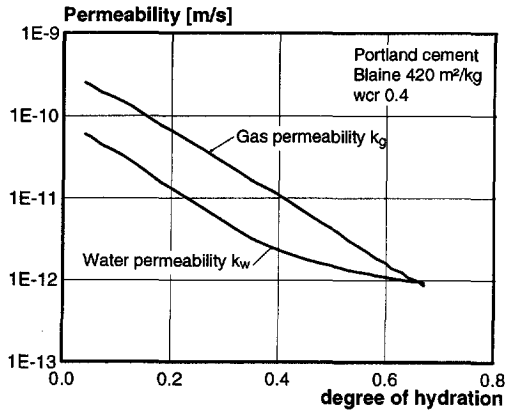

Fig. 6.21 Water and gas permeability versus degree of hydration.

to the different border limits for the intrinsic permeability. As an example, in Fig. 6.21, the water permeability k_w and gas permeability k_g versus degree of hydration of a hardening cement paste are presented. It concerns a Portland cement paste with a cement of medium fineness (Blaine 420 m^2/kg) and a water/cement ratio of 0.4. From the figure, it can be seen that the permeability of the water and gas range roughly between 10^{-9} m/s and 10^{-13} m/s. This is in good agreement with the limits as mentioned by Neville [65] (see also [83]).

The permeability depends strongly on the pore structure and the actual pore volume V_{por} of the hardening microstructure. According to equation (6.6), this pore volume is mainly a function of the water/cement ratio and the degree of hydration. In order to verify the sensitivity of the permeability to the water/cement ratio, the water permeability is

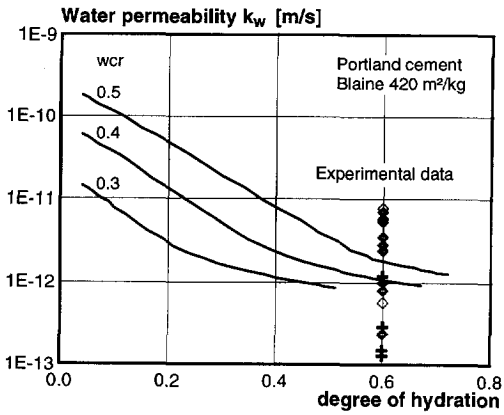

Fig. 6.22. Water permeability versus degree of hydration for three water/cement ratios. The inserted experimental data is taken from [70, 83].

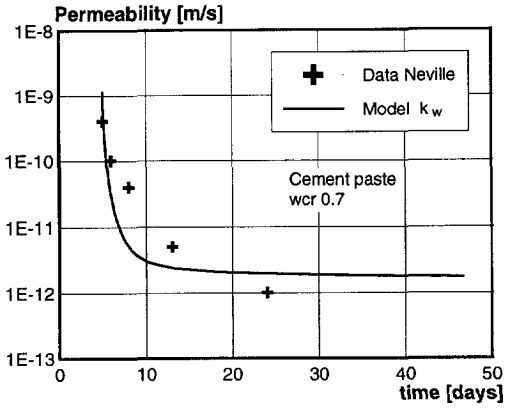

Fig. 6.23. Permeability versus time. Comparison of the model with data of Neville [65].

presented as a function of the degree of hydration in Fig. 6.22. It can be seen that the water permeability decreases for decreasing value of the water/cement ratio. For a plain Portland cement paste, based on cement of medium fineness, the water permeability for all three water/cement ratio's reaches a value of 10^{-12} m/s. This is in good agreement with the literature data [65, 83]. In Fig. 6.22, the experimental data is also shown of the permeability of various types of hardened cement with different water/cement ratio and different types of cement. For this, it is assumed that the degree of hydration of all pastes is 0.6. The experimental data gives a good impression of scatter of the permeability of the cement paste when hardened.

In Fig. 6.23, for a plain cement paste with a water/cement ratio of 0.7, the model as outlined in this section is compared with experimental data as given by Neville [65]. The model is comparable with the experimental data.

6.7.4 Permeability of ribbon paste

The permeability varies over the ribbon of a hardening cement paste. Close to the aggregate surface, the permeability differs from the permeability in the bulk paste. The variation of the water permeability as well as the variation of the gas permeability can be determined with the proposed model (see eq. (6.25) and (6.26)). In Fig. 6.24, the results are shown for the water and gas permeability of the ribbon paste. On the left hand side, a cement paste with a water/cement ratio of 0.3 is considered, whereas at the right hand side, the results are shown for a cement paste with a water/cement ratio of 0.5. The results show that the water permeability differs from the gas permeability. However, the results are rather similar. When approaching the aggregate surface, the permeability of both water and gas increases substantially. This can be attributed to the higher porosity at that particular region (Fig. 6.17). The results also show that the permeability of the paste with a water/cement ratio of 0.3 is lower than the paste with a water/cement ratio of 0.5. These differences are most pronounced at the very early ages of hardening. After hydration has ceased, both pastes (wcr 0.3 and 0.5) appear to reach an almost similar

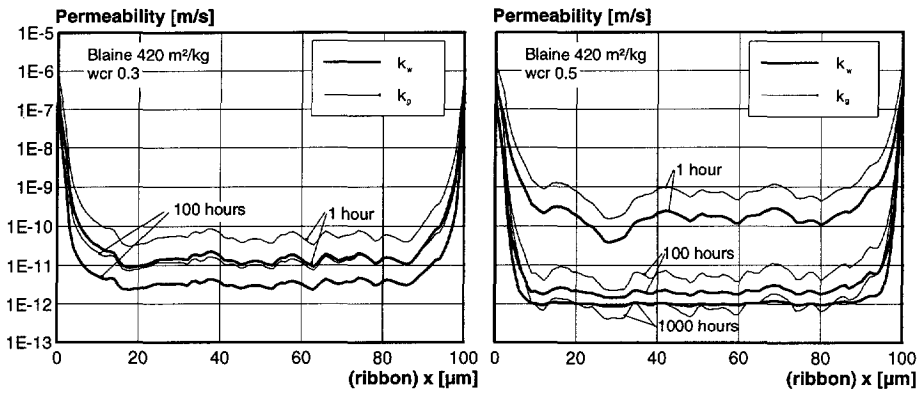

Fig. 6.24. Water and gas permeability of ribbon paste. Left: Water/cement ratio 0.3. Right: Water cement ratio 0.5. Blaine value 420m^2/kg.

permeability of about 10^{-12} m/s. This phenomenon has also been noted earlier from Fig. 6.22. The permeabilities of pastes with different water/cement ratio's converge almost to the same value. This feature can also be deduced from the literature given in [83].

6.8 Ribbon hydration with transport of water and gas

6.8.1 General

The transport of capillary water and gas through the hardening ribbon paste is accompanied by a change of the development of the hydration process and of the associated material properties. The water-rich interfacial zones may supply additional water to the bulk paste which promotes hydration in that part of the ribbon paste. A redistribution of the capillary water in the ribbon may also affect the relative humidity in the emptied pore space. A change in the relative humidity implicitly affects the autogenous shrinkage of the ribbon paste. It will also affect the internal gas pressure in the emptied pore space.

In this section, the development of the material properties of the ribbon paste will be discussed in detail. It concerns a ribbon paste with a water/cement ratio of 0.3 and 0.5 and a cement with a fineness of 420 m^2/kg. A ribbon thickness of 100 µm is adopted which can be considered as the upper boundary value for HSC mixtures [24] (see Fig. 6.5). At first, the development of the pressure in the capillary water will be discussed. The pressure gradients can be considered as the driving force behind the transport of the capillary water. After this, the development of various material properties will be presented and discussed with emphasis on the differences which are caused by the transport of capillary water.

6.8.2 Pressure in capillary water

As hydration proceeds, capillary water is bound to the cement chemically. This capillary water is taken out of the system. The rate at which the capillary water is taken out of the system strongly depends on the rate of hydration. Since the degree of hydration varies over the ribbon paste, the rate at which the water is taken out of the system will vary over the thickness of the ribbon paste as well. The different rates at which the water is consumed are accompanied by the installation of a certain pressure field. In Fig. 6.25, the pressure field is presented for a hardening cement paste with a water/cement ratio of 0.3 (Blaine 420m^2/kg). It can be noted that pressure in the capillary water reaches a maximum value of about -6.5 Pa in the middle of the ribbon (x=50μm). On both sides at the end of the ribbon, it was presumed that the pressure is equal to zero. It must be emphasised that the pressure in the capillary water must be considered relative to the pressure in the aggregate particles.

On the left hand side of Fig. 6.25, the pressure in the capillary water is presented for four different stages of the hardening process. From this figure, it can be seen that at a certain time, when the rate of hydration reaches its maximum, the pressure in the capillary water also reaches its maximum. On the right hand side of Fig. 6.25, it can be observed that the pressure in the capillary water reaches its maximum after about 25 hours of hardening. After that particular time, the pressure starts to decrease. This is the result of the change of the rate of the hydration process. At this stage, water transport becomes dominant over the pressure increase due to hydration (see eq. (6.20)).

The pressure gradient over the ribbon thickness will force the capillary water to move. According to the pressure field as presented in Fig. 6.25 (left), capillary water tends to move from the 'water-rich' ITZ to the 'water-poor' bulk paste. To what extent the movement of the capillary water will affect the development of the material properties of hardening cement paste (wcr 0.3 and 0.5), will be discussed in the next sections.

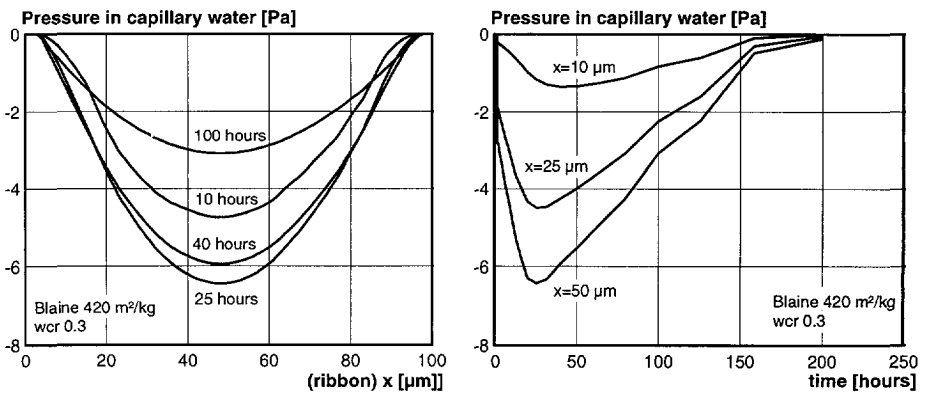

Fig. 6.25. Pressure in the capillary pore water for the ribbon paste. Left: Development of the capillary pressure at various ages. Right: Capillary pressure at different locations.

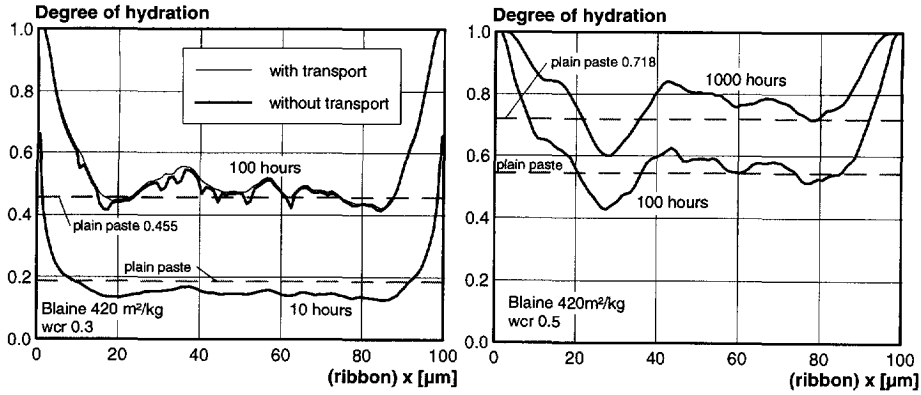

Fig. 6.26. Variation of the degree of hydration over the ribbon. Left: water/cement ratio 0.3. Right: water/cement ratio 0.5

6.8.3 Evolution of the degree of hydration in the ribbon paste

The redistribution of the capillary water over the ribbon paste is expected to influence the development of the degree of hydration. However, from the evolution of the degree of hydration as presented in Fig. 6.26 it can be seen that, according to the model, this influence is almost negligible. Minor differences appear between the results for the ribbon paste with a water/cement ratio of 0.3, if either transport of capillary water over the ribbon thickness is allowed for or if transport of capillary water is permitted. No differences were observed for the cement paste with a water/cement ratio of 0.5.

It is remarkable that the average degree of hydration of the ribbon paste (wcr 0.3) is about 16% higher than the degree of hydration of the plain paste, after 100 hours of hydration. This is in good agreement with the experimental results as presented by Roth [73]. According to Roth, the degree of hydration of mortar could exceed the degree of hydration of plain paste by 10%. This enhancement of the degree of hydration of the ribbon paste is due to the differences in the stereological packing of the cement particles.

For the ribbon paste with a water/cement ratio of 0.5 (Fig. 6.26), the average degree of hydration is also higher than the degree of hydration of the plain paste. After 100 hours of hardening, the average degree of hydration of the ribbon paste is about 12% higher than the degree of hydration of the plain paste and after 1000 hours of hardening this is 15%.

6.8.4 Degree of saturation in ribbon paste

The pressure field which develops during the hardening process (see Fig. 6.25) will discharge capillary water from the water-rich ITZ to the bulk paste of the ribbon. Pores that were emptied due to the hydration process, can become refilled again by the supply of additional water from the ITZ. The redistribution of the capillary water over the ribbon will lead to an other profile of the degree of saturation.

In Fig. 6.27, the change of the degree of saturation is presented while transport of

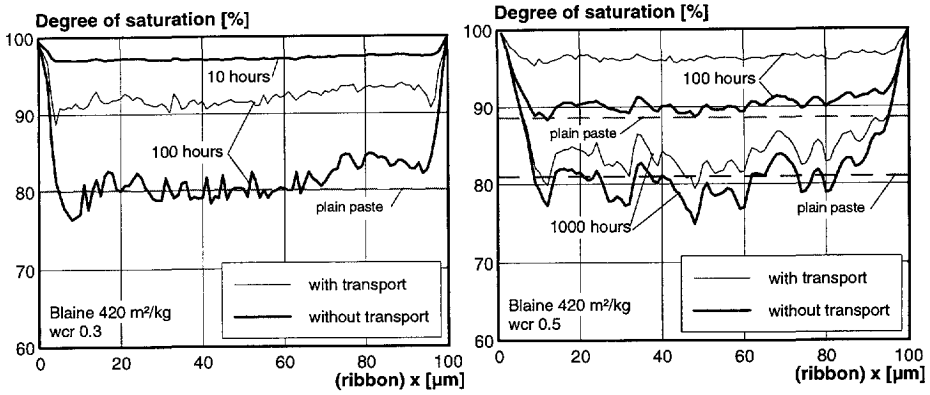

Fig. 6.27. Variation of the degree of saturation over the ribbon. Left: water/cement ratio 0.3. Right: water/cement ratio 0.5

capillary water has been accounted for. After 10 hours of hardening, no difference could be observed. However, after 100 hours of hardening, the degree of saturation in the bulk paste appears to increase from 80% to 90%. The influence of the redistribution of the capillary water appears to be substantial. For the cement paste with a higher water/cement ratio of 0.5 (right hand side), this influence turns out to be less. The degree of saturation for this paste increases about 4% due to the additional water supply from the ITZ.

From Fig. 6.28, it can be noted, that the development of the degree of saturation follows a different course if capillary water transport is accounted for. The results are shown for the centre of the ribbon (x=50µm). The additional water supply causes a substantial increase of the degree of saturation in this part of the bulk paste. The pores remain filled with capillary water for a longer time and the pores stay accumulated for a higher degree

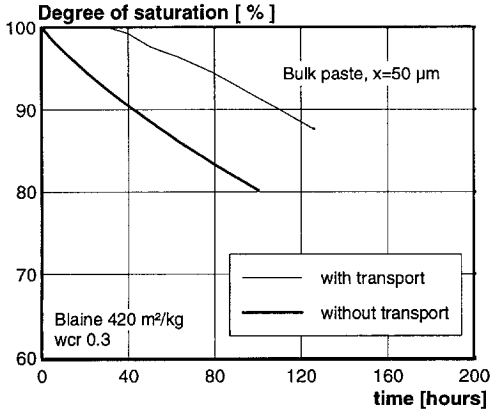

Fig. 6.28. Development of the degree of saturation with and without the influence of additional water supply due to the capillary transport (x=50 µm).

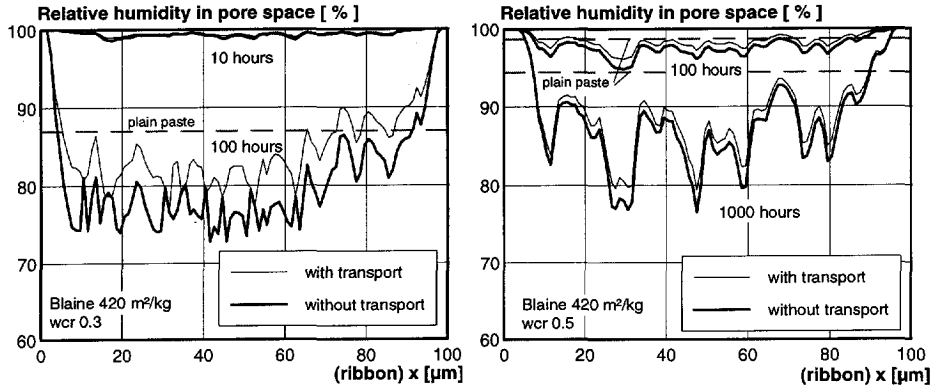

Fig. 6.29. Variation of the relative humidity over the ribbon. Left: water/cement ratio 0.3. Right: water/cement ratio 0.5.

during the hardening process. However, the increase of the overall degree of hydration due to the additional water supply appears to be negligible (see Fig. 6.26).

6.8.5 Relative humidity in the empty pore space

Thermodynamic equilibrium in the pore space requires that a change of the degree of saturation is accompanied by a change of the relative humidity. At the bulk paste region, the volume of the empty pore space decreases due to the supply of additional water. This is accompanied by an increase of the relative humidity. In Fig. 6.29 results of the relative humidity for a ribbon paste with a water/cement ratio of 0.3 (left) and a water cement ratio of 0.5 (right) are presented. The increase of the relative humidity in the bulk paste due to the transport of capillary water appears to be much more pronounced for the low water/cement ratio paste (wcr 0.3) in comparison with the high water/cement ratio paste (wcr 0.5). For the paste with a water/cement ratio of 0.3, the relative humidity appears to increase about 5% after 100 hours of hardening whereas the relative humidity of the paste with a water/cement ratio of 0.5 increases by only 1.5% after 1000 hours of hardening. These differences can be attributed to the fact that, on the one hand, the pressure gradients in the capillary water will be much smaller for the high water/cement ratio pastes, and, on the other hand, the higher water/cement ratio pastes contain enough water for the hardening process, also in the bulk paste. This appears to result in a less pronounced influence the relative humidity in the high water/cement ratio pastes.

6.8.6 Gas pressure in the empty pore space

The relative humidity in the empty pore space is defined as the ratio between the gas pressure in the empty pore and the atmospheric pressure (see section 4.2.5). This means that it is related to the gas pressure in the empty pore space (see section 4.2.6). The development of the gas pressure in the empty pore space (Fig. 6.30) shows, therefore, a similar tendency as the development of the relative humidity in the empty pore space.

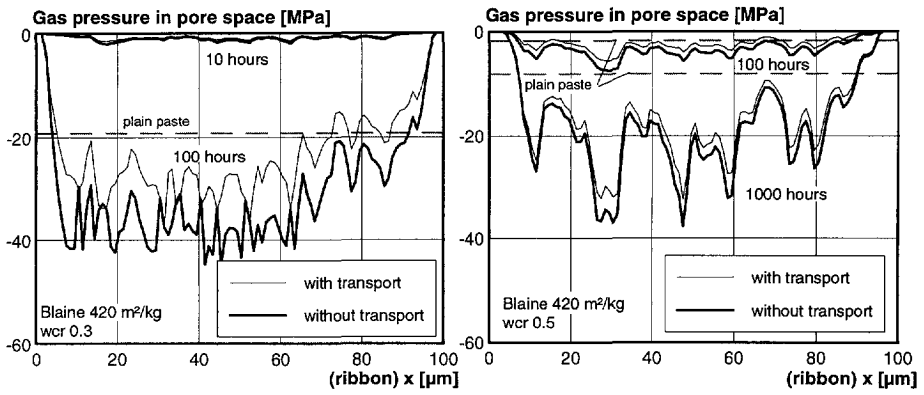

Fig. 6.30. Variation of the gas pressure over the ribbon thickness which prevails in the empty pore space. Left: water/cement ratio 0.3. Right: water/cement ratio 0.5.

In Fig. 6.30, the gas pressure in the empty pore space is presented for the two different cement pastes (wcr 0.3 and 0.5). For the cement paste on the left hand side (wcr 0.3), the influence of the additional water supply appears to result in a substantial reduction of the gas pressure in the empty pore space. This reduction is much less for the cement paste with the higher water/cement ratio (wcr 0.5).

6.8.7 Thickness of the adsorption layer in the pore space

The thickness of the adsorption layer in the pore space is determined by the actual relative humidity. A change of the relative humidity will also affect the thickness of the adsorption layer at the pore wall area. Due to a redistribution of the capillary water over the ribbon thickness, the relative humidity has changed (see Fig. 6.29). Implicitly, this also affects the thickness of the adsorption layer. However, the changes appear to be

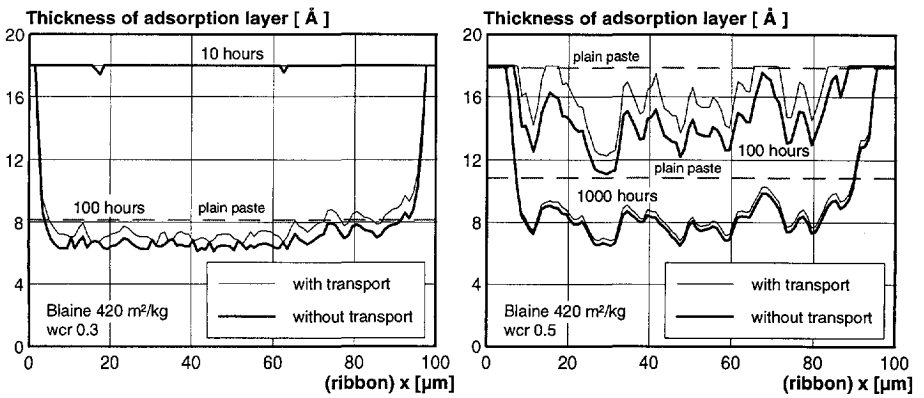

Fig. 6.31. Variation of the thickness of the adsorption layer in the pore space over the ribbon thickness. Left: water/cement ratio 0.3. Right: water/cement ratio 0.5.

very small. For the low water/cement ratio cement paste (wcr 0.3), the differences with and without allowance for transport of the capillary water turned out to be negligible. For the higher water/cement ratio paste (wcr 0.5) the average thickness of the adsorption layer appears to be 9% smaller after 100 hours of hardening when the transportation mechanism ignored. This difference reduces to about 3% after the ceasing of the hardening process (see also Fig. 4.3).

6.8.8 Surface tension in the adsorption layer

An increase of the relative humidity in the empty pore space will affect almost all parameters which determine the thermodynamic equilibrium. A parameter that is of particular importance regarding the modelling of volume changes in hardening cement paste is the surface tension in the adsorption layer. The constitutive relation, as given in equation (4.9), showed a the relationship between the surface tension in the adsorption layer and the autogenous deformation of the hardening paste. Therefore, a change of the surface tension in the adsorption layer will affect the autogenous deformation implicitly. Due to the transportation of the capillary water in the ribbon paste, the surface tension in the adsorption layer will change. In Fig. 6.32, this influence is presented for the pastes with water/cement ratio's of 0.3 (left) and 0.5 (right). For the low water/cement ratio paste (wcr 0.3), the redistribution of the capillary water causes a reduction of the surface tension of 22%, after 100 hours of hardening. This will affect the autogenous deformation of the hardening paste by the same order of magnitude. For the higher water/cement ratio paste (wcr 0.5), the surface tension in the adsorption layer appears to change much less. The average surface tension appears to be 8% smaller after 1000 hours of hardening.

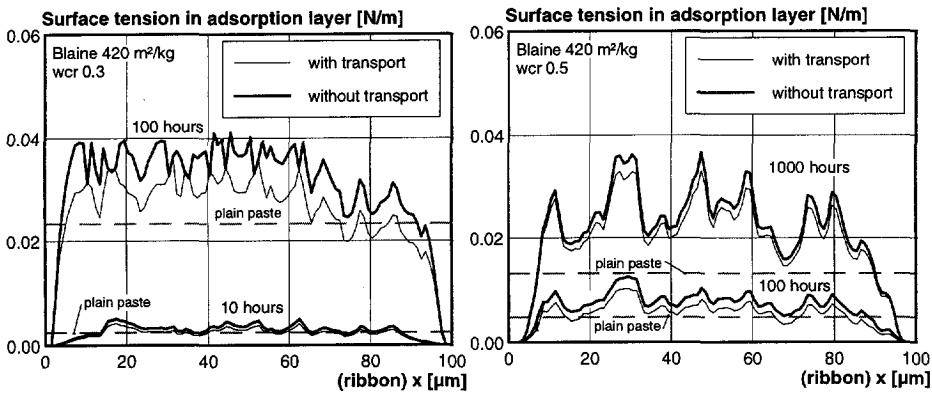

Fig. 6.32. Variation of the surface tension in the adsorption layer over the ribbon. Left: water/cement ratio 0.3. Right: water/cement ratio 0.5

6.8.9 Elastic modulus over the ribbon thickness

The evolution of the elastic modulus of the hardening cement paste is the result of the formation of interparticle contacts between the hydrating cement grains. This process is driven by the degree of hydration (see section 4.3.5). The geometrical build-up of the particle structure in the ribbon between the two aggregate particles (see Fig. 6.3) will, therefore, lead to substantial differences in the formation of the interparticle contacts and in the elastic modulus.

In Fig. 6.33, the variation of the elastic modulus over the ribbon paste is presented for the two cement pastes (wcr 0.3 and 0.5). At the ITZ, the elastic modulus is almost zero. This continuos as long as the hardening process proceeds. The elastic modulus in the bulk paste is calculated to be much higher than the elastic modulus of plain paste which is determined by the basic HYMOSTRUC model (see section 3.2.3). Conservation of volume requires a reduction of the water/cement ratio in the bulk paste to compensation for the increase of the water/cement ratio at the ITZ's (see Fig. 6.15). This results in a denser packing of the cement particles in the bulk paste and, consequently, to an increase of the elastic modulus at this particular region. From Fig. 6.33 it can be seen, that this influence affects the elastic modulus over the thickness of the ribbon paste substantially. For the cement paste with a water/cement ratio of 0.3, the elastic modulus of the bulk paste appears to increase by about 100% with respect to the plain paste, after 100 hours of hardening. For the paste with a water/cement ratio of 0.5, this effect appears to lead to an increase of about 42% after 1000 hours of hardening. This is quite an important phenomenon with respect to the prediction of the elastic modulus of concrete. The influence of the supply of additional water to the bulk paste region appears to have almost negligible influence on the development of the elastic modulus. This is in line with the results of the development of the degree of hydration as presented earlier in Fig. 6.26. The negligible change of the degree of hydration due to the additional water

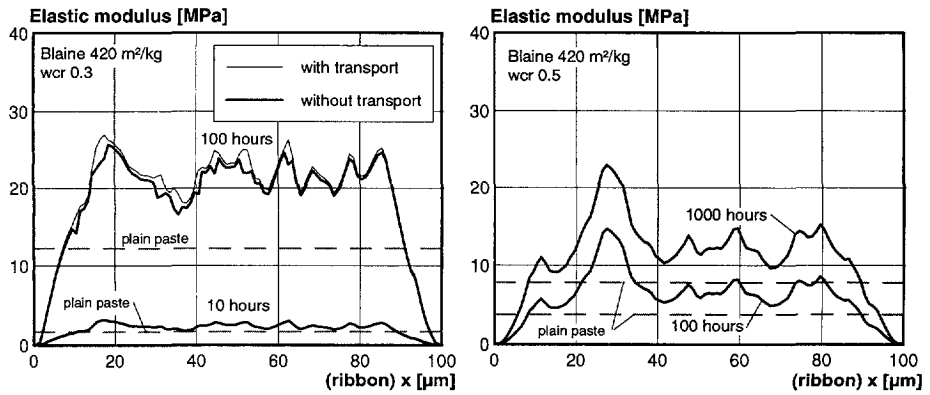

Fig. 6.33. Variation of the elastic modulus over the ribbon thickness. Left: water/cement ratio 0.3. Right: water/cement ratio 0.5

supply, implies that the formation of the microstructure is rather insensitive to this phenomenon. This also holds for the development of the elastic modulus of the hardening cement paste, since this process is driven by the degree of hydration.

6.8.10 Autogenous shrinkage over the ribbon thickness

In chapter 4, it has been shown that the development of autogenous shrinkage can be attributed to the surface tension in the adsorption layer that will establish in the empty pore space of the hardening cement paste. The actual value of the surface tension in the adsorption layer can be determined by a thermodynamic analysis of the moisture state in the empty pore space. Thermodynamic equilibrium requires equilibrium between the gas pressure in the emptied pore space and the tension in the adsorbed surface layer. The autogenous shrinkage, in turn, is strongly related to the surface tension of the hardening cement paste.

A change of the state of the capillary water due to the redistribution of the water volume which is accumulated in the ITZ and the remaining volume which is accumulated in the bulk paste, may influence the development of the autogenous shrinkage. An increase of the volume of capillary water in the dense pore structure of the bulk paste will enhance the relative humidity in the emptied pore space in that particular region. From the results in the previous figures it turned out, that this leads to a decrease of the surface tension in the adsorption layer by about 22% (wcr 0.3). From the results in Fig. 6.34 it appears, that the average autogenous shrinkage of the hardening cement paste with a water/cement ratio of 0.3 (Blaine 420m^2/kg) reduces by about 46% after 100 hours of hardening. The remaining 24% difference can be attributed to the fact that more capillary water is accumulated in the pores. Due to this, the wetted pore wall area A_{wat} will be larger, and results in a reduction of the autogenous deformation (see also eq. (4.11)).

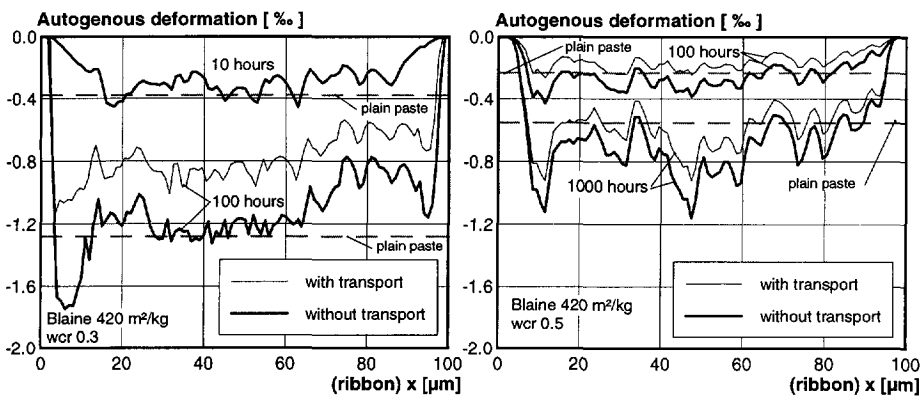

Fig. 6.34. Variation of the autogenous shrinkage over the ribbon. Left: water/cement ratio 0.3. Right: water/cement ratio 0.5

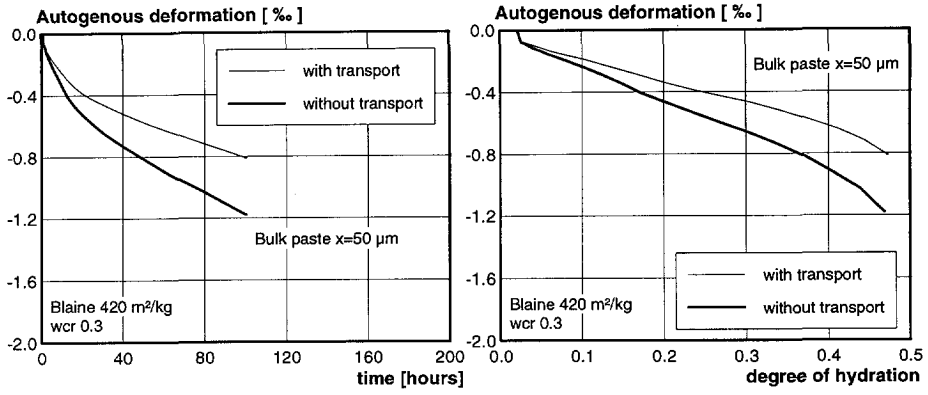

Fig. 6.35. Left: Development of the autogenous shrinkage versus time. Right: Development of the autogenous shrinkage versus the degree of hydration. Middle slice of the ribbon paste (x=50µm) with and without the transport of capillary water.

The additional water was accumulated originally in the pores of the 'water-rich' interfacial transition zone's of the ribbon. For the cement paste with a higher water cement ratio (0.5), the average autogenous shrinkage appears to reduce by about 23%. This shows that the reduction appears to be more pronounced for the low water/cement ratio pastes.

On the left hand side of Fig. 6.35, the development of the autogenous shrinkage versus time, for the middle slice of the ribbon paste (x=50µm), is presented. At the right hand side, this autogenous shrinkage is presented as a function of the degree of hydration. The results show that the autogenous shrinkage develops much faster if the transport of capillary (redistribution) is ignored. Due to the additional water supply, the autogenous shrinkage of the low water/cement ratio paste at the bulk paste region tends to be reduced.

6.8.11 Autogenous shrinkage of paste in concrete

The decrease of the autogenous shrinkage by the redistribution of the capillary water which is driven by the capillary pressure differences, may also be the reason for the fact that the autogenous shrinkage of concrete is overestimated when it is calculated from the autogenous shrinkage of cement paste using a parallel-series model (see section 5.7.2). In Fig. 5.10, it has been shown that the parallel-series model overestimates the autogenous shrinkage of concrete by about 50%. This parallel-series model only takes into account the internal restraint of the hardening cement paste induced by the stiff aggregates particles. It does not include the reduction of the autogenous shrinkage by the additional supply of capillary water. However, the development of microcracks in the cement-matrix may also affect the autogenous shrinkage of concrete.

6.9 Discussion

The analysis of the hardening process of the ribbon paste makes clear that the description of the volumetric changes of concrete is more complex than the description of the volumetric changes of plain cement paste. The geometrical packing of the cement particles and accumulation of capillary water at the ITZ regions, substantially affect the hardening behaviour of concrete.

The analysis of the ribbon paste hydration, as presented in this chapter, may contribute to a better understanding of the physical processes in concrete which play a role on a micro-scale level. A good understanding of these processes can be very useful for the development of durable concrete mixtures.
With the description of the transportation of capillary water, various changes of the material properties can be analysed. A challenging extension of the model would, therefore, be the application of adjustable boundary conditions, so that the supply of additional water from the saturated aggregate particles can be considered. In this way, it can be determined to what extent the so called *internal curing* (see Weber [96]) may influence the autogenous shrinkage of a hardening concrete. The numerical analysis of the ribbon paste hydration is considered a very useful tool in the design stage of the development of durable concrete mixtures.

7.

Applications

Autogenous shrinkage induced cracking

7.1 General

Autogenous shrinkage appears to be an inseparable property of concrete. The order of magnitude of the autogenous shrinkage is determined by the contribution of the different mix-components to the concrete. The way how autogenous shrinkage influences the quality of a hardening concrete structure will be outlined in this chapter by presenting two case studies. The first case study is a lab-scale test and the second study concerns a full-scale test. The tests provide information to what extent autogenous shrinkage influences the risk of cracking of hardening concrete.

The first case study concerns the analysis of a lab-scale structure. With the help of an experimental set-up, the stress development induced by autogenous shrinkage will be analysed on a "fibre" level. The hardening behaviour of one single fibre in a concrete can be examined quite well in the experiment carried out in this case study. Different physical as well as thermal boundary conditions can be applied to the specimen. In this way, hardening behaviour of a full-scale structure can be analysed on a lab-scale level. Emphasis will be on the way autogenous shrinkage damages the structure on a macro level.

The second case study deals with the analysis of the full-scale structure. In order to get more insight in the effect of autogenous shrinkage on cracking, the hardening behaviour of a full scale structure will be discussed in detail. A substantial increase in the probability of cracking may occur due to the influence of autogenous shrinkage induced strains.
The analysis starts with the description of the full-scale structure, followed by an overview of the boundary conditions that were applied for the simulation of the

hardening behaviour. The thermal strains as well as the autogenous shrinkage are considered to be the imposed deformations. Different degrees of external restraint give insight into the contribution of the autogenous shrinkage to the stress development of the hardening structure. This influence is also presented in terms of probability of cracking as well as in terms of the safety factor against cracking. The influence of the increase of the autogenous shrinkage as well as an increase of the degree of external restraint on the probability of cracking of a hardening full-scale structure will be discussed in this section.

7.2 Case study I: lab-scale structure[1)]

7.2.1 Temperature-Stress Testing Machine (TSTM)

The temperature stress testing machine (TSTM) is a horizontal positioned steel frame in which hardening concrete specimens can be loaded in compression and in tension, under various thermal and physical boundary conditions (see Fig. 7.1). Both load controlled and deformation controlled experiments can be performed. The specimen in the TSTM should experience the same thermal hardening conditions as a similarly shaped dummy specimen. Therefore, thermally controlled insulation and cryostat units are used to keep temperature differences between the dummy specimen and TSTM specimen within negligible ranges. With the "CLAWS" of the TSTM, the deformation of the specimen can be controlled in an active way. Any desired deformation path can be imposed on the

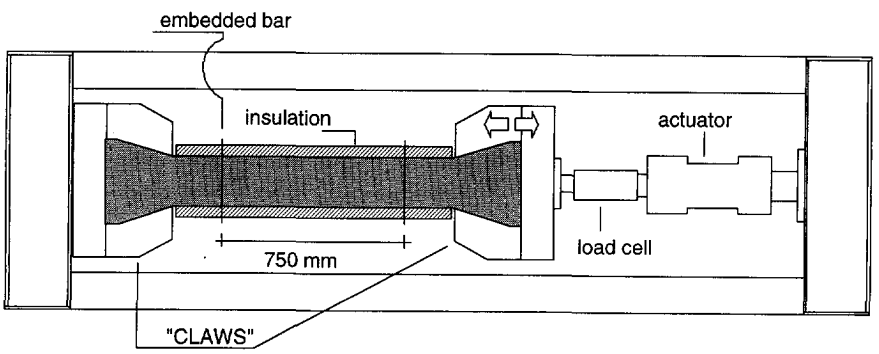

Fig. 7.1. Top view of the Thermal Stress Testing Machine (TSTM)

[1)] These tests are carried out within the scope of the research project of Mr. S. Lokhorst on *Creep and Relaxation of Hardening Concrete*. This project was supported financially by the Dutch Technology Foundation (STW), the Ministry of Traffic, Public works and Water Management (RWS) and the COAB Foundation.

Table 7.1. *Mix proportions.*

Mixture	Content	Note
Portland cement C	100 kg/m³	CEM I 52.5 R (ENCI)
Blast furnace slag cement	300 kg/m³	CEM III / 42.5 (CEMY)
Sand 0-4	46 %	
Gravel 4-16	54 %	crushed
Water	160 kg/m³	w/c=0.4
Plasticizer	1.8%	

specimen during hardening. Besides creep and relaxation tests, early-age stress development tests can be performed with this machine. The way autogenous shrinkage introduces stresses in hardening concrete will be discussed in detail in this case study.

7.2.2 Outline of the experimental set-up

At the Technical University in Delft, an experimental TSTM set-up has been developed, initially, by Lokhorst [60]. The set-up draws on the thermal-stress testing machine as was developed in Munich [85] and in Düsseldorf [89], in Germany.

With the TSTM, deformations and/or stresses can be controlled actively during testing. As a reference for the TSTM, the dummy specimen is used. If a certain degree of restraint is desired, deformations induced by temperature differences and autogenous shrinkage can be measured on the dummy specimen using LVDT's and imposed to the TSTM-specimen. It is also possible to determine stresses at a degree of restraint of 100%. For that particular situation, the dummy specimen can be omitted.

7.2.3 Description of experimental results

For this test, the TSTM set-up is used to analyse the crack-sensitivity of an ordinary concrete mixture with a water/cement ratio of 0.4 and a characteristic compressive cube strength of 65 MPa (see Table 7.1). The test is carried out under isothermal conditions and no external load is applied to the TSTM specimen. This implies that the only strain that acts on the specimen is the autogenous shrinkage. If the autogenous shrinkage is restraint, is able to induce stresses in the specimen while hardening.

The autogenous shrinkage of the hardening concrete is measured from the dummy specimen. The autogenous shrinkage appeared to cause a contraction of the concrete specimen of about 0.2 ‰ after 300 hours of hardening (see Fig. 7.2, left). The autogenous shrinkage of the TSTM-specimen was completely fully restraint. Restraining the autogenous shrinkage leads to tensile stresses in the TSTM specimen. Depending on the magnitude of the autogenous shrinkage these stresses can become quite substantial. On the right hand side of Fig. 7.2, the *autogenous stress* development is presented. This is the stress level that was measured in the TSTM-specimen, if at full restraint. The results

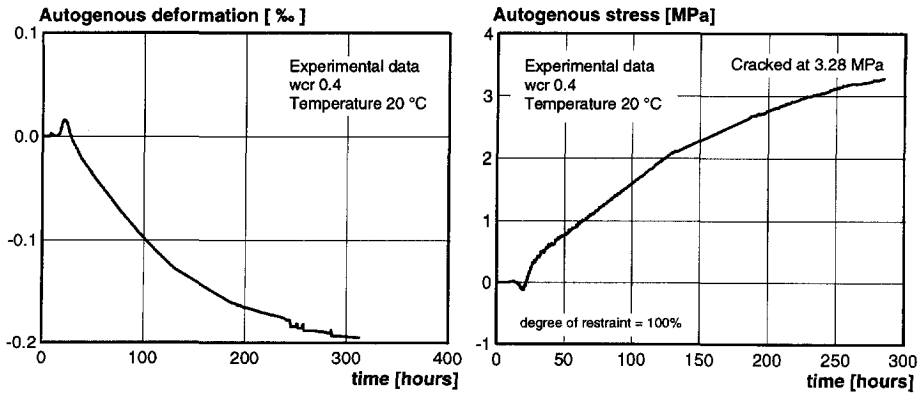

Fig. 7.2. Left: Autogenous shrinkage versus time. Right: Stress development for blended cement (see Table 7.1) versus time caused by restraining autogenous shrinkage.

show a rather continuous increase of the stresses with an increase of the autogenous shrinkage. After 285 hours of hardening, the TSTM-specimen cracked. At that time, the tensile stress reached a value of 3.28 MPa. At the moment of cracking, the mean actual tensile splitting strength was 4.78 MPa. This leads to a ratio between the uni-axial (TSTM) tensile stress and the mean tensile splitting strength at the moment of cracking of 0.69. This ratio is comparable with the ratio as found commonly for this type of concretes [90].

In order to get more insight in the stress relaxation of the considered concrete mixture, the autogenous stress development (Fig. 7.2, right) is plotted as a function of the autogenous shrinkage (Fig. 7.2, left). This result is presented in Fig. 7.3. It can be seen that the stresses develop almost linear with the development of the autogenous shrinkage.

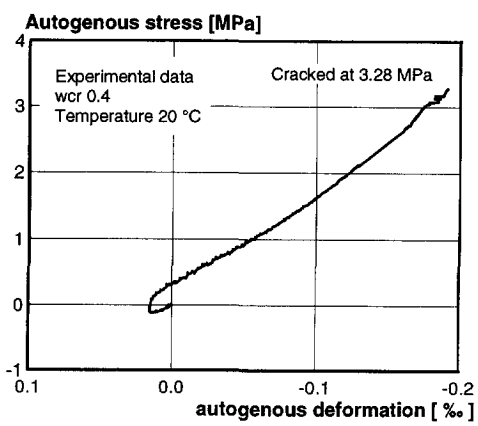

Fig. 7.3. Autogenous stress development versus autogenous shrinkage.

7.2.4 Prediction of autogenous shrinkage of blended cement concrete

In this section, the potential of the basic HYMOSTRUC model (see section 3.2.3) to simulate the autogenous shrinkage of a blended cement concrete mixture as used in this section will be outlined (see Table 7.1). The concrete contains two different types of cement. A Portland cement and a blast furnace slag cement.

In Fig. 7.2, the measured autogenous shrinkage are presented as a function of time. With the basic HYMOSTRUC model (which includes the proposed model to predict autogenous shrinkage for plain paste, see chapter 4), these autogenous shrinkage measurements of the concrete mixture are simulated. On the left hand side of Fig. 7.4, the numerical simulations are compared with the experimental results as were also presented in Fig. 7.2. Good agreement could by obtained between the numerical simulation and the experimental results. It can be seen that the proposed model to describe autogenous shrinkage of hardening cement paste and concrete as proposed in chapter 4, is also capable of simulating the volumetric changes of blended cement concretes quite well.

Note: the current version of the HYMOSTRUC model does not have the ability to simulate the swelling at the very early age of hardening. This requires the implementation of an additional swelling mechanism.

On the right hand side of Fig. 7.4, the autogenous shrinkage of the concrete is presented as a function of the degree of hydration. The figures shows a comparison between the numerical simulations and the experimental results. The agreement between these results is still quite good. However, due to swelling of the concrete mixture in the very beginning of hardening there exists some discrepancy between the simulations and the experimental results.

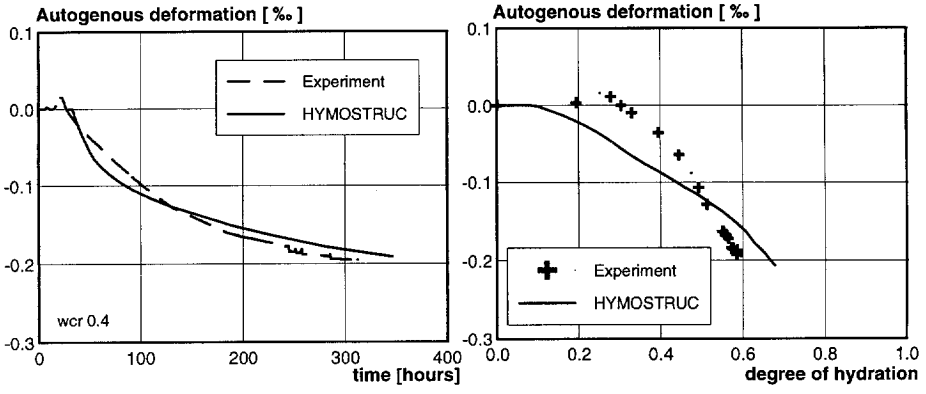

Fig. 7.4. Left : Autogenous shrinkage versus time. Right: Autogenous shrinkage versus degree of hydration. Comparison between experimental and HYMOSTRUC results.

7.2.5 Discussion

The aim of this case study was to show the effect of the autogenous shrinkage on cracking of hardening concrete. The results showed convincingly that the influence of the autogenous shrinkage on cracking of a hardening structure may not be ignored for accurate prediction of the stresses that develop during hardening. The internally imposed autogenous shrinkage may lead to cracking of a structural element in case it is restrained. It can be stated that for low water/cement ratio concretes, the influence of autogenous shrinkage on cracking in hardening concrete is of equal importance as the temperature-induced deformations which develop during the hydration process. The impact of the temperature-induced deformation on the stress development can be influenced actively by, for instance, application of cooling pipes, or low heat types of cement. On the contrary, the impact of autogenous shrinkage of the stress development is very hard to manipulate. It can be influenced by, e.g. adjusting the magnitude of the relative humidity that develops in the emptied pore space during hardening. Experiments have shown that so called "internal curing" [51], i.e. the replacement of a certain percentage of the aggregate volume by fully saturated light-weight particles, could reduce autogenous shrinkage substantially. Addition of these types of water containing particles to the concrete will increase the relative humidity in the pore system and will therefore reduce the autogenous shrinkage that will develop during hardening of the concrete. An increase of the water/cement ratio may also be an option to increase the relative humidity in the emptied pore space (see section 4.5.3), but this will be accompanied by a reduction of the compressive strength, the stiffness and the density of the concrete.
From this, it becomes clear that autogenous shrinkage of hardening concrete requires due attention with respect to the design and development of durable concrete structures. This attention concerns the mix-design, the control of the hardening process, as well as the static system of the full-scale structure.

7.3 Case study II: full-scale structure

The full-scale structure as was also discussed briefly in section 1.2, will be discussed in this section extensively. Emphasis will be on the influence of autogenous shrinkage on the probability of cracking.
From the previous section is appeared that autogenous shrinkage can cause cracking if concrete is submitted to a certain degree of external restraint. How this influence works out for a full-scale structure will be considered next.

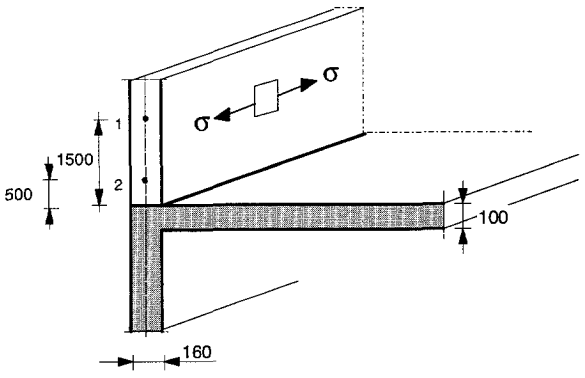

Fig. 7.5. Schematic representation of the full-scale structure.

7.3.1 Description of the structure

The full-scale structure is part of an office building which was built in The Netherlands in 1994 [50]. The structure consists of a slender wall which is cast on a rigid slab. The wall has a thickness of 0.16 m and a height of 3.5 m. The ambient temperatures were 18 ± 1 °C during hardening. The formwork was removed after 16 hours of hardening. The wall as well as the slab are made of HSC (see Table 7.3).

In this section, based on the input values as listed in Table 7.2, numerical simulations for temperature and stress development in the hardening structure are carried out with TEMPSPAN (see appendix C). In these calculations, stresses are assumed to be caused by temperature differences and also by autogenous shrinkage of the hardening concrete. The effect of the external degree of restraint on the stress development is also taken into account.

Table 7.2. Input value for numerical simulation

Parameter	**Data**	**Note**
Mixture	High Strength Concrete	see Table 7.3
Mix temperature	20 °C	
Wind velocity	2 m/s	average
Ambient temperature	18 ± 1 °C	
Formwork	thick 0.02m, λ=0.17W/m²K	wood
Removal formwork	after 16 hours	
Adiabatic hydration curve	see Fig. 7.6 (left)	
Auto. shrinkage	see Fig. 7.6 (right)	

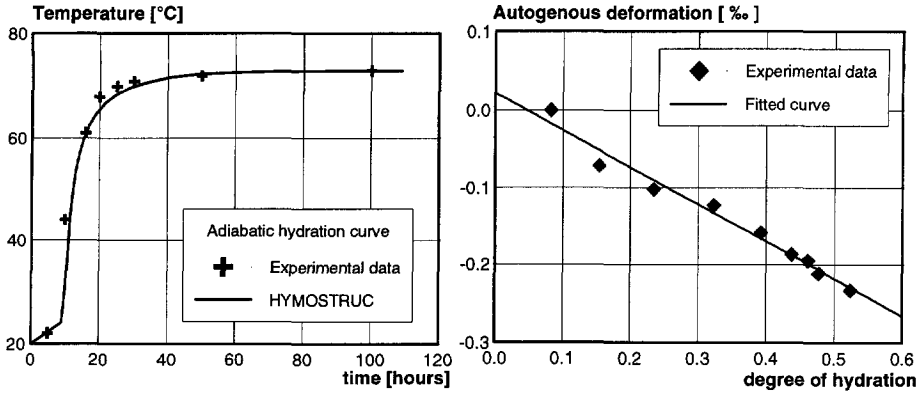

Fig. 7.6. Left: Adiabatic hydration curve versus time. Right: Autogenous shrinkage versus degree of hydration.

On the left hand side of Fig. 7.6, the adiabatic hydration curve of the HSC mixture is presented. This curve is experimentally determined at the Stevin laboratory in Delft. A detailed discussion on the test set-up that was used for this experiment is presented in [52]. The dormant stage of the applied HSC mixture is approximately 10 hours. This is due to the high dosage of plasticizers that is commonly used in HSC mixtures. After setting, hydration proceeds very fast. The high specific surface of the fine Portland cement (Blaine 550m^2/kg) provides a high reactive potential of the concrete mixture. With this type cement, the HSC mix reaches an average compressive strength of 105 MPa after 28 days of hardening. At that age, the tensile splitting strength appeared to be 5.5 MPa.

In TEMPSPAN [57], the tensile strength is described as a function of the compressive strength according to the relation as suggested by the Norwegian code NS3473. The compressive strength is related to the calculated degree of hydration. This means that the tensile strength is indirectly also related to the degree of hydration. For the modulus of elasticity a three-phase model (aggregate, unhydrated cement and gel) was used. In this way, it is also possible to relate the E-modules to the degree of hydration.

Table 7.3. *Mix proportions.*

Mixture	Content	Note
Portland cement C	475 kg/m^3	CEM I 52.5 R (ENCI)
Silica fume	50 kg/m^3	50%/50% dry/wet
Sand 0-4	44 %	
Gravel 4-16	56 %	crushed
Water	125 kg/m^3	w/b=0.3
Plasticizer	3.85%	

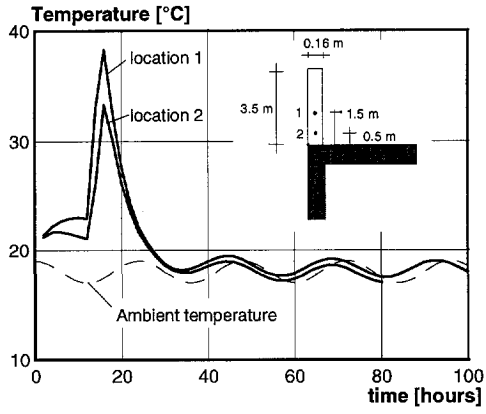

Fig. 7.7. Temperature development versus time for the locations 1 and 2 (see Fig. 7.5).

7.3.2 Temperature development in the wall

Temperature calculations are carried out for two locations (1 and 2) in the middle part of the wall as shown in Fig. 7.5. The mix temperature at casting is 20 °C. The figure shows that during the dormant stage, the temperature development is influenced by the ambient temperature. After the dormant stage has ended, the hydration process proceeds rapidly and the temperature increases. During this hardening period, the temperature in the location 1 reaches a maximum value of 38 °C. In location 2 a maximum temperature of 33 °C is reached. The maximum temperature is reached 16 hours after mixing. This particular time corresponds with the stripping of the formwork. After reaching its maximum, the temperature declines to the ambient temperature.

7.3.3 Stress development in the wall

Stress calculations are also carried out for the two different locations as given in Fig. 7.5, and for two different degrees of external restraint, viz. 100% and 0%. For location 2, the influence of the autogenous shrinkage on the stress development is also shown. The stress calculations at an external degree of restraint 0 % give a good impression of the self-equilibrating stresses which develop in the hardening structure.

On the left hand side of Fig. 7.8, the stress development is presented for the locations 1 and 2, while all external deformations are fully restrained. It can be seen that both for location 1 and location 2 the tensile stresses exceed the actual strength level to a large extent. In location 1 a maximum tensile stress of 5.8 MPa is reached and in location 2 a maximum value of 4.6 MPa. Due to these stresses, the wall would already crack within 20 hours after casting. The figure also shows the stress development if the autogenous shrinkage was ignored in the calculations. This shows a much more favourable development of the hardening stresses. A maximum tensile stress of 2.8 MPa is calculated which is lower than the actual tensile strength. This means that cracking is not likely to occur. It will be clear that this is a substantial underestimation of the stresses

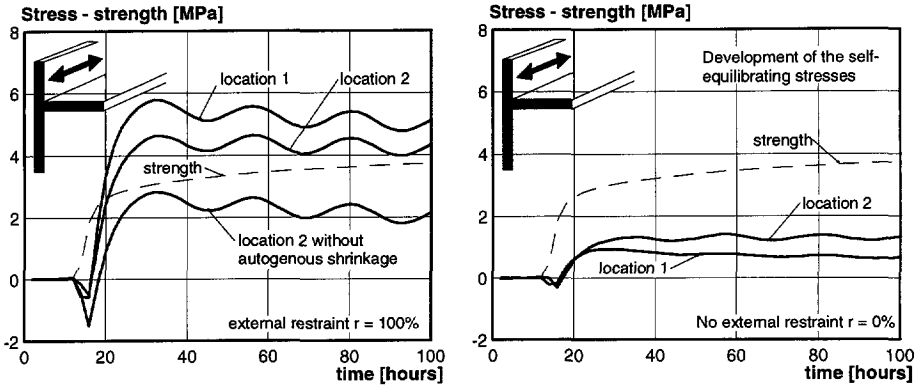

Fig. 7.8. Stress development versus time. Left: Stress development at full restraint of the external deformations. Right: Development of the self-equilibrating stresses.

which actually develop in the hardening structure. The tensile stresses are underestimated by about 65%.

On the right hand side of Fig. 7.8, the development of the self-equilibrating tensile stresses are presented for locations 1 and 2. These stresses develop without the application of any external restraint. From Fig. 7.8 it can be seen that the maximum tensile stresses which develop during hardening do not exceed the tensile strength. Due to these stresses, the structure is not likely to crack.

7.3.4 Probability of cracking

On the left hand side in Fig. 7.9, the probability of cracking is presented for the stress and strength development as given in Fig. 7.8. The standard deviations for the strength and the stress are estimated at 10 % of the actual (mean) values. For the self equilibrating stresses the probability of cracking appeared to be negligible.

From Fig. 7.9, it can be seen that the probability of cracking which is associated with the stresses that develop while the wall is under full restraint is quite high. After 20 hours of hardening the wall is likely to cracking. The probability of cracking increases very rapidly from 0% to 100% within a few hours of hardening. The figure also shows the probability of cracking for location 2 if autogenous shrinkage is not taken into account in the stress calculations. For this situation, a much more favourable situation appears regarding the probability of cracking. Ignoring autogenous shrinkage in the stress calculations would suggest that the probability of cracking is only about 25%.

In addition, autogenous shrinkage also causes an earlier increase of the probability of cracking. For the engineering practice, this means that due to the effect of autogenous shrinkage, cracks are likely to develop earlier.

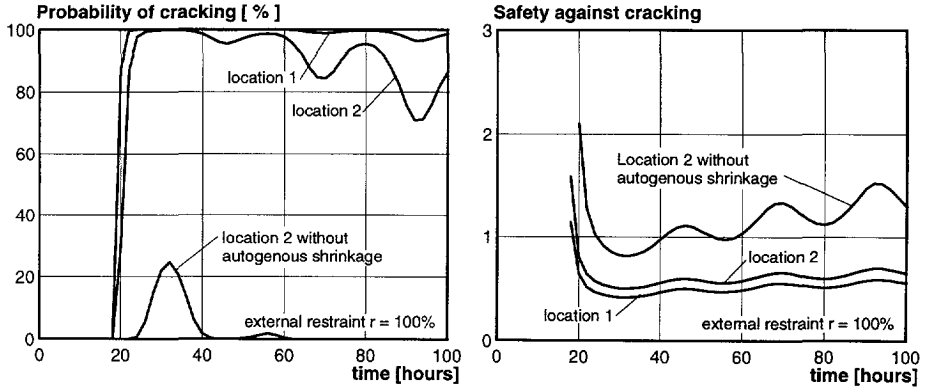

Fig. 7.9. Left: Probability of cracking versus time. Right: Safety factor against cracking versus time.

7.3.5 Safety against cracking

The safety factor against cracking is defined as the quotient of 5% lower boundary value of the tensile strength and the 95% upper boundary value of the stress. From this, the safety factor against cracking γ can be determined by (see [90]):

$$\gamma = \frac{\bar{f} - S_f}{\bar{\sigma} - S_\sigma} \tag{7.1}$$

where $\bar{f}$ is the mean tensile strength, $\bar{\sigma}$ the mean tensile stress and S_f and S_σ the standard deviation of the tensile strength and tensile stress, respectively. In TEMPSPAN the calculated values of the stress and the tensile strength are considered to be the mean values of normal distributed quantities. As stated, the standard deviations for the strength and the stresses are estimated at 10% of the actual (mean) values. With these values, it is possible to determine the safety factor γ during the course of the hydration process. On the right hand side of Fig. 7.9, the safety factor against cracking is presented for different locations in the wall. The influence of autogenous shrinkage on the safety against cracking is also taken into account. The results show that the safety against cracking of the wall drops below 1 after 20 hours of hardening. This shows also that autogenous shrinkage causes earlier cracking of a hardening concrete structure.

7.3.6 Discussion

The aim of the second case study was to show to what extent autogenous shrinkage influences the stress development and the probability of cracking in a hardening full-scale structure. For the structure as considered in this case study, it was calculated that stresses which are introduced by external restraint are substantially larger than the self equilibrating stresses. Together with the effect of autogenous shrinkage, this class of stresses influence the quality of a hardening concrete structure.

In the first case study, a degree of external restraint was imposed to the TSTM specimen. Since the stresses are related proportional to the degree of external restraint [61], the stresses will develop at similar ratio. On a fibre level, this parameter has to be established in advance. In a real structure the degree of restraint is determined by the structure itself. The geometry of the structure determines this particular value.

Autogenous shrinkage and the external restraint both have a great impact on the stress development in a hardening concrete structure. In the first case study, it was outlined that autogenous shrinkage may cause cracking of a hardening structure. However, this happens only while the structure is submitted to a certain degree of external restraint.

8.

Discussion of results and conclusions

8.1 Discussion of results

In this thesis, a consistent model based thermodynamics is proposed which has the potential to simulate the volume changes of hardening cement-based materials.
The mechanism which is responsible for the development of autogenous shrinkage during hardening of a cementitious material is modelled on the basis of a thermodynamic approach explicitly. Equilibrating the pressure in the emptied pore space with the surface tension in the adsorption layer at the pore walls turned out to be a promising approach. The satisfactory agreement between the numerical simulations and the experimental results gives confidence in the modelling approach as presented in this thesis. This is also supported by the ability of the proposed thermodynamic based model to simulate the swelling deformation of hardened cementitious material very accurately.

The parameter study carried out in chapter 4, gives an overview of the dependency of the parameters which are involved in the calculation process to establish thermodynamic equilibrium during hydration. The relative humidity in the gradually emptying pore space drops from 100% to a lower value. This value depends on the fineness of the cement and on the water/cement ratio of the paste. Generally, the relative humidity does not drop below 75%, which agrees with the limit as given by Powers (see [44]). The relative humidity in the empty pore space appears to be the main parameter in the calculation process to establish thermodynamic equilibrium. A change of the relative humidity in the pore space affects the thickness of the adsorption layer at the pore walls as well as the associated tension in this adsorption layer. If thermodynamic equilibrium is established, the surface tension in the adsorption layer showed to be a reliable parameter for the description of autogenous shrinkage of the hardening cement-based material.
Bangham showed that the surface tension could be used to describe the swelling deformation of wetting coal. Wittmann showed that this approach can also be applied to simulated the swelling of an oven-dried cement paste specimen which is exposed to a

moist environment. In general, distinction is made between two mechanisms. The first mechanism is valid for a relative humidity range between 0 and 40% (Gibbs-Bangham) and the second mechanism between the 40 and 100% (disjoining pressure). With the model as proposed in chapter 4, it is possible to determine the swelling behaviour on basis of one mechanism (thermodynamic equilibrium). By only taking into account the empty pore space and surface tension in the adsorption layer, the model determines the swelling for the hardened cement paste quite well.
In the present research it has been shown that with the surface tension concept, a good description of the contraction (*autogenous shrinkage*) of hardening cement paste is possible. This has been supported by an extensive experimental evaluation program.

For the description of autogenous shrinkage of a hardening concrete, an additional step must be made. The addition of the aggregates to the cement paste will affect the hydration properties of the hardening cement paste. Initially, the parallel-series model and the lattice model turned out to be valuable approaches to describe the internal restraint induced by the aggregates to the hardening cement paste. The lattice model was also able to visualise the internal restraint of the cement paste by the aggregates. Stress concentrations can also be visualised quite well.
The parallel-series model turned out to be very suitable for the computer modelling purpose. It is a very convenient and quick way of getting an impression on the internal restraint that is imposed by the aggregate particles. The composite model, as proposed in this thesis, is not able to simulate to reduction of the autogenous shrinkage of the cement paste induced by the aggregates very accurately. On the one hand, this can be attributed to the simplicity of the proposed composite model, but, on the other, it can also be the result of the fact that this model does not include the redistribution of the capillary water in the gradually emptying pore space.

In chapter 6 of this thesis, with the ribbon model, it has been pointed out that consumption of capillary water by the hydration process is associated with the development of a certain pressure in the capillary water. Due to the existing pressure gradients, capillary water will be transported from the 'water-rich' regions (ITZ) in the concrete to the 'water-poor' regions (Bulk paste). This transport of capillary water turned out to have a substantial effect on the hydration process and on the development of the autogenous shrinkage of the hardening cement paste. This implies that the addition of aggregates to an arbitrary concrete affects the reduction of the autogenous shrinkage in two ways. *Firstly*, the relatively stiff aggregate particles prevent the hardening cement paste to contract. *Secondly*, the autogenous shrinkage is affected by the redistribution of the capillary water in the hardening cement paste. Additional water supply to the concrete by e.g. water saturated light-weight particles, may intensify the transport of capillary water to a large extent. This has also been proven with experiments [51]. Similar test results are observed for tests which were carried out at the Stevin laboratory

[51]. This makes the transformation of cement paste properties to concrete properties quite complex.

The two case-studies as discussed in chapter 7 show that autogenous shrinkage of a hardening concrete may not be neglected. It may introduce additional stresses in the concrete structure which may cause damage and reduce the durability. A reliable model with which the autogenous shrinkage of the hardening concrete can be simulated is therefore very welcome. The model to predict autogenous shrinkage as proposed in this thesis turned out to be promising. This model is implemented in the computer program HYMOSTRUC. In this way the development of the autogenous shrinkage can be calculated as a function of the hardening process.

8.2 Conclusions

With the presented thermodynamics based model for autogenous shrinkage, the aims as briefly outlined in section 1.3 have been realised to a large extent. The model is able to predict the autogenous shrinkage of hardening Portland cement based mixtures sufficiently accurately for the use of both macro and micro-scale calculations. This holds especially true for plain Portland cement paste mixtures. The autogenous shrinkage of concrete mixtures can be calculated from the autogenous deformation of cement paste with the use of e.g. a composite model (parallel-series) or lattice model to simulate the internal restraint that is induced by the aggregate particles.
The ribbon model showed that more comprehensive processes play a role if the autogenous shrinkage of concrete is calculated from the autogenous shrinkage of plain cement paste.
From the modelling approach as presented in this thesis, the following particular conclusions and remarks can be listed:

1. Thermodynamic equilibrium in the empty pore space can be adopted as the basis for modelling autogenous shrinkage of hardening cement paste. It turned out to lead to accurate predictions.
2. The surface tension in the adsorption layer at the pore walls can be considered as the (internal) driving force behind the mechanism that causes autogenous shrinkage.
3. Due to the internal self desiccation of a hardening cement-based material, the relative humidity in the empty pore space reaches roughly between 100% and 75%.
4. The random particle structure in combination with the hydraulic radius concept can be applied to obtain reliable predictions for the pore structure of an arbitrary hardening cement paste (see chapter 3).
5. If silica fume is considered as the parameter which reduces the largest pore diameter of the actual pore structure, then, the autogenous shrinkage of a cement paste which

contains a certain percentage of silica fume can be predicted quite well with the proposed pore reduction factor as outlined in chapter 4.

6. If autogenous shrinkage of hardening concrete is calculated from the autogenous shrinkage of a hardening plain cement paste by means of a composite model, it must be born in mind that both the stiffness of the aggregates and the movement of the capillary water through the hardening microstructre are neglected.
7. The model with which the hydration process of the ribbon paste can be calculated turned out to have the potential to simulate the movement of capillary water through the hardening microstructure and its effect on the autogenous shrinkage.
8. Autogenous shrinkage may cause large strains in a hardening concrete structure. If these strains are restraint, tensile stresses will occur which can cause cracking of the structure and which may result damage.

8.3 Recommendations and outlook

The model to predict autogenous shrinkage of hardening cement paste as outlined in chapter 4 shows to be valid for a wide range of water/cement ratios and also for various finenesses of cement. The proposed model is implemented in the simulation program HYMOSTRUC. Very accurate results are obtained for Portland cement-based mixtures. This is due to the fact that the HYMOSTRUC model was originally developed for Portland cement-based mixtures. An extension of the HYMOSTRUC model to deal with more different types of cement (e.g. blast furnace cement) would also extend the applicability to simulate the autogenous shrinkage of these types of cement-based mixtures.

For further development of the HYMOSTRUC model to simulate autogenous shrinkage of hardening cement-based mixtures, the following research aspects are recommend:

1. to investigate in detail the predictability and potential of the proposed model to simulate autogenous shrinkage for a wide range of different types of cement and concretes.
2. to investigate the ability of different composite models (i.e. two phase paste-aggregate models) to predict the autogenous shrinkage of concrete.
3. to analyse the effect of the reduction of the autogenous shrinkage on a macro-scale level induced by micro-cracking in the ITZ. High stresses at the ITZ which develop during hardening may play an important role.
4. to investigate the effect of the shape of the cement particles on the pore size distribution of hardening cement paste.
5. to analyse the pore structure of the random particle structure by using the so called *random walkers* [76].

6. to simulate the effect of the supply of additional water by addition of fully water saturated light weight particles and analyse the influence on the autogenous shrinkage of a hardening concrete. For this purpose, the boundary condition of the ribbon model can be adjusted.
7. to investigate the influence of the deformation of the hardening microstructure and the affect of the transport of gas on the transport of capillary water.

The model to calculate the hydration process of a concrete ribbon as presented in chapter 6 of this thesis turned out to be a fundamental research tool with which the hardening process and the development of the material properties of hardening concrete can be analysed. Its potential to simulate the development of autogenous shrinkage by taking into account the transport of capillary water, the interfacial transition zone and the random particle structure, serves as a solid basis in this respect. The model may be a helpful tool for numerical simulations in concrete research.

References

[1] (1993), Utilisation of High Strength Concrete, Lillehammar, Norway.

[2] Amberg, C.H. and Mc. Intosh, R. (1952), A Study of Adsorption Hysteresis by means of Length Changes of a Rod of Porous Glass, Canadian Journal of Chemistry ,30, 1012.

[3] Atlassi, E. (1992), Desorption Isotherms of Silica Fume Mortar, Proc. 9th Int. Conference on the Chemistry of Cement, New Delhi.

[4] Badmann, R. et. al. (1981), J. Coll. Int. Sci ,Vol. 82, pp. 534-542.

[5] Bangham, D.H. (1937), The Gibbs Adsorption Equation and Absorption on Solids, London, Gurney and Jackson.

[6] Bangham, D. H. and Fakhoury, N. (1931), The Swelling of Charcoal, Royal Society of London ,CXXX, 81-89.

[7] Bangham, D.H. and Maggs, F.A.P. (1944), The Strength and Elastic Constants of Coal in Relation to their Ultra-fine Structure, The British Coal Utilisation Research Association, The Royal Institution, London.

[8] Bazant, Z.P. and Wittmann, F.H. (1982), Creep and Shrinkage in Concrete Structures, John Wiley & Sons.

[9] Bear, J. (1972), Dynamics of Fluids in Porous Media, New York, London Amsterdam, American Elsevier Company.

[10] Bentur, A. (1991), Microstructure of High Strength Concrete, Darmstadter Massivbau-Seminar, Darmstadt.

[11] Bentz, D.P., Garboczi, E.J. and Stutzman, P.E. (1992), Computer Modelling of the Interfacial Zone in Concrete, Interfaces in Cementitious Composites, E&FN SPON, Toulouse, France.

[12] Bentz, D. P. and Garboczi, E.J. (1991), Percolation of Phases in a Three-Dimensional Cement Paste Microstructural Model, Cement and Concrete Research ,21, 325-344.

[13] Bezjak, A. (1983), Cement and Concrete Research ,Vol 13, nr 2. pp. 186-196 and nr. 183 pp. 305-318.

[14] Bezjak, A. (1986), Cement and Concrete Research ,Vol 16, nr. 2 pp. 260-264 and nr. 264 pp. 605-609.

[15] Breugel, K. van (1980), Relaxation of Young Concrete, Delft University of Technology, Research report concrete structures, 5-80-D8.

[16] Breugel, K. van, (1991), Simulation of hydration and formation of structure in hardening cement-based materials, Faculty of Civil Engineering, Delft, Delft University of Technology, pp. 295, PhD.

[17] Breugel, K. van (1995), Numerical simulation of hydration and microstructural development in hardening cement-based materials. Theory (I) and Applications (II)., Cement and Concrete Research ,(I) Vol. 25, No. 2, pp. 319-331 (II) Vol. 25, No. 3, pp. 522-530.

[18] Chattoraj, D.K. and Birdi, K.S. (1984), Adsorption and the Gibbs Surface Excess, New York and London, Plenum press.

[19] Concrete, High Strength (1993), Utilization of High Strength Concrete, Lillehammer, Norway.
[20] Counto, W.J. (1964), The Effect of the Elastic Modulus of the Aggregate on the Elastic Modulus, Creep and Creep Recovery of Concrete, Magazine of Concrete Research ,Vol. 16.
[21] Cuperus, F. P., (1990), Characterisation of Ultrafiltration Members, Pore Structure and Top Layer Thickness, Enschede, University of Twente, pp. 103,PhD.
[22] Day, R.L. and Marsh, B. K. (1988), Measurement of Porosity in Blended Cement Pastes, Cement and Concrete Research ,Vol 18, pp. 63-73.
[23] Defay, R. Prigogine, I. and Bellemans, A. (1966), Surface Tension and Adsorption, London, Longmans London.
[24] Diamond, S. (1987), Cement Paste Microstructure in Concrete, Mat. Res. Soc. Symp. Proc. ,Vol 85, pp. 21-31.
[25] Dorcey, N.E. (1940), Properties of ordinary water-substance, Washington D.C., Reinhold Publishing Corporation.
[26] Feldman, R.F. (1968), Sorption and Length-Change Scanning Isotherms of Methanol and Water on Hydrated Portland Cement, Fifth Int. Symposium on the Properties of Cement Paste and Concrete, Tokyo.
[27] Feldman, R.F. and Cheng-yi, H. (1985), Cement, Silica Fume, Pastes, Porosity, Surface Properties, Secondary, Cement, Silica Fume, Pastes, Porosity, Surface Properties, 15, pp 766-774, 5.
[28] Ferraris, C.F. and Wittmann, F.H. (1987), Shrinkage Mechanisms of Hardened Cement Paste, Cement and Concrete Research ,Vol. 17, pp. 453-464.
[29] FIP, High Strength Concrete (1990), State of the art report, London, Fédération Internationale de la Précontrainte.
[30] Gertis, K. Kiessl, K. Werner, H. and Wolfseher, U. (1976), Hygrische Transportphänomene in Baustoffen, Deutscher Ausschuss Für Stahlbeton DAfSt ,Heft 258, pp. 110.
[31] Ghosh, R.S. (1972), Creep of Portland Cement Paste at Early Ages, Matériaux et Constructions ,Vol. 5, pp. 93-97.
[32] Ghosh, R.S. and Timusk, J. (1974), Effect of Sustained Loading at Early Ages on the Modulus of Elasticity of Cement Paste, Matériaux et Constructions ,Vol. 7, pp. 335-339.
[33] Gibbs, J.W. (1906), The scientific papers, London.
[34] Goldman, A. and Bentur, A. (1992), Effects of Pozzolanic Non-Reactive Microfillers on the Transition Zone in High Strength Concrete, RILEM Conference on 'Interfaces in Cementitious Composites', E&FN Spon, London.
[35] Grube, H., (1990), Ursachen des Schwindens von Beton und Auswirkungen auf Betonbauteile, Darmstadt, Habilitationsschrift.
[36] Grün, W. and Grün H.R. (1961), Zur Frage der Physikohemischen Verhaltensweise von Wasser des Hydratisierenden Zementes im Beton, Zement-Kalk-Gips ,nr. 11, pp. 541-520.

[37] Gutsch, A. and Rostásy, F.S. (1994), Young Concrete under High Tensile Stresses - Creep, Relaxation and Cracking, Thermal Cracking in Concrete at Early Ages, E&FN SPON London, München.

[38] Hagymassy, J. Brunauer, JR. and Mikhail, R.Sh. (1969), Pore Structure Analysis by Water Vapor Adsorption, Journal of Colloid and and Interface Science ,29-3, pp. 485-491.

[39] Hiller, K.H. (1964), Strength Reduction and Length Changes in Porous Glass Caused by Water Vapor Adsorption, Journal of Applied Physics ,35, pp. 1622-1628.

[40] Hua, C., Acker, P. and Ehrlacher, A. (1995), Analysis and Models of the Autogenous Shrinkage of Hardening Cement Paste, Cement and Concrete Research ,Vol. 25, pp. 1457-1468.

[41] Jander, W. (1927), Solid state reactions at high temperature, Zeitung anorganische und algemeine Chemie pp. 1-30.

[42] Jennings, H.M., et.al. (1996), Modelling and Material Science of Cement-Based Materials Part I: An Overview, The Modelling of Microstructure and its Potential for Studying Transport Properties and Durability, H. Jennings, Kropp, J. and Scrivener, K., London, Kluwer Academic Publishers, 304, 558.

[43] Jennings, H.M. and Johnson, S.K. (1986), Simulation of Microstructure Development During the Hydration of a Cement Compound, Journal of the American Ceramic Society ,Vol. 69, pp. 790-795.

[44] Jensen, O. (1995), Thermodynamic Limitation of Self-Desication, Cement and Concrete Research ,Vol. 25, pp. 157-164.

[45] Jonasson, J.E., (1994), Modelling of Temperature, Moisture and Stresses in Young Concrete, Civil and Mining Engineering, Luleå Sweden, Luleå University of Technology, 225,PhD.

[46] Klug, P., (1973), Creep, Relaxation and Swelling of Hardened Cement Paste, Munich, Technical University of Munich, pp. 69,PhD.

[47] Koenders, E.AB. and Breugel, K. van (1995), The Effects of Autogenous Shrinkage on Cracking in Hardening High Strength Concrete, Concrete 95 Toward Better Concrete Structures, FIP-CIA, Brisbane Australia.

[48] Koenders, E.A.B., Veen, C. van der and Kaptijn, N. (1995), Application of High Strength Concrete in Cantilever Bridge Construction, International Conference, The Concrete Future, NCS & CCAN, Auckland, New Zealand.

[49] Koenders, E.A.B., Lokhorst, S.J. and Breugel, K. van (1995), Cracking in Hardening Concrete due to Temperature Effects, International Conference, The Concrete Future, NCS & CCAN, Auckland, New Zealand.

[50] Koenders, E.A.B., Breugel, K. van, Ouwerkerk, H. and Töllner, M. (1996), Design and Construction of an Office Building in High Strength Concrete, Structural Engineering in consideration of Economy Environment Energy, Copenhagen Denmark.

[51] Koenders, E.A.B. (1997), An investigation to the material properties of concrete B65, Delft University of Technology, Delft, Stevin report, 25.5-97-1.

[52] Koenders, E.A.B. and Breugel, K. van (1994), Numerical Sensitivity Analysis of Adiabatic Hydration Curves, 29 Forschungskolloquium, Deutscher Ausschuss Für Stahlbeton pp. 157-164.

[53] Koenders, E.A.B. Töllner, M., Breugel, K. van and Obladen, B. (1996), Evaluation of a Full-Scale Test of a U-Shaped Element in High Strength Concrete, Fourth International Symposium on Utilization of High-Strength / High-Performance Concrete, Paris France.

[54] Kukko, H., (1992), Frost effects on the microstructure of HSC and methods for their analysis, Technical Research Centre of Finland, Espoo, pp 133,VTT Publication 126, PhD.

[55] Larbi, J.A., (1991), The Cement Paste-Aggregate Interfacial Zone In Concrete, Faculty of Civil Engineering, Delft, Delft University of Technology, 127,PhD.

[56] Laube, M., (1990), Werkstoffmodell zur Berechnung von Temperaturspannungen in Massiven Betonbauteilen im Jungen Beton, Braunschweig, TU-Braunschweig, 251,PhD.

[57] Lokhorst, S.J., (1991), Simulation of Strength and Stress Development in Hardening Concrete (in Dutch), Faculty of Civil Engineering, Delft, Delft University of Technology, Master thesis.

[58] Lokhorst, S.J. (1996), Young Concrete, Stresses and Cracking (in Dutch), Cement ,nr. 3, pp. 23-30.

[59] Lokhorst, S.J. and Breugel, K. van (1994), From Microstructoral Development Towards Prediction of Macro Stresses in Hardening Concrete, Thermal Cracking in Concrete at Early Ages, E&FN SPON London, München.

[60] Lokhorst, S.J. and Breugel, K. van (1995), Experimental and Numerical Analysis of Stress Development in Hardening Concrete, Progress in Concrete Research ,Vol. 4, pp. 11-20.

[61] Lokhorst, S.J. and Breugel, K. van (1995), Prediction of Thermal Cracking in Hardening Concrete Structures: Effects of Various Degrees of Restraint, FIP-CIA conf. Concrete 95, Toward Better Concrete Structures, Brisbane, Australia.

[62] Maggs, F.A.P. (1944), The Absolute Evaluation of Surface Areas of Solid Materials, Ultra-fine Structure of Coals & Cokes, The British Coal Utilisation Research Association, The Royal Institution, London.

[63] Mayer, L. (1991), Hochfester Beton im Hochhausbau, Darmstadter Massivbau-Seminar, Darmstadt.

[64] Moukwa, M. and Aitcin, P. C. (1988), The effect of Drying on Cement Pastes Pore Structure as Determined by Mercury Porosimetry, Cement and Concrete Research ,Vol. 18, pp. 745-752.

[65] Neville, A.M. (1978), Properties of Concrete, Great Britain, The Pitman Press.

[66] Pommersheim, J. M. en Clifton, J. R. (1980), Conceptual and mathematical models for tri-calcium silicate hydration, 7th Int. Conference on Chemistry of Cements.

[67] Powers, T.C. (1947), A discussion of Cement Hydration in Relation to the Curing of Concrete, Portland Cement Assn ,Vol. 27, 178.

[68] Powers, T.C. and Brownyard, L.T. (1947), The Thermodynamics of Adsorption of Water on Hardened Cement Paste, American Concrete Institude ,Vol. 18, pp. 549-602.

[69] Ramachandran, V.S., Feldman, R.F. and Beaudoin, J.J. (1981), Concrete Science, Treatise on Current Research, Division of Building Research, National Research Council, Canada, Heyden.

[70] Reinhardt, H.W. (1985), Concrete as a building material (in Dutch), Delft, The Netherlands, Delft University Press.
[71] Renhe, Y., Baoyuan, L. and Zhongwei, W. (1990), Study on Pore Structure of Hardened Cement Paste by SAXS, Cement and Concrete Research ,Vol. 20, pp. 385-393.
[72] Rooij, de M. R., Bijen, J.M.J.M. and Frens, G., (1997), Syneresis: An explanation for the interfacial zone, To be published in: Advanced cement-based materials 1997.
[73] Roth, W., (1970), Heat of Hydration and Degree of Hydration of Portland Cement, Aachen, Germany, Technical University of Aachen, PhD.
[74] Sarkar, S.L. (1993), High Strength Concrete and its Microstructure, New Delhi, India.
[75] Schlangen, E., (1993), Experimental and Numerical Analysis of Fracture Processes in Concrete, Faculty of Civil Engineering, Delft, Delft University of Technology, 121,PhD.
[76] Schwartz, L. (1996), Transport and Diffusion in Porous Media: The Interplay Between Physics and Geometry, 7th ACBM/NIST computer modelling workshop - 1996, NIST, Washington USA.
[77] Scrivener, K.L. and Nemati, K.M. (1996), The Percolation of Pore Space in the Cement Paste/Aggregate Interfacial Zone, Cement and Concrete Research ,26, pp 35-39.
[78] Sellevold, E., Bjøntegaard, ø, Justens, H. and Dahl, P.A. (1994), High Performance Concrete: Early volume Change and Cracking Tendency, Thermal Cracking in Concrete at Early Ages, E&FN SPON London, München.
[79] Setzer, M., J. (1978), Einfluss des Wassergehalts auf die Eigenschaften des erhärteten Betons, Deutscher Ausschuss Für Stahlbeton DAfSt ,Heft 280, pp. 43-79.
[80] Setzer, M.J. A model of hardened cement paste for linking shrinkage and creep phenomena, Technical University Munich, Munich, Technical report,
[81] Setzer, M. J., (1972), Oberflächenenergie und Mechanische Eigenschaften des Zementsteins, München, TU München, pp. 113,PhD.
[82] Setzer, M.J. (1976), A Method for Describtion of Mechanical Behaviour of Hardened Cement Paste by Evaluating Adsorption Data, Cement and Concrete Research ,6, 37-48.
[83] Society, The Concrete (1985), Permeability of concrete and its control, The concrete society, London, Proceedings report.
[84] Somerville, G. (1995), Developments in Design and Performance Requirements for Post-Tensioned Bridges in the U.K., Concrete 95 Toward better concrete structures, Brisbane Australia.
[85] Springenschmid, R., Breitenbücher, R. and Mangold, M. (1994), Development of the Cracking Frame and the Temperature-Stress Testing Machine, RILEM Conference onThermal Cracking in Concrete at Early Ages, E&FN SPON, Munich.
[86] Taylor, H.F.W. (1992), Cement Chemistry, San Diego, Academic press inc.
[87] Tazawa, E. and Miyazawa, S. (1992), Autogenous shrinkage caused by self desiccation in cementitious material, 9th Int. Conf. on Chemistry of Cement, New Delhi.

[88] Tazawa, E. and Miyazawa, S. (1993), Autogenous Shrinkage of Concrete and its Importance in Concrete Technology, Creep and Shrinkage of Concrete, E&FN Spon, Barcelona, Spain.
[89] Thielen, and Hinzen (1994), RILEM Conference onThermal Cracking in Concrete at Early Ages, E&FN SPON, Munich.
[90] Veen, C. van der, Koenders, E.A.B. and Kaptijn, N. (1996), Thermal Craking in a Cantilever Bridge made of HSC, ASCE Third Congress on Computing in Civil Engineering, Los Angeles.
[91] Verruijt, A. The Development of Reduced Pore Pressure in Partially Saturated Sand, pp. 305-312.
[92] Verruijt, A. (1969), Elastic Storage of Aquifers, Flow Through Porous Media, R. J. M. d. Wiest, New Jersey, USA, Academic press New York and London, 331-375.
[93] Verruijt, A. (1987), Soil Mechanics, Delft, Delft University Press.
[94] Vonk, R. A., (1986), Stress Development and Reological Behaviour of Hardening Concrete, Civil Engineering, Mechanica and Structures, Delft, The Netherlands, Delft University of Technology, MSc.
[95] Wardenier, P. (1994), Determination of the degree of hydration of High Strength Concrete, Delft University of Technology, Delft, Stevin report, 25.1-94-09.
[96] Weber, S., (1996), Nachbehandlungsunempfindlicher Hochleistungsbeton, Institut für Werkstoffe im Bauwesen (IWB), Stuttgart, University of Stuttgart, 211,PhD.
[97] Whiting, D. and Kline, E. (1977), Pore size distribution in epoxy impregnated hardened cement pastes, Cement and Concrete Research ,Vol. 7, pp 53-60.
[98] Winslow, D.L. (1990), The Pore Structure of Paste in Concrete, Cement and Concrete Research ,Vol. 20, pp. 227-235.
[99] Wisman, W.H. (1994), Introduction in Thermodynamics, Delft, Delft University Press.
[100] Wittmann, F., (1968), Physikalische Messungen an Zementstein, München, TU München, Habilitationsshrift.
[101] Wittmann, F.H. (1976), On the Action of Capillary Pressure in Fresh Concrete, Cement and Concrete Research ,Vol 6, pp. 49-56.
[102] Wittmann, F.H. (1977), Grundlagen eines Modells zur Beschreibung charakterisstischer Eigenschaften des Betons, Deutscher Ausschuss Für Stahlbeton (Dafst) ,Heft 290.
[103] Yates, D. J. C. (1954), The Expansion of Porous Glass on the adsorption of Non-Polar Gases, Proceedings of the Royal Society of London ,224, 526-543.
[104] Young, J.F., et.al Materiaux et Construction pp. 377-382.

Appendix A Cement characteristics

The characteristic properties of three types of Portland cement used in this thesis are listed in detail in Table A.1. The clinker composition, the fineness of the cement (Rosin Rammler parameters (n_{RR} and b_{RR})), but also the HYMOSTRUC input parameters (k_0, δ_{tr}, β_1, β_2) that are required for a numerical simulation are listed in the table.

Table A.1. Cement characteristics.

Parameter	CEM I 52.5 R	CEM I 42.5 R	CEM I 32.5 R
Q_{pot} [J/g]	440	430	419
C_3S	60	54	43
C_2S	12	20	28
n	1.030	1.076	1.107
b	0.067	0.041	0.023
K_0 [μm/hr]	0.055	0.045	0.04
δ_{tr} [μm]	5.5	3	3
β_1	2	2	2.5
β_2	2	2	2
Vol. mass [kg/m³]	3150	3150	3150
Blaine [m²/kg]	550	420	300

Appendix B Numerical solution of differential equation for moisture transport

General

In this section, it will be outlined how the partial differential equation (6.21) is solved numerically. Several numerical techniques can be applied to solve this equation. In this thesis, it is chosen to solve the set of equations by using the implicit numerical approach according to Euler. Application of this method has the advantage that the numerical process is always stable, independent of the size of the applied time step. However, the time step must be restricted with respect to the accuracy of the solution.
Various numerical schemes can be applied to make the differential quotients of the partial differential equation discrete. Most known methods of discretisation are, for instance, the finite difference method, the finite volume method or the finite element method. In this thesis, the finite difference method is applied for the discretisation of the set of differential quotients.
In this appendix, an outline will be given on the way how the partial differential equation (PDV) is solved. To get a good overview of the applied procedure, the following sequence is adopted. First, the problem definition will be given. Emphasis will be on the validity area of the PDV and on the boundary conditions that have to be faced. Thereafter, the discretisation the PDV will be show. Finally, it will be shown how the set of equations can be solved by application of the implicit Euler approach.

Problem definition
In chapter 6, the formal derivation of a partial differential equation was shown that describes the relationship between the change of the volumes of solid, water and gas as a function of the development of the microstructure. This *parabolic* PDV has the following form:

$$\frac{\partial p_w}{\partial t} = \frac{1}{n\beta}\frac{\partial}{\partial x}\left(\frac{k_w}{\gamma_w}\frac{\partial p_w}{\partial x}\right) - \frac{0.4\rho_{ce}}{n\beta(\rho_w + \rho_{ce}\omega_0)}\frac{\partial \alpha}{\partial t} \qquad \text{(B.1)}$$

where: p_w: pressure in the capillary water
n: porosity
β: compression coefficient of water
k_w: permeability of water
γ_w: specific density of water
ρ_w: specific mass of water

ρ_{ce}: specific mass of cement
ω_0: water/cement ratio
$\partial\alpha/\partial t$: rate of the hydration process

Time integration
The PDV as shown by equation (B.1) can be solved by the implicit Euler approach. The discretisation of this PDV is based on the finite difference approach. Application of this method yields into the following set of equations:

$$(I - \Delta t S)p^{n+1} = p^n + \Delta t \cdot f \tag{B.2}$$

where f is the vector which contains the pressure that is induced by hydration. According to the adopted discretisation, the matrix S has the shape of a so called tri-diagonal matrix. This matrix can be solved very easily by a direct solution method.
A row of the matrix S can be denoted as follows:

$$\frac{1}{n\beta\gamma_w\Delta x^2}\left(k_{w,i-\frac{1}{2}} - 2\left[k_{w,i-\frac{1}{2}} + k_{w,i+\frac{1}{2}}\right] + k_{w,i+\frac{1}{2}}\right) \tag{B.3}$$

The variation of the permeability k_w has also be taken into account since this parameter changes throughout the length of the ribbon. Especially at the ITZ, the permeability gradients are quite large.
The time integration can be performed by a sequential stepwise calculation procedure. The set of equations (B.2) must be solved for every time step. This implies that a matrix must by solved by either a direct or an indirect method. Since the matrix dimensions are not very large (about 100x100) this matrix can be solved directly by e.g. Gauss elimination or LU-decomposition.

Appendix C The program TEMPSPAN

Numerical simulation of thermal cracking with TEMPSPAN

The computer code TEMPSPAN was developed to calculate the probability of thermal cracking in hardening concrete structures. The code consists of two modules. In the module TEMP the development of the hydration process and the temperature is calculated, taking into account the ambient conditions (temperature, wind and solar radiation), the thermal properties of the formwork, the mix composition and the dimensions of the structure. In the module SPAN the development of thermal stress due to internal and/or external restraint is calculated. In the code the (calculated) degree of hydration plays a paramount role in the calculation of the temperatures and the development of material properties, including early-age relaxation.

Temperature development

The transfer of heat through a material can be carried out according to the partial differential equation of Fourier (eq. (C.1)). This equation is based on the balance of the thermal gradients. Internal or external heat sources may influence the heat development in the material. The equation can be written as follows:

$$\frac{\partial \bar{T}}{\partial t} = D \; div \; grad \; T + \bar{f}(t,x,y,z) \qquad (C.1)$$

where D [m²/s] is the coefficient of thermal diffusivity, T [°C] temperature, x,y,z co-ordinates of a point in the structure, t[s] time and $\bar{f}$ [J/g] the heat source, e.g. heat of hydration

Stress development

The calculation of the stress development is based on elastic and time-dependent deformational behaviour of concrete. Elastic stress increment is calculated according to:

$$\Delta\sigma(\tau_i,t) = (\Delta T_i \cdot \alpha_{c,i} + \Delta\varepsilon_a) \cdot E(\alpha_{\tau_i}) \cdot R \qquad (C.2)$$

in which:
- ΔT_i : temperature increment in time step i
- $\alpha_{c,i}$: coefficient of thermal expansion of concrete at time τ_i
- $\Delta\varepsilon_a(\alpha_{\tau i})$: *autogenous deformation* increment
- $E(\alpha_{\tau i})$: elastic modulus of concrete at time of loading τ_i
- R : degree of restraint

The external degree of restraint depends on the physical boundary conditions of the structure. It can vary between 0 and 100 % and is constant throughout the calculation.

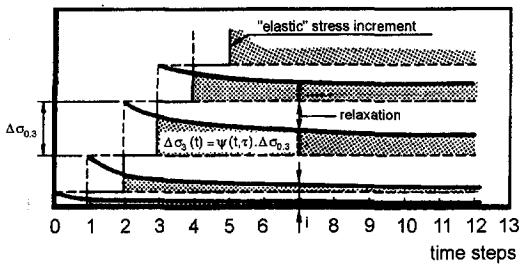

Fig. C.1. Schematic representation of the superposition principle

The superposition principle [15] is used to take into account the stress history (see Fig. C.1):

$$\sigma(t) = \sum_{i=1}^{n} \Delta\sigma(\tau_i, t) \cdot \psi(\tau_i, t, \alpha_{\tau,i}, \alpha_t) \tag{C.3}$$

where the stress relaxation is determined by

$$\psi(\tau_i, t, \alpha_{\tau,i}, \alpha_t) = \exp(-[\frac{\alpha_h(t)}{\alpha_h(\tau_i)} - 1 + 1.34 \cdot \omega^{1.65} \cdot \tau_i^{-d} \cdot (t - \tau_i)^n \cdot \frac{\alpha_h(t)}{\alpha_h(\tau_i)}]) \tag{C.4}$$

in which $\psi(\tau_i,t,\alpha_{\tau i},\alpha_t)$ is the relaxation factor pertaining to a particular stress increment $\Delta\sigma(\tau_i)$ [15] and α_h the degree of hydration. In this formula the rate of the hydration process influences the relaxation. In this formula n is 0.3 for compression and 0.6 for tension; d varies from 0.3 to 0.4 for a low heat cement and a rapid hardening cement respectively; ω is the water/cement ratio (w/c) of the mix.

Probability of cracking

When comparing the thermal stresses with the actual tensile strength, the probability of cracking can be predicted. In TEMPSPAN the calculated values of the stress and the tensile strength are considered to be the mean values of normal distributed quantities. The standard deviations for the strength and the stress are both estimated at 10 % of the actual (mean) values. Thus a strength criterion is adopted. For the probability of cracking it holds:

$$P_{crack} = P\{\sigma(t) > f_{ct}(t)\} \tag{C.5}$$

Appendix D

Description of the drying-wetting model

General

In this appendix, an overview and description is given of the model with which the drying or wetting deformation of an arbitrary cement paste can be determined on the basis of a thermodynamic approach. The equations used in the model will be outlined in the sequence at which the calculation process can be carried out. The equations which describe the pore size distribution are taken from the thesis of van Breugel [16]. The model can easily be programmed with a spread-sheet program.

Model description

Consider a cement paste that follows the following pore size distribution:

$$V_{por}(\alpha) = a \ln\left(\frac{\phi}{\phi_0}\right) \tag{D.1}$$

This formula is originally proposed by Van Breugel [16]. It turned out to give a reliable approximation of the pore structure in a hardening paste.
For the total pore volume it holds that:

$$V_{por}(\alpha) = \frac{\rho_{ce}}{\rho_w + \rho_{ce}\omega_0} \cdot (\omega_0 - 0.3375\alpha) \cdot V \tag{D.2}$$

From the pore size distribution and the total pore volume, the maximum pore diameter ϕ_{por} can be found. It holds that:

$$\phi_{por}(\alpha) = \phi_0 \exp\left(\frac{V_{por}(\alpha)}{a}\right) \tag{D.3}$$

The total pore wall area can be determined by:

$$A_{por}(\alpha) = -4 \cdot a \cdot (\phi_{por,\alpha}^{-1} - \phi_0^{-1}) \tag{D.4}$$

The total pore volume can be subdivided into a part which consists of the capillary water and another part which is induced by the chemical shrinkage. This can be denoted as:

$$V_{por}(\alpha) = V_{cap}(\alpha) + V_{chsh}(\alpha) \tag{D.5}$$

The capillary water volume can be determined according to:

$$V_{cap}(\alpha) = \frac{\rho_{ce}}{\rho_w + \rho_{ce}\omega_0} \cdot (\omega_0 - 0.4\alpha) \cdot V \qquad (D.6)$$

If the relative humidity is known (ranging between 0% and 100%), the thickness of the adsorption layer Γ in the pore structure can be determined according to the relation as given by Setzer [79] (based on data of Hagymassy [38]):

$$\Gamma = 3\left(\frac{-2.7}{\ln(RH)}\right)^{1/3} \qquad (D.7)$$

From the actual relative humidity and the thickness of the adsorption layer, the surface tension in the adsorption layer can be determined by:

$$\sigma = RT \int_{p_g/p_0}^{p_g/p_0=1} \Gamma \, d\left(\ln(p_g / p_0)\right) \qquad (D.8)$$

If the volume of capillary water and the thickness of the adsorption layer are known, the volume of water that is adsorbed at the pore wall area can be determined according to:

$$V_{ad}(\alpha) = 4 \cdot a \cdot \left(\Gamma\left(\frac{1}{\phi_0} - \frac{1}{\phi_{por,\alpha}}\right) + \frac{\Gamma^2}{2}\left(\frac{1}{\phi^2_{por,\alpha}} - \frac{1}{\phi^2_0}\right)\right) \qquad (D.9)$$

Subtracting the adsorbed water volume from the capillary water volume results in the volume of free capillary water which is available for further hydration. The volume of free capillary water can be determined by:

$$V_{free}(\alpha) = V_{cap}(\alpha) - V_{ad}(\alpha) \qquad (D.10)$$

The largest pore diameter which is still completely filled with capillary water can be determined according to:

$$\phi_{wat}(\alpha, RH) = \phi_0 \exp\left(\frac{V_{free}(\alpha)}{a}\right) \qquad (D.11)$$

ϕ_{wat} is also defined as a function of the relative humidity. This is done since the volume of free water depends on the thickness of the adsorption layer which in turn, a function of the relative humidity.

The area of the pores which are completely filled with water can be determined by:

$$A_{wat}(\alpha) = -4 \cdot a \cdot (\phi^{-1}_{wat,\alpha,RH} - \phi^{-1}_0) \qquad (D.12)$$

With the elastic modulus, the specific mass of the cement paste and the above given equations, all parameters are known which are necessary to determine the proportionality factor λ. Therefore, the proportionality factor can be determined according to:

$$\lambda(\alpha, RH, wcr) = C\frac{\Sigma(\alpha, RH)\cdot\rho_{pa}(wcr)}{E_p(\alpha)} \qquad (D.13)$$

where: $\Sigma(\alpha,RH)$ = $A_{por}(\alpha)$-$A_{wat}(\alpha,RH)$ is the pore wall area of the empty pores
$\rho_{pa}(wcr)$ = specific mass of the cement paste
$E_p(\alpha)$ = modulus of elasticity of the cement paste
C = constant = 3

Together with the surface tension in the adsorption layer σ, the increment of the drying or wetting deformation can be determined according to:

$$\Delta\varepsilon_s = \lambda\cdot\Delta\sigma \qquad (D.14)$$

The total drying or wetting deformation must be determined incrementally since the proportionality factor λ depends on the relative humidity (not a constant !).
The total deformation can be determined by summation of all increments:

$$\varepsilon_s = \sum_{RH}\Delta\varepsilon_s \qquad (D.15)$$

Notations and symbols

A	area	$[m^2]$
A_{por}	total pore wall area	$[m^2]$
A_{wat}	wet pore wall area	$[m^2]$
a	pore structure constant	[--]
b_{RR}	Rosin Rammler constant	[--]
C	cement content	$[kg/m^3]$
c_c	specific heat of cement	[J/kg.K]
c	molar concentration	[--]
e	volume strain	[--]
E_p	elastic modulus of cement paste	[MPa]
F	particle fraction	[--]
$G(x)$	cumulative mass distribution of cement	[g]
g	gravity constant of the earth	$[m/s^2]$
I_x	cell with centre particle x	$[m^3]$
k_g	gas permeability	[m/s]
k_w	water permeability	[m/s]
L	ribbon length	[m]
L_x	mean particle spacing	[m]
N	number of particles per gram cement	[1/g]
$n = n(\alpha)$	porosity	[--]
n_{RR}	Rosin Rammler constant	[--]
n_i	number of molecules in phase i	[--]
p	pressure	[Pa]
p_0	atmospheric pressure	[Pa]
p/p_0	relative pressure	[--]
p_g	gas pressure	[Pa]
p_w	water pressure	[Pa]
Q	heat exchange between system and surroundings	[J]
Q_{cap}	discharge of capillary water	$[m^3/s]$
Q_g	discharge of gas	$[m^3/s]$
Q_w	discharge of water	$[m^3/s]$
Q_{pot}	potential heat of hydration	[J/g]
q	specific discharge	[m/s]
R	universal gas constant	[J/K.mol]
RH	relative humidity	[--]
R_H	hydraulic radius	[m]
R_m	max. radius of random particle structure	[m]
R_t	ribbon thickness	[m]
r	degree of restraint	[--]
r_m	radius for random position of a particle	[m]
S	entropy	[J/T]
S_a	total specific surface area of aggregates	$[m^2]$
$s = s(\alpha)$	degree of saturation	[--]
T	temperature	[K]
t	time	[s]

U	internal energy	[J]
V_{c0}	initial cement volume	[m^3]
V_g	volume of gas	[m^3]
V_p	paste volume	[m^3]
V_w	volume of capillary water	[m^3]
V_{w0}	initial water volume	[m^3]
V_s	volume of solid material	[m^3]
V	volume	[m^3]
W	mechanical work	[J]
x	length	[m]
α	overall degree of hydration	[--]
α_x	degree of hydration of particle with diameter x	[--]
β	compression coefficient of water	[m^2/N]
ε_a	autogenous deformation strain	[--]
ε_s	swelling deformation strain	[--]
ϕ	general pore diameter	[m]
ϕ_{por}	largest pore diameter in pore structure	[m]
ϕ_{wat}	maximum pore diameter of filler pores	[m]
ϕ_0	minimum diameter of capillary pores	[m]
γ_w	specific density of water	[N/m^3]
γ_g	specific density of gas	[N/m^3]
κ_w	intrinsic permeability of water driving pores	[--]
κ_g	intrinsic permeability of gas driving pores	[--]
λ	proportionality factor	[m/N]
φ	angle for random particle structure	[--]
ϑ	angle for random particle structure	[--]
Σ	pore wall area of the empty pores	[m^2]
Γ	thickness of adsorption layer	[Å]
μ_g	dynamic viscosity of gas (air)	Pa.s
μ_w	dynamic viscosity of water	Pa.s
ν_g	kinematic viscosity of gas (air)	[m^2/s]
ν_w	kinematic viscosity of water	[m^2/s]
ν	ratio: volume of hydration products / reactant	[--]
ρ_{ce}	specific mass of cement	[kg/m^3]
ρ_s	specific mass of the solid material	[kg/m^3]
ρ_w	specific mass of water	[kg/m^3]
ρ_{pa}	specific mass of paste	[kg/m^3]
σ	surface tension	[N/m]
ω_0= wcr	water/cement ratio	[--]
ζ_{pa}	volumetric paste density	[--]

Summary

Durability requirements have become an important issue for the design of concrete structures today. The improvement of the quality of a concrete structure starts with the control of the hardening process. The main parameters that may damage the concrete structure during the hardening process are considered to be the hydration induced temperature development and also the autogenous deformations (swelling or shrinkage). Considering autogenous shrinkage to be a parameter that is responsible for durability loss of a concrete structure is a rather new concept. For conventional concretes with a high water/cement ratio, this effect of autogenous shrinkage on the durability loss is generally neglected. This effect appears to be more pronounced for low water/cement ratio concretes, such as high strength concrete or high performance concrete made with non-expansive cements. The range within which this research is carried out is therefore limited to low water/cement ratio concretes and associated cement pastes.

In chapter 1, the research topic and the aim of the research project are outlined. This also includes a survey of the field of interest.

In chapter 2, an overview is given on the main parameters that play an important role in the hardening process of low water/cement ratio concretes. The chapter starts with a discussion on the mix constituents of low water/cement ratio concretes. After that, the various aspects of the hardening process of low water/cement ratio concretes are discussed. Issues including are the degree of hydration, the rate of hydration, the volume changes during hydration and also the special locations in concrete (interface zone, bulk paste, plain paste) are mentioned.

Since the cause of the autogenous shrinkage lies in the microstructural development, chapter 3 starts with an overview of the existing numerical models with which hydration processes of cement-based material can be simulated. From this point on, the extension of the HYMOSTRUC model is elucidated. A random particle structure is developed to form the basis of the hydration model. From this random particle structure, the pore structure is determined with help of the hydraulic radius.

An reliable description of the pore structure is required forms the basis the thermodynamic analysis of the microstructure. This can be used to model autogenous shrinkage of a hardening cement paste. The way in which autogenous shrinkage can be modelled on the basis this approach is outlined in detail in chapter 4. The parameters that play an important role in this model are presented and discussed extensively. A flow chart is given which shows the way in which thermodynamic equilibrium in the pore space can be established. A parameter study is also part of chapter 4. The parameters which are involved in the calculation process to establish thermodynamic equilibrium are presented for different values of the water/cement ratio and also for three different finenesses of the cement of the hardening cement paste.

The proposed model to simulate and predict autogenous shrinkage of a hardening cement paste is validated by experiments in chapter 5. An extensive experimental program was carried out to verify the predictability and accuracy of the proposed model to simulate autogenous shrinkage. The effect of silica fume on the autogenous shrinkage of hardening cement paste is also taken into account in the experimental program. The effect of the autogenous shrinkage of hardening cement paste is also considered for a concrete. The addition of stiff aggregate particles prevent the hardening cement paste to shrink. This results in a reduction of the autogenous shrinkage of the hardening concrete. A composite model, as well as a lattice model, is proposed to derive the autogenous shrinkage of concrete from the autogenous shrinkage of the hardening cement paste. The lattice model is also used to visualise the stress concentrations in the hardening cement paste which develop in the vicinity of the aggregate particles.

In chapter 6, a model is proposed with which the volume changes of a ribbon of a hardening concrete can be simulated. The model consists of a random particle structure which is bordered by two aggregate particles. The model also takes into account the discontinuity of the packing of the cement particles close to the aggregate surface. Water is accumulated in these relatively porous regions. A transport model is proposed which shows that these water-rich regions serve as water suppliers for the bulk paste during hydration. Due to this process, the emptied pore space in the bulk paste may become filled with capillary water again, resulting in a reduction of the autogenous shrinkage. This effect is shown for two cement pastes with different water/cement ratios. The results show a reduction of the autogenous shrinkage for low water/cement ratio pastes.

The way in which autogenous shrinkage induced deformation may damage a hardening concrete structure is presented in chapter 7. Two case studies are presented to show the effect of the autogenous shrinkage on a lab-scale as well as on a full-scale level. The results show that autogenous shrinkage itself may cause cracking of a concrete structure while under a certain restraint.

The discussion of the results and conclusions of the findings are summarised briefly in chapter 8. This chapter also deals with some recommendations for further research and development of the model.

Samenvatting

Duurzaamheideisen worden in toenemende mate belangrijk bij het ontwerpen van betonconstructies. Het verbeteren van de kwaliteit van een betonconstructie begint bij het controleren van het verhardingsproces. De hoofdparameters die verantwoordelijk zijn voor het veroorzaken van schade aan een verhardende betonconstructie zijn met name de temperatuurontwikkeling als gevolg van het verhardingsproces en ook de autogene krimp. Het beschouwen van de autogene krimp als een parameter die verantwoordelijk is voor het verminderen van de duurzaamheid van een betonconstructie is tamelijk nieuw. In het algemeen wordt voor conventionele betonsoorten het effect van de autogene krimp op het verminderen van de duurzaamheid verwaarloosd. Echter, autogene krimp blijkt duidelijk op te treden bij betonmengsels met een lage watercementfactor, zoals hoge-sterkte beton soorten. Het gebied waarvoor dit onderzoek is uitgevoerd is daarom gericht op cementpasta's en betonsoorten met een lage water/cement factor.

In hoofdstuk 1 wordt het onderzoeksdoel en het aandachtsveld van dit promotiewerk besproken. In dit hoofdstuk wordt eveneens een overzicht gegeven van het interessegebied waarvan het promotiewerk deel uitmaakt.

Om meer inzicht te verkrijgen in de parameters die een belagrijke rol spelen in het verhardingsproces van betonmengsels met een lage watercementfactor, wordt in hoofdstuk 2 een overzicht gegeven over deze parameters. Het hoofdstuk begint met een discussie over de verschillende ingredienten waaruit een beton met een lage watercement factor is opgebouwd. Hierna worden verschillende aspecten van het verhardingsproces besproken. Onderwerpen die aan de orde komen zijn de hydratatiegraad, de hydratatiesnelheid, volumeveranderingen die optreden tijdens het verhardingsproces en ook worden de "speciale gebieden" die in beton voorkomen. (grenslaag tussen toeslag en cementpasta, bulkpasta, pure cement pasta).

Hoofdstuk 3 begint met een overzicht van de bestaande numerieke modellen waarmee het hydratatieproces van cementgebonden materialen kan worden gesimuleerd. Hierop-volgend wordt de uitbreiding van het hydratatiemodel HYMOSTRUC uiteengezet. Een *random* korrelstructuur vormt nu de basis van het hydratatiemodel. Vanuit deze *random* korrelstructuur kan ook de porieverdeling worden afgeleid met behulp van de hydraulische straal. Een betrouwbare beschrijving van de poriestructuur vormt de basis van de thermodynamische analyse van de microstructuur. Het kan worden toegepast voor het beschrijven van de autogene krimp van verhardende cementpasta.

Hoe te komen tot een model dat is gebaseerd op het thermodynamische evenwicht wordt uitgebreid besproken in hoofdstuk 4. De parameters die een belangrijke rol spelen in dit model worden beschouwd en uitgebreid besproken. Middels een stroomschema wordt aangegeven hoe het thermodynamisch evenwicht in de lege porieruimte kan worden bewerkstelligd. In hoofdstuk 4 worden ook de resultaten van een parameterstudie weergegeven. De parameters die zijn betrokken bij het rekenprocess ter verkrijging van

thermodynamisch evenwicht worden weergegeven voor verschillende waarden van de watercementfactor en ook voor verschillende waarden van de maalfijnheid van de cementsoort die is toegepast in de cementpasta.
Het model waarmee autogene krimp van verhardende cementpasta kan worden voorspeld, zoals dat is afgeleid en besproken in het vorige hoofdstuk, wordt gevalideerd in hoofdstuk 5. Een uitgebreid experimenteel programma is opgesteld om het voorspellend vermogen en de nauwkeurigheid van het model te analyseren. In dit experimentele programma wordt ook de invloed van de toevoeging van silica fume op de ontwikkeling van de autogene krimp van het verhardende cementpasta meegenomen. De autogene krimp van de verhardende cementpasta kan worden beschouwd als de oorzaak van de autogene krimp van het verhardende beton. Door toevoeging van stijve toeslagkorrels wordt de verhardende cementpasta verhinderd om vrij te vervormen. Dit zal resulteren in een vermindering van de autogene krimp van het verhardende beton. Een composiet-model, evenals een "*lattice*"-model, is toegepaste met als doel de autogene krimp van het verhardende beton af te leiden van de autogene krimp van verhardende cementpasta. Met het *lattice*-model kan ook een beeld worden verkregen van de spanningsconcentraties die zich ontwikkelen in de nabijheid van de toeslagkorrels.
In hoofdstuk 6 wordt een model gepresenteerd waarmee het hydratatieproces van een beton*ribbon* kan worden berekend. Het model behelst een *random* korrelstructuur van cementkorrels welke is omsloten met twee toeslagkorrels. Het model houdt daarom ook rekening met de invloed van de grenslaag tussen de toeslagkorrel en de cementpasta. Door de aanwezigheid van de toeslagkorrel is de pakking van de cementkorrels in de nabijheid van het oppervlak van de toeslagkorrel enigszins verstoord. Hydratatiewater zal zich verzamelen in deze poreuze gebieden. Een transportmodel wordt voorgesteld waarmee kan worden aangetoond dat gedurende het hydratatieproces, deze waterrijke gebieden dienen als een wateropslagvoorziening voor de bulkpasta. Door dit proces kan het voorkomen dat de lege poriën weer worden gevuld met capillairwater waardoor ook de autogene krimp zal afnemen. Dit proces wordt getoond voor twee verschillende cementpasta's met verschillende watercementfactoren.
In hoeverre de autogene krimpvervorming verantwoordelijk kan zijn voor het beschadigen van een betonconstructie wordt besproken in hoofdstuk 7. Twee case-studies worden gepresenteerd om het effect van autogene krimp op een laboratoriumnivo en op constructieniveau te laten zien. Het resultaat van deze case-studies laat zien dat autogene krimp alleen al genoeg kan zijn om scheurvorming te veroorzaken in een betonconstructie indien een zekere mate van vervormingsverhindering aanwezig is.
Een discussie van de resultaten en conclusies van de bevindingen zijn samengevat in hoofdstuk 8. In dit hoofdstuk worden ook enkele aanbevelingen gedaan voor verder onderzoek en ontwikkeling van het model.

Curriculum vitae

Eddie Koenders is geboren op 23 maart 1967 in Groenlo in de provincie Gelderland. Na zijn basis opleiding aan de st. Canisiusschool te Groenlo te hebben voltooid, begon hij in 1979 aan zijn opleiding bouwkunde aan de Technische School te Winterswijk. Het diploma van deze opleiding ontving hij in 1984. Hij vervolgde zijn studie bouwkunde aan de Middelbare Technische School te Enschede. Drie jaar later stapte hij over naar de Hogere Technische School te Hengelo, om zich daar verder te ontwikkelen in de richting Constructieve Bouwkunde. Tijdens deze studie spraken met name de richtingen mechanica en wiskunde hem zeer aan. Hierdoor aangetrokken besloot hij twee jaar later, in 1989, zijn kennis verder te ontwikkelen aan de Faculteit der Civiele Techniek van de Technische Universiteit in Delft. Zijn afstudeerrichting werd Offshore Technologie. Het afstudeerwerk voerde hij uit onder begeleiding van prof. J. Blaauwendraad. Dit afstudeerwerk betrof het modelleren van het vloeigedrag van betonnen platen en het implementeren van een vloeicontour in het eindig-elementen pakket TILLY. Zijn ingeniersdiploma ontving hij in 1992.
Bij prof. J.C. Walraven en onder begeleiding van dr K. van Breugel van de sectie Betonconstructies van de Faculteit der Civiele Techniek van de Technische Universiteit in Delft begon hij in 1993 met zijn promotieonderzoek. Dit onderzoek betroft het verhardingsproces van hoge-sterkte beton. Tijdens zijn onderzoek specialiseerde hij zich in de krimpmechanismen welke optreden tijdens het verhardingsproces van cement-gebonden materialen.

Tijdens zijn promotieonderzoek heeft hij diverse onderzoeksprojecten begeleid, uitgevoerd waarvan hij de onderzoeksresultaten heeft gepubliceerd en gepresenteerd op diverse international conferenties. Tevens heeft hij artikelen geschreven in vakbladen en internationale tijdschriften. Naast zijn promotieonderzoek heeft hij ook studenten begeleid tijdens hun afstudeerwerk en was hij medeorganisator van een studiereis voor 40 onderzoekers van de Faculteit der Civiele Techniek naar de Verenigde Staten.

Op 1 mei 1997 begint hij als wetenschappelijk medewerker bij de sectie Numerieke Mechanica van TNO-bouw.